UNIVERSIDADE DE SÃO PAULO

Faculdade de Filosofia, Ciências e Letras de Ribeirão Preto

Departamento de Física

Pedro Henrique Rodrigues da Silva

Redes cerebrais estruturais e funcionais: das conexões à cognição. Um estudo aplicado em Doença Cerebral de Pequenos Vasos

Brain structural and functional networks: from connections to cognition. A study applied to Cerebral Small Vessel Disease

Ribeirão Preto, São Paulo, Brasil

2022

Pedro Henrique Rodrigues da Silva

Redes cerebrais estruturais e funcionais: das conexões à cognição. Um estudo aplicado em Doença Cerebral de Pequenos Vasos

Brain structural and functional networks: from connections to cognition. A study applied to Cerebral Small Vessel Disease

Tese apresentada ao Programa de Pós-Graduação em Física Aplicada à Medicina e Biologia do Departamento de Física da Faculdade de Filosofia, Ciências e Letras de Ribeirão Preto da Universidade de São Paulo, para a obtenção do título de Doutor em Ciências.

Universidade de São Paulo – USP

Faculdade de Filosofia, Ciências e Letras de Ribeirão Preto – FFCLRP

Programa de Pós-Graduação em Física Aplicada à Medicina e Biologia

Versão Corrigida

Supervisor: Drª. Renata Ferranti Leoni

Ribeirão Preto, São Paulo, Brasil

2022

Pedro Henrique Rodrigues da Silva

Redes cerebrais estruturais e funcionais: das conexões à cognição. Um estudo aplicado em Doença Cerebral de Pequenos Vasos

Brain structural and functional networks: from connections to cognition. A study applied to Cerebral Small Vessel Disease

Tese apresentada ao Programa de Pós-Graduação em Física Aplicada à Medicina e Biologia do Departamento de Física da Faculdade de Filosofia, Ciências e Letras de Ribeirão Preto da Universidade de São Paulo, para a obtenção do título de Doutor em Ciências.

Ribeirão Preto, São Paulo, Brasil, 09 de fevereiro de 2022

Aprovado em:___/___/_____

Banca Avaliadora

Prof. Dr.:_____ Instituição: _____

Julgamento:_____ Assinatura: _____

Prof. Dr.:_____ Instituição: _____

Julgamento:_____ Assinatura: _____

Prof. Dr.:_____ Instituição: _____

Julgamento:_____ Assinatura: _____

Ribeirão Preto, São Paulo, Brasil

2022

"Wild horses run unbridled or their spirits die."
Mariah Carey, 1997.

Agradecimentos

Meus mais sinceros agradecimentos à professora Renata Ferranti Leoni, pela orientação, conhecimento, apoio e amizade em todos esses anos de pós-graduação. Foi uma jornada incrível e espero que a colaboração se mantenha no futuro. Gratidão eterna! Claro, muita saúde para o bebê que está a caminho.

Não poderia deixar de agradecer aos membros do laboratório Inbrain André Paschoal, Kaio Felippe, Ícaro Agenor, Bruno Hebling, Fábio Otsuka, Hohanna Gabriela, Carlo Rondinoni e professor Carlos Garrido. Desejo todo o sucesso do mundo a cada um deles. Agradeço também aos membros do Laboratório de Neurologia Vascular e Emergências Neurológicas pelo apoio.

Ao senhor Heinz Jorg Gruber, muito obrigado pelo apoio e interesse em minha pesquisa em todos esses anos. Agradecimento especial à colaboradora Maria Clara Zanon Zotin por todo o apoio, conhecimento e colaboração, os quais foram essenciais para a realização desse trabalho.

My most sincere thanks to Dr. Frank-Erik de Leeuw and Dr. Anil Man Tuladhar from Radboud University for the database of patients with cerebral small vessel disease and the support, without which it would not have been possible to complete the thesis.

Aos amigos de longa data e que recebem com carinho meus anseios e comemoram minhas vitórias, Cláudio Vasconcelos, Beatriz Dotta, Vanessa Masini e Fabiana Nicolau, deixo aqui meus agradecimentos. Também agradeço minha tia Márcia Massoni por todo o apoio e torcida.

Finalmente, agradeço aos meus pais, Joana e Valdir, por todo o apoio e amor desde sempre. Aos nossos pets Beethoven e Malévola também não poderia deixar de agradecer.

Resumo

As redes estruturais cerebrais modulares e hierárquicas são especialmente bem adaptadas à integração funcional de processos neuronais locais que sustentam a cognição. De fato, padrões alterados de conectividade anatômica ou funcional foram evidenciados em muitas doenças cognitivas e afetivas, que foram definidas como síndromes de "desconexão".

A hipótese central no presente estudo é que a conectividade estrutural restringe, mas não determina a conectividade funcional, e essa relação é a base do desempenho cognitivo. Além disso, as rupturas nas redes estruturais e funcionais estão relacionadas a deficiências cognitivas. Portanto, ao estudar as redes estruturais e funcionais cerebrais, podemos entender melhor como o cérebro funciona e sua relação com a cognição. Procuramos, então, responder a essas perguntas avaliando como a conectividade estrutural está relacionada à conectividade funcional e à cognição em participantes saudáveis e como alterações de conectividade cerebral se relacionam com o desempenho cognitivo em participantes clínicos.

Nesse contexto, avaliamos a localização e integração funcional em resposta à execução de uma tarefa cognitiva, o Teste de Modalidades de Símbolos-Dígitos (Symbol Digit Modalities Test, SDMT), que avalia a velocidade de processamento da informação (VPI), adaptada ao ambiente de ressonância magnética (RM). Mais especificamente, nosso objetivo foi investigar como as regiões dentro da rede cerebral de VPI interagem funcionalmente umas com as outras, estudando a conectividade efetiva, definida como a forma como uma região influencia ou causa atividade em outra durante um determinado processo neural e sua conectividade estrutural. Para fins de aplicação clínica, os pacientes com doença cerebral de pequenos vasos (DCPV) são de grande interesse, dado seu impacto na saúde pública global, sua classificação como Síndrome de desconectividade, e as questões em aberto sobre os danos estruturais e funcionais da conectividade que a doença causa, além da alta incidência de déficit de VPI. Nesse caso, avaliamos VPI com uma variação do SDMT: a Tarefa de Substituição de Letras-Dígitos (Letter-Digit Substitution Test, LDST).

Foi possível constatar que a rede estrutural restringe, mas não determina a rede funcional de VPI nos participantes saudáveis jovens. Além disso, ao avaliarmos a rede funcional de VPI durante a execução do SDMT, a ativação e conectividade funcional de nós da rede de modo padrão (Default Mode Network, DMN), importante para a saúde cognitiva, foi suprimida durante a realização do teste de VPI. Além disso, o nó pré-cúneo esquerdo (BA 7) apresentou comportamento modulatório dependente do contexto experimental. Avaliando as associações entre conectividade estrutural e funcional com escores de LDST em pacientes com DCPV, os achados sugeriram que DCPV deve ser considerada uma síndrome global e não localizada. Os efeitos de mediação da conectividade funcional da rede sensório-motora entre a lesão e os escores do LDST apontam o papel desta rede como uma importante rede funcional afetada neste grupo clínico. Usando uma abordagem de mapeamento lesão-sintoma

chamada "Brain disconnectome mapping", descobriu-se que as associações entre probabilidade de desconexão e escores de LDST envolveram áreas cerebrais amplas em pacientes com DCPV não dementes. Além disso, efeitos distintos foram observados conforme a carga de lesão e sua distribuição topográfica. Ambos os estudos com pacientes DCPV, embora com metodologias diferentes, apontam para o achado geral de que a DCPV é uma síndrome de desconectividade com amplo impacto pelo cérebro.

Assim, com o desenvolvimento do presente trabalho, investigamos a dinâmica das redes funcionais, sua relação com redes estruturais e desempenho cognitivo em VPI em indivíduos saudáveis, com os achados sugerindo que a rede estrutural restringe mas não determina a rede funcional. Também avaliamos as alterações de conectividade relacionadas ao desempenho de tarefas de VPI em DCPV, cujos resultados apontam para a importância de avaliar os efeitos da lesões focais na conectividade cerebral para compreender a heterogeneidade de desfechos clínicos.

Palavras-chave: conectividade cerebral, imagens por ressonãncia magngética funcional, imagens por tensor de difusão, Teste de Modalidades de Símbolos-Dígitos, Tarefa de Substituição de Letras-Dígitos, Doença Cerebral de Pequenos Vasos.

Abstract

Modular and hierarchical brain structural networks are especially well adapted to the functional integration of local neuronal processes that underpin cognition. Altered anatomical or functional connectivity patterns were evidenced in many cognitive and affective diseases, defined as "disconnectivity" syndromes.

The central hypothesis in the present study is that structural connectivity constrains but does not determine functional connectivity, and this relationship is the basis of cognitive performance. Furthermore, disruptions in structural and functional networks are related to cognitive impairments. Therefore, by studying the brain structural and functional networks, we can better understand how the brain works and its relationship to cognition. We then sought to answer these questions by assessing how structural connectivity is related to functional connectivity and cognition in healthy participants and how changes in brain connectivity relate to cognitive performance in clinical participants.

We evaluated the location and functional integration in response to executing a cognitive task, the Symbol Digit Modalities Test (SDMT), which evaluates the information processing speed (IPS), adapted to the MRI environment. More specifically, we aimed to investigate how regions within the IPS brain network interact functionally, studying effective connectivity, defined as how one region influences or causes activity in another during a given neural process and its related structural connectivity. For clinical application purposes, cerebral small vessel disease (cSVD) patients are of great interest given their impact on global public health, their classification as Disconnectivity Syndrome, and the open questions about the structural and functional disruptions of connectivity that the disease causes and the high incidence of IPS deficit, here evaluated with a variation of the SDMT: the Letter-Digit Substitution Test (LDST).

It was possible to verify that the structural network restricts but does not determine the functional network of IPS in young, healthy participants. In addition, when evaluating the IPS functional network during SDMT execution, activation and functional connectivity of nodes in the default mode network (DMN), essential for cognitive health, was suppressed during the performance of the IPS test. In contrast, the left precuneus (BA 7) node showed a modulatory behavior dependent on the experimental context. Assessing the associations between structural and functional connectivity with LDST scores in patients with cSVD, the findings suggested that cSVD should be considered a global rather than a localized syndrome. The mediation effects of the functional connectivity of the sensorimotor network between the lesion and the LDST scores point to the role of this network as another critical functional network affected in this clinical group. Using a lesion-symptom mapping approach called "Brain disconnectome mapping," the associations between the probability of disconnection

and LDST scores involved large brain areas in non-demented cSVD patients. Lesion load and its topographical distribution affected the cSVD patients differently. Both studies with cSVD patients, although with different methodologies, point to the general finding that cSVD is a syndrome of disconnection with a broad impact on the brain.

Thus, with the development of the present work, we investigated the dynamics of functional networks, their relationship with structural networks, and cognitive performance in IPS in healthy individuals. The findings suggest that the structural network constrains but does not determine the functional network. We also evaluated connectivity alterations related to the performance of IPS tasks in cSVD, whose results point to the importance of assessing the effects of focal lesions on brain connectivity to understand the heterogeneity of clinical outcomes.

List of Figures

List of Tables

Contents

1 General Introduction

1.1 The brain structure-function paradox

Modular and hierarchical brain structural networks are especially well adapted to the functional integration of local neuronal processes that underpin cognition (1). Altered anatomical or functional connectivity patterns were evidenced in many cognitive and affective diseases, defined as "disconnectivity" syndromes (2). Furthermore, spontaneous activity measures indicate functional connectivity patterns comparable to structural patterns, implying that structural networks impose constraints on functional networks (3).

However, how complex functioning comes from a brain with a relatively unchangeable structure remains a major puzzle in neuroscience (4, 5). As a result, understanding the nature of brain networks requires mapping the degenerate structure-function (many-to-one) relationship. In addition to understanding the nature of brain functioning, we will be able to understand the impact of brain damage on cognition and evaluate the effects of interventions.

1.2 Brain Connectivity

Complex brain networks are topologically organized in a non-trivial way (small world architecture and modular structure) that supports the efficient processing of information in the brain. Brain connectivity (structural or functional) is usually represented by a binary network whose topological organization can be evaluated using graph theory (6). Approaches based on graph theory model the brain as a complex network graphically represented by a collection of nodes (anatomical regions, for example) and connections (the temporal correlation between the signals of the regions defined by the nodes). In the virtual graph, nodes indicate anatomical elements (e.g., brain regions), and connections represent the relationship between nodes (e.g., connectivity). After the network modeling procedure, several theoretical measures of the graphs can be used to investigate the organizational mechanism behind the relevant networks. By statistical analysis of network properties, we can find possible neuromarkers of brain disease (7).

Structural connectivity (SC) or anatomical connectivity is a concept that aims to describe the white matter connections that link cortical regions. This structural network can be studied using diffusion tensor imaging and diffusion spectrum imaging (8). Diffusion Tensor Imaging (DTI) is a magnetic resonance imaging (MRI) technique that measures the anisotropic diffusion of water molecules in tissues that provide useful structural information about the white matter and the orientation of neural tracts, providing a view of the micro-architecture of these tracts (9). This method has been promising in understanding and

investigating neuronal tracts and structural connectivity between human brain regions (10). However, there is still a lot to understand about the brain structure and how it conditions its functionality.

Concerning functional connectivity (FC), we refer to the interregional synchrony of low-frequency fluctuations in the MRI signal (11). FC is of great value, considering its biological basis and its description of organizing the brain into functional networks. A functional network can be broadly defined as a set of brain regions that are consistently synchronous; the functional connectivity between two or more areas being due to synchronization within or between networks. In the context of neuroimaging, the functional connectivity framework provides researchers with opportunities to formulate and test hypotheses about functional networks, using methods such as seed-based correlation or the temporally and spatially Independent Component Analysis (ICA) (12).

MRI-FC studies are primarily performed using functional MRI (fMRI) based on the Blood Oxygenation Level Dependent (BOLD) contrast. It is correlated with the spontaneous neural activity of a brain region through neurovascular coupling, thus being considered as physiologically significant (13). BOLD contrast is based on the difference in magnetic susceptibility of hemoglobin molecules, which depends on their oxygenation state. When in the presence of a stimulus or task, neural activity occurs, causing a local demand for oxygen to produce energy, which is supplied by blood vessels through increased local cerebral blood flow (CBF). As the increase is greater than necessary, there is a decrease in the oxygen extraction fraction (OEF), causing an increase in the MRI signal weighted in relaxation time T2* (14). As the BOLD signal comes from large vessels, there is low spatial specificity regarding the neuronal activity. On the other hand, due to its sensitivity and temporal resolution, fMRI is useful in functional studies with or without tasks (15).

Measurements of spontaneous activity by BOLD-fMRI reveal patterns of functional connectivity that are similar to structural connectivity measured by DTI, suggesting that structural networks constrain functional networks in the resting state. However, task-related responses that require context-sensitive integration reveal a divergence between function and structure that appears to rest mainly on long-distance connections (16). The functional network architecture identified in resting state is present during task performance and may plausibly reflect the routes through which activity flows during cognitive task performance. In short, neuronal interactions represent the dynamics of fixed structural connectivity that underlies cognition and behavior. This divergence between function and structure is perhaps the brain most intriguing property and invites intensive research.

Thus, in addition to SC and FC, it is of interest to study effective connectivity, defined as how one region influences or causes activity in another during a particular neural process (17). The assessment of effective connectivity over time may indicate the occurrence of adaptive neuroplasticity (18).

1.3 Information Processing Speed, Symbol Digit Modalities Test (SDMT), and Letter Digit Substitution Test (LDST)

Information Processing Speed (IPS) is defined as "the amount of time required to process a set of information or the amount of information that can be processed in a given unit of time" (19). Many cognitive functions require sufficient processing speed to execute relevant operations the allowed timeframe; delayed IPS often underlies attention deficits. IPS can be assessed by the Symbol Digit Modalities Test (SDMT) (20, 21, 22). The SDMT consists of a key at the top of the test paper with nine symbols and nine corresponding numbers. Below the key, there is a random sequence of symbols, and below each symbol, there is a blank space. In the written version, the participant must write the number corresponding to the symbol as faster as possible. In the oral SDMT, the participant must say the corresponding number.

A meta-analysis reported the brain regions associated with the performance of the SDMT adapted for the MRI environment (23).It showed activation in bilateral middle frontal gyrus (Brodmann Area (BA) 6), left superior parietal lobule (BA 7), left precuneus (BA 7), left inferior frontal gyrus (BA 9), right cuneus (BA 17), left lingual gyrus (BA 17) and left declive (part of the cerebellum). Since IPS underlies other cognitive functions such as working memory, attention, and immediate visual memory (24, 25), we cannot just study IPS simply by mapping the individual areas involved but rather the connectivity between these areas. SDMT is interesting for such an application, as it is a robust and straightforward task, and its execution does not allow the use of different strategies by different subjects, better isolating the processing speed (26). Thus, functional and effective connectivity of the brain regions activated with the SDMT task were investigated in healthy subjects (27).

As previously described in the literature, FC studies revealed a highly linked network for IPS, involving the recruitment of frontoparietal regions involved to selective attention processes, occipital areas related to visual attention, and the cerebellum (21, 22). TThe activation of the areas associated with top-down attention management, such as the middle and superior frontal gyrus and the superior and inferior parietal gyrus, and of mechanisms of response selection, such as the posterior cingulate gyrus and the supplementary motor area (28) were also reflected in the findings. Activation in the temporoparietal and inferior frontal cortices might also be linked to detecting behavior-relevant inputs (29). The effective connectivity analysis identified a probable network architecture, with information propagating serially from the cuneus, passing through the lingual gyrus and the declive. Then, it bifurcates to the superior parietal lobe and the precuneus, converges to the inferior frontal gyrus and bifurcates again to the bilateral middle frontal gyrus.

To create more specific measures of IPS, the Letter Digit Substitution Test (LDST) (30) was made from SDMT and Digit Symbol Substitution Test (DSST) (31). During the LDST

performance, the participant must associate a letter to the digit. Unlike the other two tests, in which the participant must learn the exposed abstract symbols, in LDST the letters and digits are previously known. So, LDST is less dependent on complex visual and memory processes and, therefore, more specific on the IPS. It has been applied in cerebral small vessel disease studies (32, 33).

1.4 Cerebral Small Vessel Disease

Cerebral small vessel disease (cSVD) is a syndrome of significant impact on public health worldwide, with pathological, clinical, and imaging findings associated as a result of pathologies that lead to the perforation of arterioles, capillaries, and cerebral venules (34). cSVD is commonly associated with aging and may present as a stroke, dementia, cognitive decline, gait impairment, or mood disturbances, or it may have few or no symptoms. cSVD causes up to 45% of dementia cases and represents about 20% of all strokes worldwide. 25% are ischemic (or lacunar) stroke, of which 20% end in disabled patients (35). cSVD often coexists with neurodegenerative diseases and can exacerbate physical and cognitive deficits, particularly in IPS and executive functions (32, 36, 34). Given the difficulty in visualizing cSVD-related pathologies in vivo, the diagnosis of cSVD has been heavily based on neuroimaging, including white matter hyperintensity (WMH) (37), recent small subcortical infarcts (RSSI), lacunes of presumed vascular origin (38), microbleeds (39), perivascular spaces (40) and brain atrophy (34).

MRI techniques such as DTI and BOLD-fMRI are expected to contribute to the understanding of the pathophysiology of white matter lesions (and of cSVD in general) and their clinical correlates (37) through studies of structural and functional brain connectivity. Recently, researchers have demonstrated an association between global and local disruption of brain structural networks with diffusion markers and an increase in overall cSVD severity or burden of patients with a first transient ischemic attack or stroke (41). On the other hand, functional neuroimaging studies reported reduced functional connectivity in cSVD distributed networks. Three networks that are commonly affected are the Default Mode Network (DMN), the Dorsal Attention Network (DAN), and the Frontoparietal Control Network (FPCN). They all play an important role in attention directed by goals and executive functions (42, 43). Studies have reported that reduced functional connectivity within the FPCN, DAN, and DMN was related to an increased degree of cognitive impairment (44, 45). Evidence suggests that cognitive impairments due to cSVD result from disruption of frontal-subcortical circuits and long association fibers that, in turn, impair communication among crucial neural networks responsible for cognitive control or attention, such as DMN, FPCN, and DAN (43). However, there is still a lot to understand about the damage to the brain structure due to cSVD and how it alters brain functionality and cognition conditioned to the affected brain areas.

Therefore, in this work, we first investigated the dynamics of functional networks, their relationship with structural networks, and the cognitive performance of IPS in healthy individuals. Then, we assessed the different outcomes in a clinical group with cSVD from empirical data obtained with multimodal magnetic resonance imaging and neuropsychological assessment.

We organized the thesis based on the studies that we performed. In chapter 2, we present the general and specific goals of the work. In chapters 3 and 4, we present the methodology and results of two studies on young, healthy participants. In the first one, we investigated the brain structural-functional connectivity relationship underlying the IPS. Then, we focused on the non-classical behavior of the DMN regions during an IPS task. Both studies were already published.

In chapter 5, we present the results of a systematic review on the use of contrast-agent-free, state-of-the-art MRI on cSVD to investigate from lesions to connections and cognition. Here, we focused on DTI and BOLD-fMRI. However, the full article submitted for publication also included other MRI techniques. In chapters 6 and 7, we present the results of two studies of a clinical group with non-demented cSVD individuals from empirical data. In the first one, we investigated the WMH effects on cortical thickness, brain networks, and IPS through a mediation study. Then, we assessed the neural substrates of IPS deficits using a brain disconnectome mapping method.

Finally, chapter 8 shows our general conclusions and future steps.

2 Objectives

The general objective was to investigate the dynamics of functional networks, their relationship with structural networks and cognitive performance in IPS in healthy individuals, and the connectivity disruptions related to IPS performance in a clinical group with cSVD. We used empirical data obtained with multimodal magnetic resonance imaging and neuropsychological assessment. Our specific goals include:

- To investigate the dynamics of the IPS functional network, its relationship with the structural network, and the cognitive performance of IPS in healthy individuals based on multimodal MRI and neuropsychological evaluation.

- To investigate the activation and functional connectivity of the DMN regions in young, healthy controls during the performance of the SDMT task adapted for the BOLD-fMRI experiment.

- To evaluate the previous findings of cSVD effects using brain imaging performing a systematic review of the use of contrast-agent-free state-of-the-art MRI on cSVD, from the effects on brain connectivity to the clinical outcomes.

- To investigate the effects of WMH load and distribution patterns on cortical thickness, structural and functional connectivity, and LDST performance in cSVD patients and whether the association between lesion and IPS is mediated by brain connectivity and/or cortical thinning.

- To investigate WMH lesion anatomy that results in impaired IPS in cSVD patients without dementia using a lesion-symptom mapping approach.

3 Brain Structural–Functional Connectivity Relationship Underlying the Processing Speed

3.1 Introduction

Human cognition and behavior emerge from dynamic neuronal interactions on a brain structural architecture. Nevertheless, the convergence (or divergence) between dynamic functional connectivity (FC) and structural connectivity (SC) is still a pivotal and challenging question (4). The central hypothesis is that the anatomic architecture constrains the neural network dynamics, but does not determine it (46, 47).

Studies have found moderate to strong correlation between SC and FC measures obtained from multimodal magnetic resonance imaging (MRI) (48); others have inferred resting-state FC from SC, showing consistent results corroborating the hypothesis that structure influences, but does not determine brain function (48). The comprehension about the structure–function relationship is essential to clarify the normal neural mechanisms and provide biomarkers of the healthy aging process (49, 50), and the so-called disconnectivity syndromes (2), such as schizophrenia and dementia (51).

The structure–function relationship studies have relied on neuroimaging techniques such as multimodal MRI and sophisticated computational data modeling, with additional contributions from neuropsychological tests to provide information about cognition (4). SC describes the white matter connections between cortical regions and can be studied using diffusion tensor imaging (DTI) and diffusion spectrum imaging (10). DTI is an MRI technique that measures anisotropic diffusion of water molecules in tissues, providing useful structural information about the white matter, such as the orientation of the neural tracts (52).

Reconstruction of DTI includes model-based and model free methods. The model-free method, generalized q-sampling imaging (GQI), quantifies the density of diffusing water at different orientations, providing a spin distribution function. The GQI method was then generalized, originating the q-space diffeomorphic reconstruction method considering group analysis in a specific template space (53). The study of structure–function relationship using the GQI method is interesting once it presented the highest number of valid bundles in a worldwide competition concerning the human structural connectome mapping using diffusion tractography, which involved 96 distinct submissions from 20 research groups (54).

Regarding FC, we refer here to the interregional synchronization of low-frequency fluctuations in MRI signal based on the blood oxygenation level-dependent (BOLD) contrast (11). It correlates with spontaneous neural activity of a brain region through the neurovascular coupling and is thus considered to be physiologically significant (13).

BOLD contrast is based on the difference in magnetic susceptibility of hemoglobin molecules, which depends on their oxygenation state. When in the presence of a stimulus or task, neural activity occurs, causing local oxygen demand for energy production, which is supplied by the blood vessels through increasing local cerebral blood flow. As the increase is greater than the demand, there is a decrease in the oxygen extraction fraction, causing an increase in T2*-weighted MRI signal (14). As the BOLD signal comes from vessels larger than capillaries, there is low spatial specificity regarding the neuronal activity. In contrast, because of its sensitivity and temporal resolution, BOLD-MRI is useful in functional studies with or without tasks (15).

FC is of great value considering its biological basis and its description in terms of brain organization in functional networks. A functional network can be broadly defined as a set of brain regions that show consistent synchronous activity, with FC between two or more regions due to synchronization within or between networks. FC is also studied using the effective connectivity (EC) concept, a complementary approach that relies on the biophysics of context-sensitive neuronal mechanisms.

EC is defined as how one region influences or causes activity in another during the particular neural process (17). It can be modeled using dynamic causal modeling (DCM) that estimates and makes inferences over the neuronal coupling and its changes due to the controlled experimental disturbance (55). It uses a realistic coupled neurovascular model and estimates its parameters such as those from the bilinear neural state: the endogenous connectivity, the modulatory connectivity, and the driving inputs. DCM presents advantages over similar methods due to its more plausible generative model of measured brain responses, once it considers their nonlinear and dynamic nature (55).

In this context, we evaluated the brain functional integration in response to the execution of a cognitive task, the Symbol Digit Modalities Test (SDMT) (20), which evaluates information processing speed (IPS), adapted to the MRI environment (27, 23). IPS was chosen because several cognitive functions require sufficient speed for relevant operations to be performed within the allowed timeframe; delayed IPS usually underlies attention deficits (18). Therefore, we investigated the dynamics of the IPS functional network, its relationship with the structural network, and the cognitive performance of IPS in healthy individuals based on multimodal MRI and neuropsychological evaluation. We hypothesize that SC constrains but does not determine FC, and their relationship is closely related to IPS cognitive performance assessed by the SDMT.

3.2   Methods

Participants and cognitive evaluation

Fourteen right-handed Portuguese speakers, both genders (nine men, five women),

with a mean age of 28 – 7 years (range: 18–43 years), asymptomatic for neurological and psychiatric disorders, were recruited. The research ethics committee of the institution approved the study. Exclusion criteria were abuse of alcohol or illicit drugs verified by the CAGE questionnaire ([56]); sensory or motor problems that could interfere with task performance, verified by the 9-Hole Peg Test ([57]); previous experience with cognitive tests for 6 months; language other than Portuguese; psychiatric disorders; presence of partial or total carotid stenosis, unilateral or bilateral; presence of injury from stroke or brain tumor; MRI contraindications; claustrophobia; myopia; and pregnancy.

The cognitive evaluation was performed by a neuropsychologist or supervised trainee to investigate differences within the group. The oral and written versions of the SDMT (Lezak et al., 2012) were administered according to the manual instructions. In brief, the SDMT ([20]) presents a key of numbers paired with symbols, followed by rows of symbols to which the participant provides the correct numbers as rapidly as possible, orally (oSDMT) or written (wSDMT). The higher the SDMT score, the better the information processing speed performance.

Image acquisition

MRI was performed on a 3T system (Philips Achieva, The Netherlands), using a full-body transmission coil and a dedicated 32-channel head coil for signal reception. BOLD images were acquired using a 2D echo-planar imaging (EPI) sequence with the following parameters: time of repetition (TR)/time of echo (TE) = 2000/30 ms, flip angle = 80°, matrix = $80 \cdot 80$, field-of-view (FOV) = $240 \cdot 240$ mm² , number of slices = 31, slice thickness = 4 mm, gap between slices = 0.5 mm, number of repetitions = 165 (during task) and 200 (during resting state).

Diffusion-weighted imaging was acquired using a spin-echo sequence with EPI readout, and the following parameters: TR/TE = 9300/54 ms, pixel size = $2 \cdot 2$ mm², slice thickness = 2 mm, EPI factor = 67, FOV = $256 \cdot 256$ mm², acquisition matrix = $128 \cdot 128$ pixels, 60 slices, 33 diffusion gradients (32 with b = 1000 s/mm² and 1 with b = 0), and overplus = no. For anatomical reference, images were acquired using a T1-weighted gradient-echo sequence with the following parameters: TR/TE = 7/3 ms, flip angle = 8°, matrix = $240 \cdot 240$, FOV = $240 \cdot 240$ mm², number of slices = 160, and slice thickness = 1 mm.

SDMT task for fMRI

The block-designed paradigm consisted of five 30-sec blocks of task intercalated by six 30-sec blocks of control. The task was an adaptation of the SDMT test. As previously described, the participants should associate numbers with corresponding symbols based on a "response key." During each task block, a symbol was displayed every 2 sec, totaling 15 symbols per block. During control blocks, a number was displayed every 2 sec, totaling 15 numbers per

block, and the participant should silently read the displayed number (23).

The commands were developed in PsychoPy (58), and presented on a monitor positioned in front of the MRI machine. The participant viewed the monitor through a mirror system coupled to the head coil. Before image acquisition, all participants were instructed to perform the task inside the MRI environment. Details about the task adaptation are available in a previous study (23).

Image processing and analysis

Functional images. Functional image preprocessing was performed using the Statistical Parametric Mapping (SPM12), and included reorientation using the anterior commissure as reference point for the origin; slice time correction; realignment for correction of motion artifacts; coregistration with anatomical images; normalization to Montreal Neurological Institute (MNI) space; and spatial smoothing using a Gaussian filter (full width at half maximum = 6 mm).

Statistical parametric maps were obtained for each subject and the group, using the General Linear Model with a boxcar regressor convolved with a canonical hemodynamic response function (p-FDR < 0.01, cluster size [k] ≥ 50 voxels). Based on a previous meta-analysis (23) and the obtained activation maps, a task-related template was created using the WFU PickAtlas Toolbox (59), and included eight regions: left and right middle frontal gyri (MFG, Brodmann area [BA] 6), left superior parietal lobule (SPL, BA 7), left precuneus (BA 7), left inferior frontal gyrus (IFG, BA 9), right cuneus (BA 17), left lingual gyrus (BA 17), and left declive (portion of cerebellum). More details about the activation maps and the regions of interest were previously reported (23).

We used the CONN toolbox (60) to assess the FC among regions during task performance. First, to remove unwanted fluctuations in BOLD signal, we used motion correction residual and their first-time derivatives, global signals of white matter and cerebrospinal fluid, and finite impulse response task timing, as regressors (61). We performed a region of interest (ROI)-to-ROI analysis considering the task-related templates. A correlation matrix was obtained from the bivariate correlation between the time series of each ROI. Correlation values were considered significant for p < 0.05, corrected for false discovery rate (FDR).

We used the DCM12 implemented in SPM12 to assess EC and investigate the best network model considering task-positive regions. Task-related regions were inserted as nodes in three models for the EC analysis. The first model was created based on the FC analysis, considering bidirectional connections (top-down and bottom-up) and signal propagation from visual, through cognitive, up to motor regions. The second and third models considered only top-down and bottom-up connections, respectively, of the first model. For each node, we considered the principal component extracted from the set of time series of all voxels that

constitute each ROI. Intrinsic connections were considered within and between each region (node).

For DCM, we used parametric regressors for "all SDMT" contrast as a single input, and "SDMT minus control" contrast as a modulator of EC (62). The first regressor ("all SDMT minus implicit baseline") modeled nonspecific information-processing effects relative to baseline, whereas the second regressor ("SDMT minus control") modeled information-processing effects during SDMT performance. Such regressors were orthogonal to each other. We used Bayesian model selection (BMS) to choose the best model and obtain EC parameters (endogenous connections, modulations, and driving inputs). The BMS determines the most likely random effects model among a set of hypotheses about the mechanisms that generated the observed data considering between-subjects heterogeneity.

The model evidence or the probability that the data are explained by the model is approximated by the negative variational free energy as an optimal compromise between accuracy and complexity of a model and is used to compare among alternative models (63). The best model was chosen based on the expected probability and exceedance probability. The former represents the probability that a specific model generated the data of a randomly chosen subject, and the latter represents the probability that a model is more likely than the other models (64).

Endogenous and modulatory connectivity parameters of the winning model were correlated with the SC metrics, described later in the text (65, 66). The endogenous (forward and backward) and modulatory (backward) connectivity among regions are rates of change (in units of hertz) expressing what one region causes in others due to intrinsic and experimental conditions, respectively. If the value is positive, it is said that the connection is excitatory, with one region causing an increase in the activity of the other region; otherwise, the connection is inhibitory, with one region causing a suppression in the activity of the other region (67, 68).

Diffusion-weighted images. First, we performed eddy current and motion correction (69), and extracted the brain (70) of diffusion-weighted images using the FSL (71). Then, using DSI Studio, we reconstructed the images in the MNI space using q-space diffeomorphic reconstruction (53) to obtain the spin distribution function (65). A diffusion sampling length ratio of 1.25 was used. The restricted diffusion was quantified using restricted diffusion imaging (66) and a deterministic fiber tracking algorithm (72) was used with a quantitative anisotropy (QA) threshold of 0.0455 (73).

We performed a preliminary study to determine the best angular threshold setting that gives similar results as the tractography atlas (74), testing for 40°, 50°, 60°, 70°, and 80°. The step size was 0.5 mm. Then, the fiber trajectories were smoothed by averaging the propagation direction with a percentage of the previous one. The percentage was randomly selected from 0% to 95%. Tracks with a length <10 or >400 mm were discarded. A total of 106 seeds were

placed.

We calculated several SC metrics for each tract linking two cortical regions from task-related template: number, volume, and length of the tracts; fractional anisotropy (FA); axial (AD), radial (RD), and mean diffusivities (MD) in unit of 10^{-3}mm²/s; QA and normalized quantitative anisotropy (NQA); isotropic diffusion component (ISO); and density of restricted diffusion (RDI) and nonrestricted diffusion (nRDI) given a displacement distance ([65], [66]).

Statistics

Demographic variables, neuropsychological scores, and BOLD metrics were evaluated with the Shapiro–Wilk normality test ($p < 0.05$). Once they presented normal distribution, parametric Pearson's correlation was performed among the described structural, functional, and cognitive measures. Otherwise, we used the nonparametric Spearman correlation. Moreover, SC measures of each tract were obtained and correlated with EC measures from the respective cortical regions pair. Both SC and EC measures from each tract/associated cortical regions pair were correlated with both written and oral SDMT scores. We considered significant correlations at $p < 0.05$. We also used the Bonferroni's method to correct for multiple comparisons.

3.3   Results

Demography and neuropsychological evaluation

The sample consisted of 14 participants (5 women) with a mean age of 28 ± 7 years. Most of them (78.6%) had >12 years of education (17 ± 4 years). Mean scores of wSDMT and oSDMT were 55.6 – 7.71 and 59.2 – 12.1, respectively, which are consistent for cognitively healthy subjects.

Brain connectivity

The statistical parametric map for the whole group showed activations in all regions of the task-related template. Task-based FC patterns showed interactions among all regions of the network (Figure 1). Random effects BMS considering the three models and based on modulatory parameters showed that the top-down model (Figure 2, model 3) presented the highest expected probability (0.415) and exceedance probability (0.585).
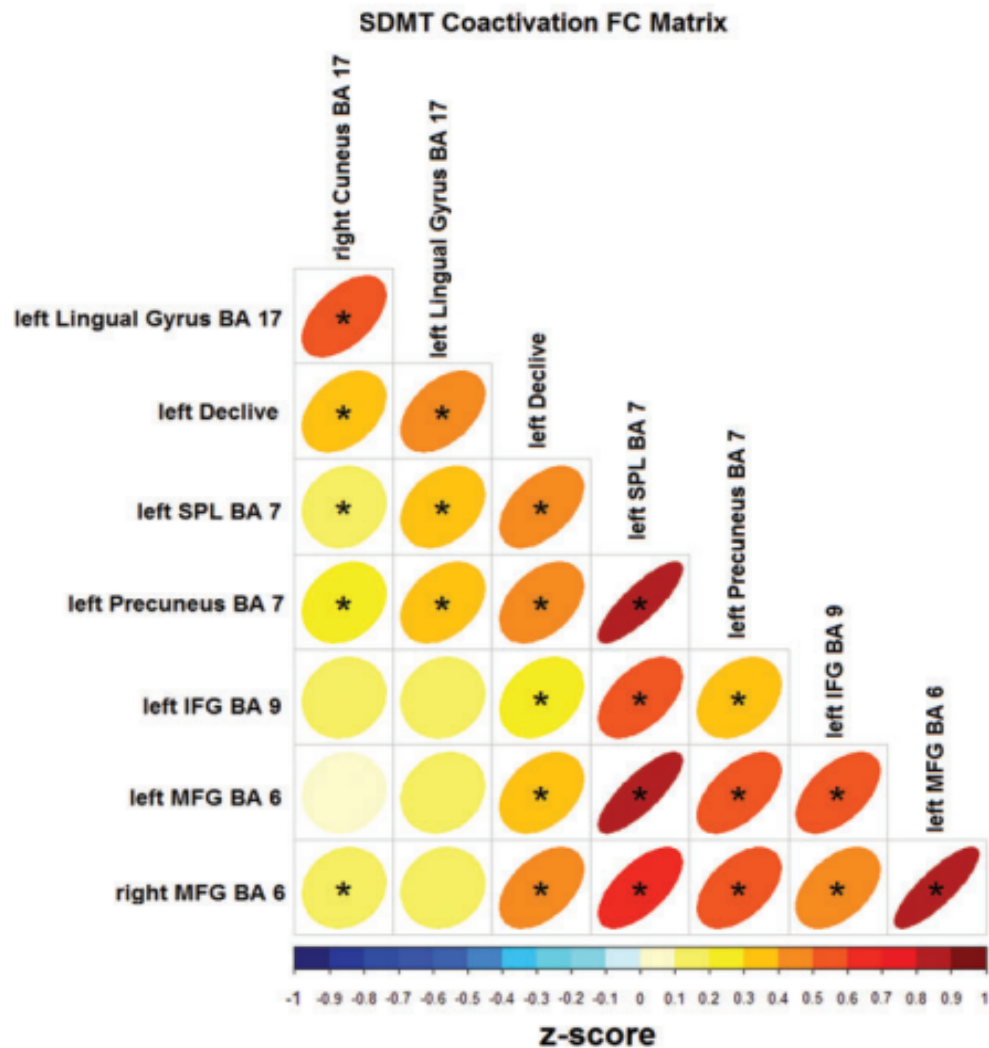
Figure 1 – Functional connectivity analysis using bivariate Pearson's correlation and task-related regions. SDMT coactivation matrix: the ellipsoid shape is related to the correlation strength; circles represent low correlation, whereas ellipses represent high correlation. Asterisks indicate significant correlations for p-FDR < 0.05. MFG, middle frontal gyrus; SDMT, Symbol Digit Modalities Test; SPL, superior parietal lobule.
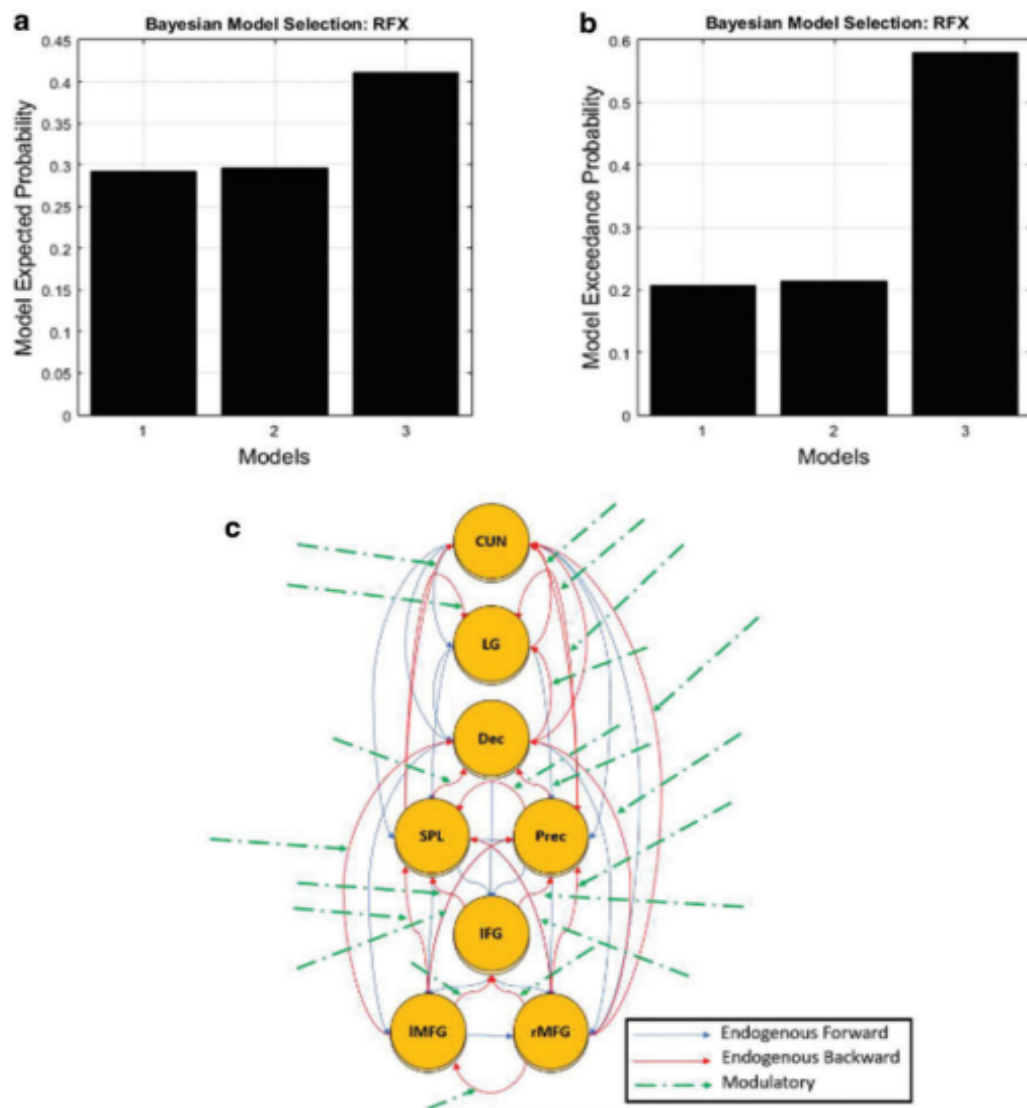
Figure 2 – Results of Bayesian model selection. Bar charts show the expected model probabilities (a) and exceedance probabilities (b) of bidirectional (1), bottom-up (2), and top-down (3) models. (c) The top-down model was the winner. BA, Brodmann area; Cun, right cuneus (BA 17); Dec, left declive; IFG, left inferior frontal gyrus (BA 9); lMFG, left middle frontal gyrus (BA 6); LG, left lingual gyrus (BA 17); Prec, left precuneus (BA 7); rMFG, right middle frontal gyrus (BA 6); SPL, left superior parietal lobule (BA 7).

For the structural analysis, we obtained the tracts from a preliminary study (Supplementary Table S1) using the HCP1021 tractography atlas to identify the fibers passing through every two ROI pairs from which task-based FC survived the FDR correction. All pairs of ROIs were connected by at least one tract, except for the left declive with the left IFG. Moreover, the corpus callosum tract connected most of the regions.

IPS structural and EC relationship

The correlations between SC and EC parameters showed significant associations involving interactions among 19 pairs of cortical regions. When considering only statistically significant associations after correcting for multiple comparisons, we mainly observed correlation of endogenous backward EC metrics with the tract length, MD, AD, and RDI from five cortical pairs (Table 1 and Figure 3). Moreover, most of these associations involved the precuneus or the declive.

IPS SC and SDMT performance relationship

When considering only statistically significant associations after correcting for multiple comparisons, we found negative correlations between the scores of the SDMT and diffusivity metrics of the corpus callosum connecting six pairs of cortical regions (Table 2 and Figure 4).

When considering associations without multiple comparisons and for $p < 0.05$, the correlations between SC parameters and cognitive scores showed significant associations involving interactions among 19 pairs of cortical regions. The associations presented a consistent pattern: tract's physical characteristics such as volume and number correlated positively with cognitive scores, whereas MD, RD, AD, and NQA presented negative associations with both oSDMT and wSDMT scores. It was not possible to identify a correlation pattern of FA and tract length with cognitive scores due to a similar number of positive and negative correlations.

IPS EC and SDMT performance relationship

We found only one significant association after correcting for multiple comparisons using a less restricted p-value ($p < 0.15$): endogenous backward connections between left declive and right cuneus correlated with oSDMT scores. However, when considering no correction for multiple comparisons, the correlations between EC parameters and cognitive scores showed significant associations involving interactions mainly among 6 of the 22 pairs of cortical regions: right cuneus with left declive, left precuneus, and right MFG, and left lingual gyrus with left SPL. The corpus callosum tract appeared in five connections. Modulatory connections showed mainly positive associations with both scores, whereas endogenous connections correlated mainly negatively with cognitive scores.
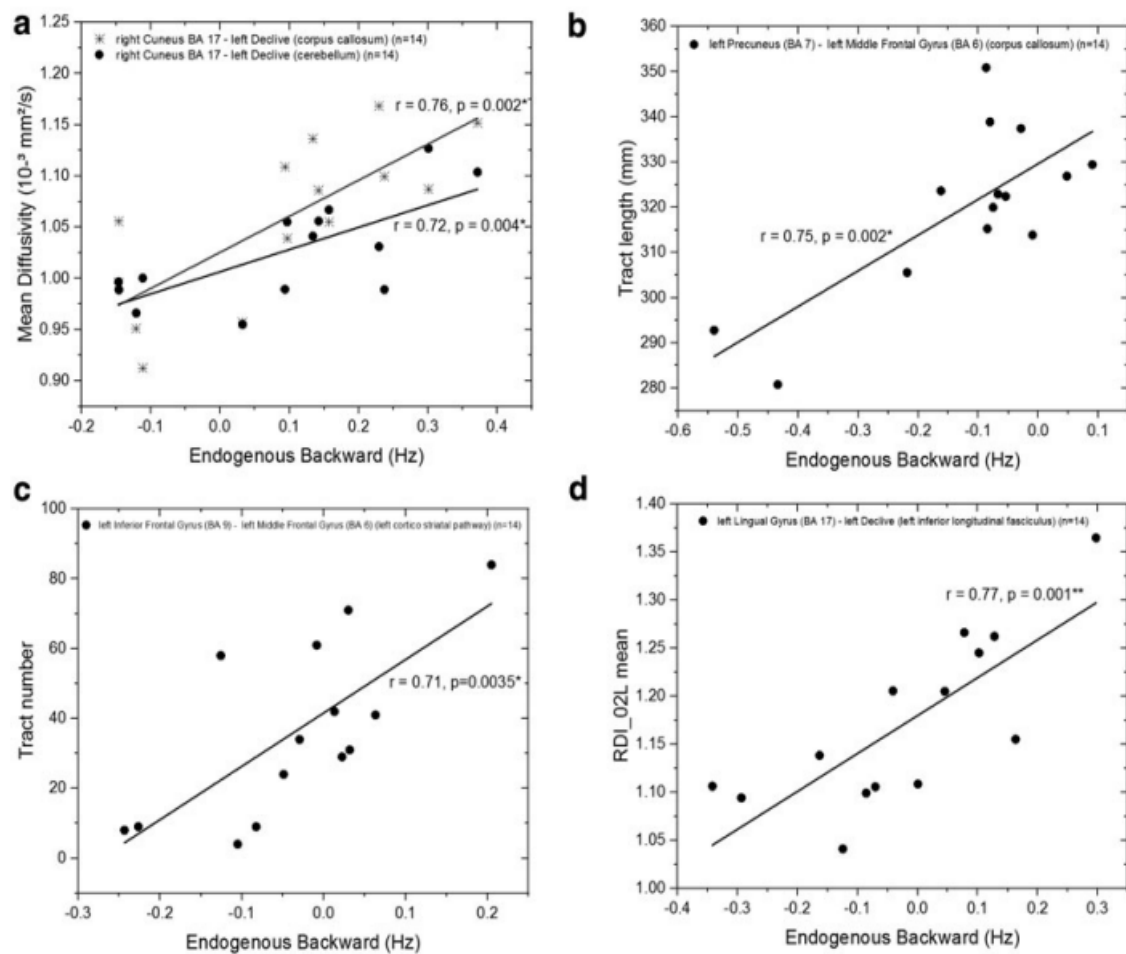
Figure 3 – Associations between (a) mean diffusivity and endogenous backward measures of the right cuneus (BA 17) and left declive considering the corpus callosum and cerebellum tracts, (b) tract length and endogenous backward measures of the left precuneus BA (7) and left middle frontal gyrus (BA 6) considering the corpus callosum tract, (c) tract number and endogenous backward measures of the left inferior frontal gyrus (BA 9) and left middle frontal gyrus (BA 6), considering the left corticostriatal pathway tract, and (d) RDI_02L mean and endogenous backward measures of the left lingual gyrus (BA 17) and left declive considering the left inferior longitudinal fasciculus. Cortical pairs, their related tract, sample number, r and p-values are shown. *Is statistically significant at $p < 0.1$ after multiple comparison correction using the Bonferroni method. **Is statistically significant at $p < 0.05$ after multiple comparison correction using Bonferroni method.

Structural–functional connectivity relationship underlying IPS performance

When considering only statistically significant associations after correcting for multiple comparisons, the following structural–functional significant relationship was associated with oSDMT performance: endogenous backward connections between left declive and right cuneus correlated with AD measurement of corpus callosum tract (5a).

When considering associations without such a correction, the following structural–functional

Table 1 – Correlations Between Structural and Effective Connectivity Measures. AD, axial diffusivity; BA, Brodmann area; FA, fractional anisotropy; ISO, isotropic diffusion component; MD, mean diffusivity; nRDI, density of nonrestricted diffusion in a displacement L; r, Pearson correlation coefficient; RDI, density of restricted diffusion; q, Spearman correlation coefficient. *Statistically significant at p < 0.1 after multiple comparison correction using Bonferroni method.

Cortical Regions Pair	Tracts	Effective connectivity parameters	Structural Connectivity Measures (Statistics)
right Cuneus (BA 17) - left Declive	corpus callosum	Endogenous Backward	MD (r = 0.76, p = 0.002)[1] AD (r = 0.73, p = 0.003)[1]
left Lingual Gyrus (BA 17) - left Declive	cerebellum	Endogenous Backward	MD (r = 0.72, p = 0.004)[1]
	left inferior longitudinal fasciculus	Endogenous Backward	RDI_02 (r = 0.77, p = 0.001)[2] RDI_04 (r = 0.77, p = 0.001)[2] RDI_06 (r = 0.77, p = 0.001)[2] RDI_08 (r = 0.77, p = 0.001)[2] RDI_10 (r = 0.77, p = 0.001)[2] RDI_12 (r = 0.77, p = 0.001)[2] nRDI_02 (r = 0.77, p = 0.001)[2] nRDI_04 (r = 0.77, p = 0.001)[2] nRDI_06 (r = 0.77, p = 0.001)[2]
	corpus callosum	Endogenous Backward	RDI_02 (r = 0.71, p = 0.004)[1] RDI_04 (r = 0.71, p = 0.004)[1] RDI_06 (r = 0.71, p = 0.004)[1] ISO (r = 0.72, p = 0.003)[1]
	left cerebellum	Endogenous Backward	RDI_02 (r = 0.73, p = 0.003)[1] RDI_04 (r = 0.73, p = 0.003)[1] RDI_06 (r = 0.73, p = 0.003)[1] RDI_08 (r = 0.73, p = 0.003)[1] RDI_10 (r = 0.73, p = 0.003)[1] RDI_12 (r = 0.73, p = 0.003)[1] nRDI_02 (r = 0.73, p = 0.003)[1] nRDI_04 (r = 0.72, p = 0.003)[1]
left Precuneus (BA 7) - left Inferior Frontal Gyrus (BA 9)	left u fiber (n = 8)	Endogenous Forward	ISO (ρ = 0.90, p = 0.002)[2] RDI_02 (ρ = 0.90, p = 0.002)[2] RDI_04 (ρ = 0.90, p = 0.002)[2] RDI_06 (ρ = 0.90, p = 0.002)[2] RDI_08 (ρ = 0.90, p = 0.002)[2] RDI_10 (ρ = 0.90, p = 0.002)[2] RDI_12 (ρ = 0.90, p = 0.002)[2] nRDI_02 (ρ = 0.90, p = 0.002)[2] nRDI_04 (ρ = 0.90, p = 0.002)[2] nRDI_06 (ρ = 0.95, p = 0.000)[2]
left Precuneus (BA 7) - left Middle Frontal Gyrus (BA 6)	corpus callosum	Endogenous Backward	Tract length (r = 0.75, p = 0.002)[2]
left Inferior Frontal Gyrus (BA 9) - left Middle Frontal Gyrus (BA 6)	left cortico striatal pathway	Endogenous Backward	Tract number (r = 0.71, p = 0.0035)[2]

[1] Statistically significant at p < 0.1 after multiple comparison correction using Bonferroni method.
[2] Statistically significant at p < 0.05 after multiple comparison correction using Bonferroni method..

significant relationships were associated with oSDMT performance: endogenous backward connections between left declive and right cuneus correlated with MD and AD measures of corpus callosum tract (5a), and MD, AD, and RD values of right u fiber tract (5b); endogenous forward connectivity between right cuneus and left precuneus correlated with AD and RD measures of corpus callosum (5c); modulatory connectivity values between right cuneus and left precuneus correlated with RD values of right cingulum tract (5d). Moreover, the correlation of the endogenous forward connectivity between right cuneus and left precuneus with
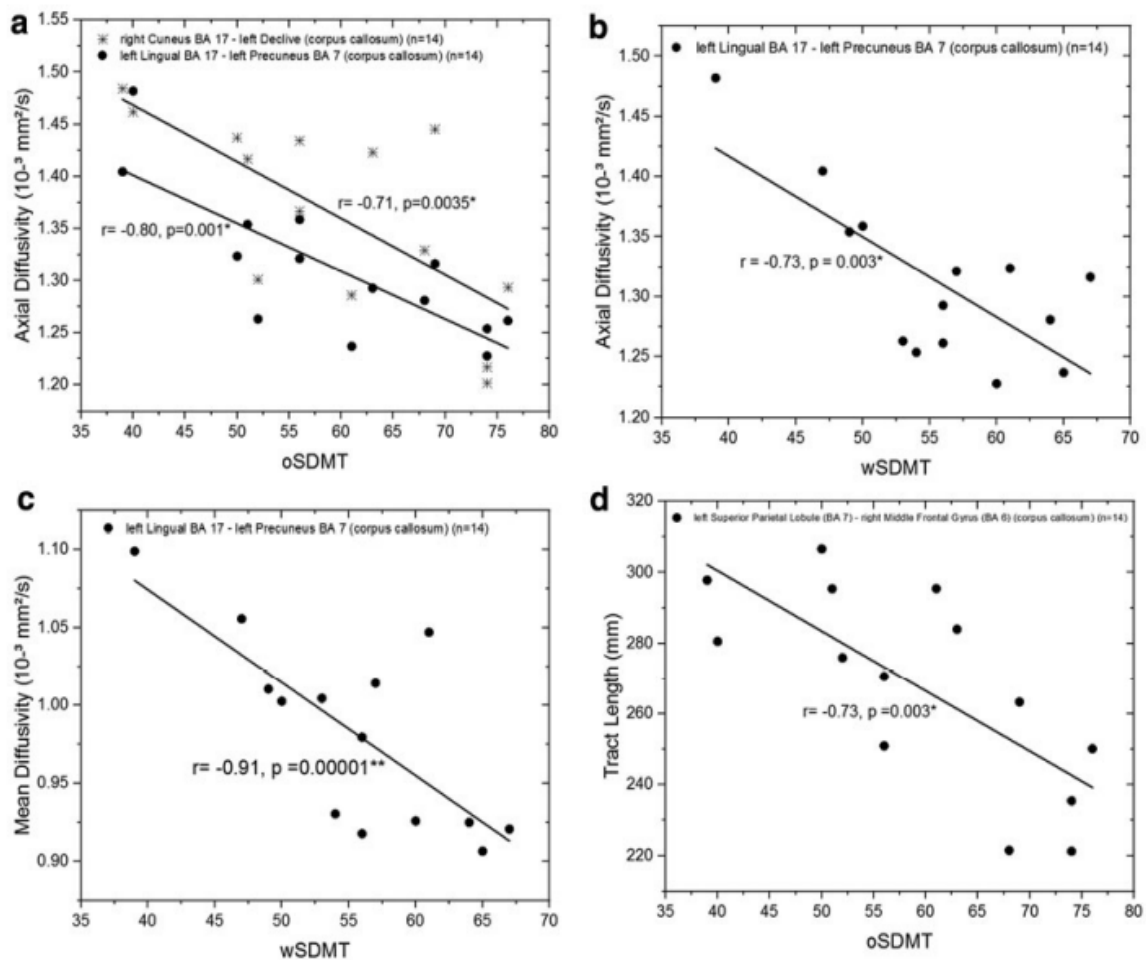
Figure 4 – Associations between (a) axial diffusivity and oSDMT scores, (b) axial diffusivity and wSDMT scores, (c) mean diffusivity and wSDMT scores, and (d) tract length and oSDMT scores. Cortical pairs, their related tract, sample number, r, and p-values are shown. o, oral; w, written.

AD measures of the corpus callosum tract (5a), and right u fiber tract (5a), showed significant association with the wSDMT performance.

3.4   Discussion

We investigated the dynamics of functional networks in response to the execution of an MRI-adapted cognitive task (SDMT), which evaluates IPS, their relationship with structural networks, and cognitive performance in healthy individuals, based on empirical data obtained from multimodal MRI and neuropsychological evaluation.

The dynamics of functional networks were studied using BOLD-fMRI data and DCM, which allows specifying models of EC among selected brain areas, to estimate their parameters (endogenous and modulatory connections) and compare hypotheses (67). Our winning model among the tested hypotheses was the one with top-down modulations. Top-down

Table 2 – Correlations Between Structural Connectivity Measures and SDMT. o, oral; RD, radial diffusivity; SDMT, Symbol Digit Modalities Test; w, written.

Cortical Regions Pair	Tracts	Neuropsychological measures	Structural Connectivity Measures (Statistics)
right Cuneus (BA 17) - left Declive	corpus callosum	oSDMT	AD (r = -0.71, p = 0.0035)[1]
left Lingual Gyrus (BA 17) - left Declive	vermis	wSDMT	FA (r = 0.77, p = 0.002)[1]
left Lingual Gyrus (BA 17) - left Precuneus (BA 7)	corpus callosum	oSDMT	MD (r = -0.91, p = 0.000)[2] AD (r = -0.80, p = 0.001)[2] RD (r = -0.86, p = 0.000)[2]
left Declive - left Superior Parietal Lobule (BA 7)	middle cerebellar peduncle (n=9)	wSDMT	MD (r = -0.75, p = 0.002)[1] AD (r = -0.73, p = 0.003)[1]
		wSDMT	Tract volume (ρ = 0.93, p = 0.000)[2]
left Superior Parietal Lobule (BA 7) - right Middle Frontal Gyrus (BA 6)	corpus callosum	oSDMT	Tract length (r = -0.73, p = 0.003)[1]
left Inferior Frontal Gyrus (BA 9) - right Middle Frontal Gyrus (BA 6)	corpus callosum (n =10)	wSDMT	MD (r = -0.86, p = 0.001)[2] RD (r = -0.88, p = 0.001)[2]

[1] Statistically significant at p < 0.1 after multiple comparison correction using Bonferroni method.
[2] Statistically significant at p < 0.05 after multiple comparison correction using Bonferroni method..

visual attention is described as a voluntary process that selects internally and focuses upon a particular thing of interest (29), as the association between the symbols and the number in the SDMT task. Studies suggest that the prefrontal cortex and areas in the posterior parietal cortex are the source regions related to not only the top-down process but also the bottom-up process (75).

The top-down and bottom-up processes have been widely considered as two systems responsible for attentional demands, both being critical for efficient information processing (76). It can be the reason behind the considerable exceedance probability involving bottom-up and bidirectional models, even if the top-down model was the dominant one in our study. Moreover, intersubject variability regarding strategies to achieve goal-directed behavior may explain that result.

Our results about the IPS structural and EC relationship show a positive association between the diffusion parameters and tract features between two cortical regions and the effects on endogenous connections across these regions. On the contrary, lower diffusivity parameters and lower tract characteristics tend to cause inhibitory effects in intrinsic connections. As an exploratory analysis, results suggest a step further in the understanding of structure–function relationship. As diffusivity and tracts features decrease, both the excitatory additive changes in endogenous connections and the inhibitory influences in intrinsic connections among regions increase. This is due to the modulation impinged by the experimental conditions.

Different methodologies were previously used to assess SC and its relationship with
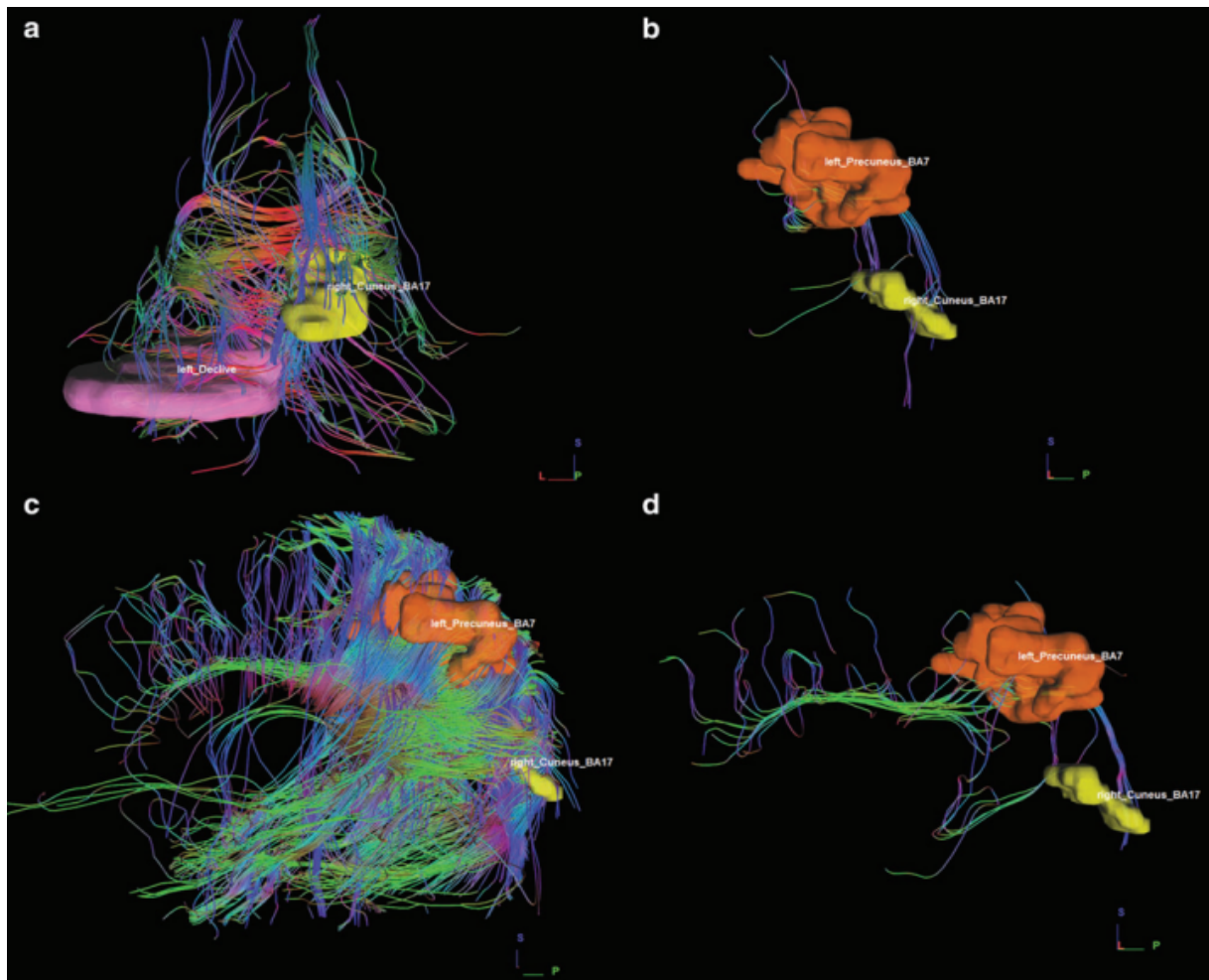
Figure 5 – Individual deterministic tractography results regarding structural–functional correlates related to SDMT performance. (a) Corpus callosum tract crossing right cuneus (BA 17) and left precuneus (BA 7), (b) right u fiber tract crossing right cuneus (BA 17) and left precuneus (BA 7), (c) corpus callosum tract crossing right cuneus (BA 17) and left declive and (d) right cingulum tract crossing right cuneus (BA 17) and left precuneus (BA 7). Anatomical masks of the right cuneus (yellow), left precuneus (orange), and left declive (pink) are represented. Tracts' colors represent their directionality. L, lateral; P, posterior; S, superior.

function and cognition. Huang and Ding (77) reported that conditional Granger causality (GC) correlated significantly with the weight of the edges of the structural network, suggesting that observed using metrics obtained from deterministic tractography within resting-state networks, although no convergence with resting-state FC changes was found (78). Resting-state FC was shown to be constrained by the large-scale anatomical structure using fiber counts among 66 cortical regions (48).

Graph analysis using fiber bundles FA, MD, AD, and RD connectivity matrices showed that children with the highest intellectual abilities present strong inter- and intrahemispheric white matter integrity (79). In our study, we considered DCM as the measure of EC, which is complementary to the GC (80). GC characterizes EC with a generic inferential approach,

whereas DCM focuses on specific models previously selected, describing hidden dynamics from observations. Our choice relies on the fact that DCM englobes a biologically plausible background (81), providing a more reliable interpretation of our results. Concerning the structural measures, we decided to evaluate diffusion parameters with neurobiological background and wide application in clinical studies.

Moreover, our study provides a methodology wherein SC analysis is performed between cortical regions related to the performance of a cognitive task, assessed by the statistical parametric map (in opposition to the inclusion of all cortical regions or fiber bundles from atlas) and inserted in functional and EC analysis of task-based data (in contraposition to the usual resting-state data). Although some studies reported associations between structure and function and others between structure and cognition, we were able to identify associations among structure–function–cognition, providing a more complete method of analysis of such a challenging question.

Moreover, recent studies have reported altered measures of SC, such as MD, RD, and AD in different diseases. Increased MD, RD, and AD values were found when comparing progressive supranuclear palsy–Richardson's syndrome patients with Parkinson's disease patients, conditions with complicated diagnostic accuracy due to its similar clinical symptoms (82). Another study stated that MD is an essential correlate of cognition and predictor of motor impairment in Parkinson's disease, allowing its stratification (83).

Higher MD in specific white matter regions was significantly correlated with Alzheimer's disease stage, clinical severity (84), and preceding dementia symptoms (85). RD correlated positively with worse sleep quality scores, whereas both MD and RD were associated with increased depressive symptoms in individuals with mild traumatic brain injuries when compared with healthy controls (86). Higher MD values also correlated with aging (78). Therefore, once MD, RD, and AD correlated significantly with both functional and cognitive measures in our healthy group and presented associations with various conditions reported in recent publications even with various methodologies, we suggest that the methodology we used can be a useful tool to investigate diseases that presents alterations in diffusivity measures.

Notably, both diffusivity measurements (such as MD, AD, and RD) and density measurements (such as QA, ISO, RDI, and nRDI), and tract features (tract volume and length) correlated significantly with EC metrics and cognitive score. Diffusivity measurements are more sensitive to identify pathological conditions, whereas density measurements are better to detect individual and physiological differences (53). In clinical applications, it can be useful to detect the structural intactness using the diffusivity measurements and to evaluate the SC using density measurements, once the latter quantifies the total amount of diffusing water (53).

Regarding the structural–functional connectivity correlates of IPS performance, we found associations related to the connection between the right cuneus, left precuneus, and left

declive. It was previously shown that the posterior part of precuneus has strong connections with the cuneus, related to visual information processing (87). In addition, the precuneus is considered "pivotal for conscious information processing" (88), once its disruption has been linked to impaired consciousness pathophysiological conditions such as vegetative state, Alzheimer's disease, and schizophrenia (88).

It was also shown that the posterior lobe of the cerebellum is responsible for visual perceptual learning (89). The visual information processing requires coordinated processing in time to enable appropriate behavior. Once the categorization of visual images is related to many stages, it can be affected by any of the processing stages (90). Then, perceptual learning can improve visual processing speed, and due to the many stages of processing, it can also improve nontrained visual functions. Our findings suggest the importance of such areas in IPS performance, suggesting that interindividual variability in SDMT scores can be related to the structural–functional connectivity differences.

Despite the interesting findings, our study also has some limitations. Regarding our sample size (n = 14), it was reported that in DCM studies, the number of subjects required for a study to observe the effect of interest is similar for detecting group activation in fMRI studies (91), with 12 volunteers providing 80% of power (92). In addition, different DCM models and nodes can be tested to address individual variability and clinical groups. More specifically, due to brain changes in clinical conditions, other ROIs can be part of the IPS network to perform the task. Such changes must be considered to get more reliable EC parameters. Finally, confounders such as age and gender can also be included in future analyses to find stronger associations.

It is also important to note that our hypothesis is broad and encompasses a challenging question in neurosciences, that is, the relationship between brain function and cognition and its underlying structure. In this exploratory study, we also considered results without correcting for multiple comparisons. As reported before, in cases of confirmatory studies, which can cause a change in clinical practice or approval of a new treatment, it is more important to guard against the possibility of false-positive results. In the case of exploratory studies or post-hoc analysis of existing data, a strict adjustment for multiple comparisons is less critical. Then, we also considered no correction for multiple comparisons to explore the results. However, we also added the findings that survived such a correction to assess which parameters best fit our general hypothesis.

Increasing the number of subjects, applying to different cognitive domains, and in clinical groups are the next steps to make our results well grounded and allow the asking for more precise hypotheses.

3.5   Conclusion

Our findings suggest that IPS functional network is related to the highest SDMT scores when its effective endogenous connections are suppressed to the detriment of modulation caused by the experimental conditions, with the underlying structure providing low diffusivity (as measured by MD, RD and AD) and density diffusion (as measured by NQA) environments. Therefore, IPS SC network constrains but does not determine IPS FC network, and both are related to the SDMT performance. Moreover, the use of neuroimaging techniques such as multimodal MRI, sophisticated computational data modeling with increasingly plausible neurobiological background, and neuropsychological tests seems to be useful to provide more reliable and robust information about the structure–function–cognition relationship assessed by cognitive tasks.

This study was already published (93).

4 Non-classical behavior of the Default Mode Network (DMN) regions during an Information Processing task

4.1 Introduction

The human brain at rest, when mind-wandering, shows patterns of connectivity among distinct brain regions that seem to reflect intrinsic characteristics of neural organization (94). In such a context, the behavior of the Default Mode Network (DMN) has aroused interest, including its association with cognition and regulation of attention (95). The four DMN nodes are the precuneus/posterior cingulate cortex (PCC), the medial prefrontal cortex (mPFC), and left and right lateral parietal (LP) lobules (60). This network shows higher activation at rest and deactivation during the performance of goal-directed tasks, where behavior is oriented toward achieving a particular goal and requires the focus and selection of relevant information in the scenario (96). However, despite the consensus on the antagonistic role of the DMN during task performance, recent studies have shown the opposite behavior in some cases, with regions of the network possibly exhibiting different connectivity patterns from and into the network as a whole (87, 97, 94, 98, 99, 100).

One of the four regions of the DMN functional template – the DMN-PCC node - comprises portions of the PCC and precuneus in a single area (60, 94). While many studies considered the DMN-PCC node as an indivisible structure (101, 102, 103, 104), studies have shown structural and functional differences within this region (87, 105). Leech et al. reported that the DMN-PCC is considered the functional core of the DMN, but presents different connectivity pattern from the whole network. The dorsal portion of this region showed connectivity with both DMN and task-positive networks at rest. However, as task difficulty increases, its ventral and dorsal portions present opposite behaviors from the entire DMN (97). Increased activation in such a region has also been reported during emotional stimulus processing (106), autobiographical memory retrieval (107), and reward outcome (108).

Moreover, although the precuneus has presented a high rate of metabolism during the resting state (109), it has shown connectivity patterns involving higher association regions, suggesting an essential role in integrating both internally and externally driven information (88). Considered as a region separated from the DMN-PCC node, the precuneus has shown a positive association with an Information Processing Speed (IPS) task (27), the same used in the present study. Besides, the angular gyrus, included in the DMN-LP node, is also involved in different tasks such as visuospatial perception (110), visuospatial attention decision making (111), imagined music performance (112), and semantic processing (113). Different functional properties were also expressed in the left and right angular gyrus (114). Such results suggest that the DMN regions have important multimodal cognitive roles, functional activation, and

connectivity patterns. However, there is no consensus about what such roles and patterns are.

IPS is an individual cognitive ability defined as "the amount of time required to process a set of information or the amount of information that can be processed in a certain unit of time" (19). IPS-related deficits are present in several clinical and neurological diseases (115, 116, 117, 118, 26, 119, 120, 121). Therefore, the integrity of brain regions and their functional connections are essential for this cognitive function. The Symbol Digit Modalities Test (SDMT), a screening neuropsychology tool created by Smith (20), is the gold-standard to assess IPS. Due to the consensus over its easy application, shorter time, low cost, and not exhausting for the patient (122, 22, 123), the SDMT has been used to study IPS deficits in a variety of clinical and neurological conditions, including traumatic brain injury (TBI) in adults (116, 118), Alzheimer's disease (117), Parkinson's disease (119), Huntington's disease (115), small vessel disease (120), depression (121), and multiple sclerosis (MS) (26).

Beyond its presence and severity evaluated by a neuropsychological test, IPS impairment should be assessed regarding its brain function network. In this context, the functional Magnetic Resonance Imaging (fMRI) based on the blood oxygenation level-dependent contrast (BOLD-fMRI) is a preferable technique due to its non-invasive nature and a reasonable level of reliability (124). A recent meta-analysis reported that the bilateral middle frontal gyri (Brodmann Area (BA) 6,) left inferior frontal gyrus (BA 9), left declive (cerebellum portion), left superior parietal lobule (BA 7), right cuneus (BA 17), left lingual gyrus (BA 17), and left precuneus (BA 7) are related to the performance of an adapted version of the SDMT inside the MRI scanner (23). The four DMN nodes were also associated with SDMT task performance within the MRI environment (27).

Optimal DMN suppression during tasks demanding external focus, such as the IPS, has been considered essential for healthy cognition (96). However, DMN regions have shown distinct connectivity patterns during goal-directed tasks. Therefore, we investigated the activation and functional connectivity of the DMN regions in young, healthy controls during the performance of the SDMT task adapted for the BOLD-fMRI experiment.

4.2   Methods

Participants

Twenty-four right-handed volunteers, mean age of 29 ± 7 years (14 men, 21-43 years; 10 women, 18-35 years), native Portuguese speakers, both genders, minimum age of 18 years, asymptomatic for neurological and psychiatric disorders, were recruited. The Research Ethics Committees of the Faculty of Philosophy, Sciences, and Letters of Ribeirao Preto (FFCLRP), and the Clinical Hospital, both of the University of Sao Paulo, have approved the study. Written informed consent was obtained from all participants before their participation. Exclusion criteria included abuse of alcohol or illicit drugs verified by the CAGE questionnaire (O'Brien,

2008); sensory or motor problems, confirmed by the 9-HPT ([57]); previous experience with cognitive tests for six months; language other than Portuguese; psychiatric disorders; the presence of partial or total carotid stenosis, unilateral or bilateral; the presence of injury from stroke or brain tumor; magnetic resonance imaging (MRI) contraindications; claustrophobia; and myopia.

Cognitive evaluation

A neuropsychologist performed the cognitive assessment. The oral and written versions of the SDMT were applied according to the manual instructions. In brief, the SDMT presents a key of numbers paired with symbols, followed by rows of symbols to which the participant provides the correspondent numbers as rapidly as possible, orally (oSDMT) or written (wSDMT) ([20], [122]). The higher the SDMT score, the better the information processing speed performance.

Image acquisition

MRI was performed on a 3T system, using a full-body transmission coil and a dedicated 32-channel head coil for signal reception. BOLD images were acquired using a 2D EPI sequence with the following parameters: TR/TE = 2000/30 ms, flip angle = 80°, matrix = 80 x 80, FOV = 240 x 240 mm2, number of slices = 31, slice thickness = 4 mm, gap between slices = 0.5 mm, number of repetitions = 165 (during task) and 200 (during resting state). For anatomical reference, images were acquired using a T1-weighted gradient-echo sequence with the following parameters: TR/TE = 7/3 ms, flip angle = 8°, matrix = 240 x 240, FOV = 240 x 240 mm2, number of slices = 160, slice thickness = 1mm. Pads were used next to the patients' heads to add comfort and reduce movement.

We acquired both task-based (section SDMT task for fMRI) and resting-state fMRI (section Resting-state fMRI) data. Task-based data was used in both functional localization and connectivity analysis. Resting-state data was used to compare with task condition in functional connectivity analysis to isolate better FC effects specific to the task-state since there is evidence that the spontaneous covariance present during the resting-state is also present during the performance of a task ([61]).

SDMT task for fMRI

The block-designed paradigm consisted of five blocks of task performance (30 seconds each) intercalated by six blocks of control (30 seconds each). The task was an adaptation of the SDMT test, as previously described ([23]). Briefly, during each task block, a symbol was displayed every 2 seconds, totaling 15 symbols per block, and the participants should mentally associate the numbers with the corresponding symbols based on a response key. During control blocks, a number was displayed every 2 seconds, totaling 15 numbers per block,

and the participant should silently read the displayed number. The stimuli were designed using PsychoPy ([58](#)) and presented on a monitor positioned in front of the MRI machine. The participant viewed the monitor through a mirror system coupled to the head coil.

Resting-state fMRI

During the resting-state (RS) acquisition, participants were asked to stay still with their eyes fixed on a cross and in the absence of any specific thought or intention. The acquisition occurred before the task-based scan and lasted 6 minutes and 40 seconds.

Image preprocessing

Image preprocessing was performed using the Statistical Parametric Mapping software SPM12 <www.fil.ion.ucl.ac.uk/spm/>. The procedure for BOLD-based images included reorientation using the anterior commissure as the origin; slice time correction; realignment to account for head movement during acquisition using a six-parameter (rigid body) spatial transformation ([125](#)); and co-registration with anatomical images. T1-weighted images were segmented into gray matter (GM), white matter (WM), and cerebrospinal fluid (CSF) ([126](#)). Functional and structural images were normalized to the standard Montreal Neurological Institute (MNI) space. Finally, fMRI images were smoothed using a Gaussian filter (FWHM = 6 mm).

For quality control for head motion during fMRI acquisition, we calculated frame-wise displacement (FD), mean FD, and the root mean squared (RMS) values of the realignment estimates ([127](#), [128](#)). FD provides an index for head movement from one volume to the next and is calculated as the sum of the absolute values of the differentiated realignment estimates at every timepoint. We used a MATLAB code from the BRAMILA pipeline v2.0 to calculate both FD and RMS (available at <https://git.becs.aalto.fi/bml/bramila/>). We adopted the threshold of maximum FD of 2mm or 2° ([129](#)), mean FD of 0.5mm or 0.5°, and RMS movement of 0.5 mm or 0.5°. Subjects with any acquisition exceeding these thresholds were removed from the analysis.

Functional localization

A statistical parametric map was obtained for the group using a one-sample t-test General Linear Model (GLM) with a boxcar regressor convolved with a canonical hemodynamic response function. The contrast images of task versus control were used as dependent variables. The group-level analysis considered a voxelwise threshold of two-sided p = 0.001 (Chen et al., 2019), with 23 degrees of freedom and false discovery rate (FDR) = 10%. The obtained map was masked using the SDMT task-positive templates of a previous meta-analysis ([23](#)), and the DMN and posterior cingulate gyrus (PCG) templates of the CONN Harvard-Oxford functional atlas ([60](#)). Once we were interested specifically in DMN nodes, we searched

for the peak coordinates of the clusters when masking T maps with each DMN template. If clusters were remaining under the reported statistical threshold, we reported the anatomical composition of the clusters in percentage values. SPM12 software provided this information.

The task-positive templates were obtained with the WFU PickAtlas Toolbox ([59]) for each of the following regions: left and right middle frontal gyri (l and r MFG, BA 6), left superior parietal lobule (l SPL, BA 7), left precuneus (l Prec, BA 7), left inferior frontal gyrus (l IFG, BA 9), right cuneus (r cuneus, BA 17), left lingual gyrus (l lingual gyrus, BA 17) and left declive (part of the cerebellum). The Human Atlas (AAL atlas), included in the SPM "WFU-PickAtlas" toolbox, was used in the present study to define the task-positive templates. The coordinates were in MNI space ([130]). The DMN template provided by the CONN toolbox included the medial prefrontal cortex (mPFC) (1, 55, -3), left lateral parietal lobule (-39, -77, 33), right lateral parietal lobule (47, -67, 29), and posterior cingulate cortex (1, -61, 38). We used the same terminology in the present study. This template was obtained using the independent component analysis (ICA) of 497 subjects from the HCP dataset ([131]). In our study, the DMN-PCC node contains portions of the left precuneus (BA 7), a task-positive region, and PCG. The PCG is the most ventral part of the DMN-PCC node.

Functional connectivity analysis

We used the CONN toolbox <www.nitrc.org/projects/conn,RRID:SCR_009550> to assess FC among brain regions during RS and task performance. Based on the SPM results, for both conditions, the templates of the task-positive network obtained from the previous meta-analysis (Silva et al., 2018), the DMN template, except for the DMN-PCC node, and the PCG template were used as regions of interest (ROIs). The CONN toolbox provided DMN and PCG templates. Time courses from the mentioned ROIs were extracted. Then, to remove unwanted fluctuations in the time courses, the motion correction residual and their first-time derivatives, global signals of white matter and cerebrospinal fluid, and task timings and its first-time derivatives were used as regressors. The finite impulse response (FIR) regression was applied to the task time-series to reduce spurious correlations ([61]), using customized MATLAB scripts. The FIR regression consists of fitting the cross-trial/cross-block mean response for each time point in a set window length that is time-locked to the trial/block onset for a given task condition. Each of the task blocks was fitted with a series of regressors, one per time point. Each condition window length matched the duration of the event with an additional 18s (9 regressors) to account for the likely duration of the HRF ([61]).

Then, we performed ROI-to-ROI analyses for both RS and task conditions using the templates mentioned above (task-related regions and DMN nodes). A correlation matrix was obtained from the bivariate Pearson's correlation between the time series of each ROI. Inferences about individual connections were made using the standard Benjamini and Hochberg's FDR algorithm ([132]) to compute a connection-level FDR-corrected p-value for each connec-

tion (between all pairs of ROIs). As performed in recent studies, we considered a connection-level p-FDR < 0.05 threshold to select significant connections (with larger effects than what we could reasonably expect under the null hypothesis) (133, 134, 135, 136, 137).

We also compared ROI-to-ROI FC between RS and task conditions using paired t-tests (p-FDR < 0.05). This analysis was performed to isolate better FC effects specific to the task-state since there is evidence that the spontaneous covariance present at rest is also present during the performance of a task (61).

4.3   Results

Demographic Variables and SDMT Scores

No participant was excluded due to head motion, so the group consisted of 24 participants with a mean age of 29 ± 7 years (14 men, 21-43 years; 10 women, 18-35 years). Most of them (79.2%) had more than 12 years of education (16 ± 4 years). Mean scores of wSDMT and oSDMT were 56.62 ± 7.18 and 60.17 ± 11.11, respectively, which are consistent for cognitively healthy subjects.

Statistical Parametric Mapping

Statistical parametric maps for the group showed activations in all regions of the task-related template for the task > control contrast (Figure 6A). The left DMN-LP and DMN-PCC presented voxel with positive and negative values in the task > control contrast (Figure 6A).

Considering the positive values of the task > control contrast, the PCC node (Figure 7A; peak activation at 6, -40, 48 mm, MNI coordinates) comprised the right precuneus (56%), not-labeled voxels (14.5%), left precuneus (12.2%), right cerebral white matter (10.7%), right superior parietal lobule (6.5%) and right cuneus (0.2%). For the DMN contrast, the PCC node (Figure 7A; peak activation at -6, -54, 26, MNI coordinates) comprised the left precuneus (36.7%), left cerebral white matter (36.4%), left posterior cingulate cortex (19.9%), right precuneus (5.4%), and right posterior cingulate cortex (1.6%). There was an evident difference in the activated area composition between the positive and negative values of the contrast. Compared with the positive values of the task > control contrast, a smaller area of the precuneus and part of the posterior cingulate cortex was activated for the negative values of the task > control contrast. Based on these findings, we separated the DMN-PCC node into two regions centered in the precuneus and posterior cingulate gyrus (PCG) to perform the functional connectivity analysis (Figure 7B). We used PCG, instead of PCC, to highlight the different ROI.

Moreover, for the positive values of the task > control contrast, the left LP node (Figure 7A; peak activation at -28, -74, 42, MNI coordinates) comprised the left angular gyrus (40.3%), left superior parietal lobule (23.3%), left cerebral white matter (15.7%), left middle frontal
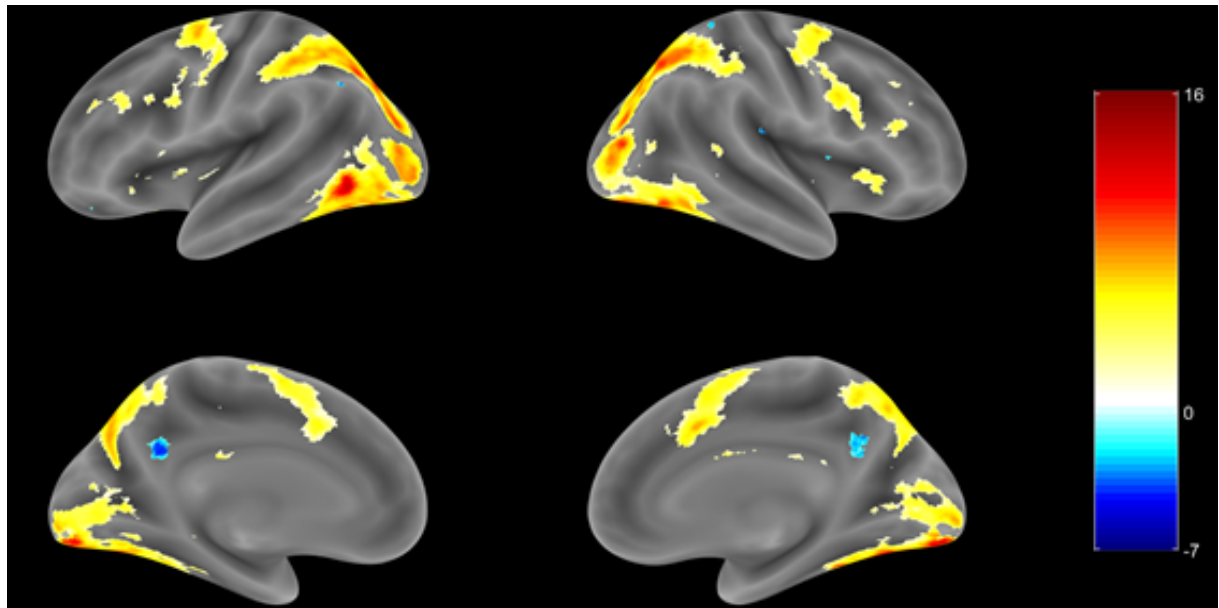
Figure 6 – Group statistical parametric map during the performance of the SDMT (positive values in hot colors, and negative values in cold colors), using a voxelwise threshold of two-sided p = 0.001, with 23 degrees of freedom and FDR = 0.1. The color bar indicates t-values. The cerebellum was excluded for visualization purposes.

gyrus (9.8%), not-labeled voxels (6.2%), and left superior occipital gyrus (4.7%). For the negative values of the task > control contrast, the left LP node (Figure 7A; peak activation at -48, -72, 26, MNI coordinates) comprised the left angular gyrus (40.1%), left middle occipital gyrus (31.2%), not-labeled voxels (25.8%), and the left cerebral white matter (2.8%). There was a difference in the composition of the regions inside the T map masked with the DMN LP mask, once the left middle occipital gyrus comprised a bigger area with negative than positive values in the task > control contrast. Unlike the DMN-PCC node, we did not separate the DMN LP because the activation region in both contrasts was small, which would make a reliable separation of the node difficult.

Functional connectivity analysis: effects of node selection

FC results showed a fully connected network during the RS condition (p-FDR < 0.05) (Figure 8A). Anticorrelations between visual areas and bilateral DMN-LP nodes could be observed. During the SDMT performance, a reorganization of the functional architecture was observed with the appearance of two anticorrelated systems (Figure 8B). The first system is composed of the task-positive regions, while DMN nodes and PCG compose the second system. These two systems showed anticorrelated interactions, except for the right DMN-LP with the right MFG, and the PCG with the left precuneus. Moreover, compared to the resting-state, the left DMN-LP and mPFC nodes showed a decreased correlation with the precuneus and left SPL during task performance (Figure 8C). Additionally, task performance resulted in different activation/deactivation patterns of the left precuneus when compared to the RS
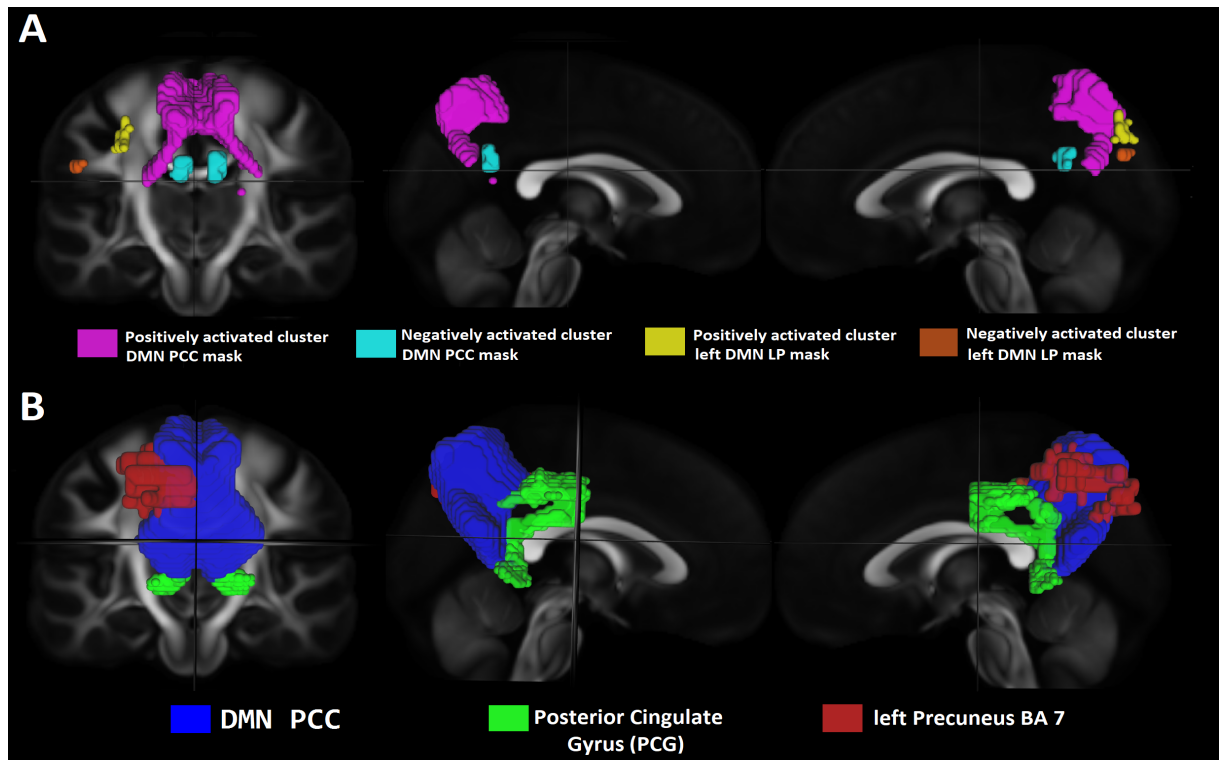
Figure 7 – (A) Tridimensional representation of the clusters resulting from the statistical parametric map (task > control, two-sided p = 0.001 and FDR = 0.1) masked with the DMN template: from left to right, positively activated voxels using DMN-PCC mask, negatively activated voxels using DMN-PCC mask, positively activated voxels using DMN-LP mask, negatively activated voxels using DMN-LP mask. (B) Anatomical templates of the DMN-PCC node (dark blue) and posterior cingulate gyrus (PCG) (light green), provided by the CONN toolbox, and the left part of the precuneus (BA 7) (dark red) from the task-related template. Posterior coronal, right, and left sagittal views are shown.

condition. The precuneus was, at the same time, positively correlated with the left lingual gyrus, a task-positive region, and negatively correlated with left DMN-LP and DMN-mPFC nodes.

4.4 Discussion

We investigated the DMN functional localization during the performance of an information processing task in healthy young subjects. Functional connectivity analysis was performed for data acquired during resting-state and task performance. We also compared both conditions to isolate better FC effects specific to the task-state since there is evidence that the spontaneous covariance present during the resting-state is also present during the performance of a task (61).

Two anticorrelated systems were observed during the performance of the SDMT task. One task-positively related control system consisted of the dorsal attention network,
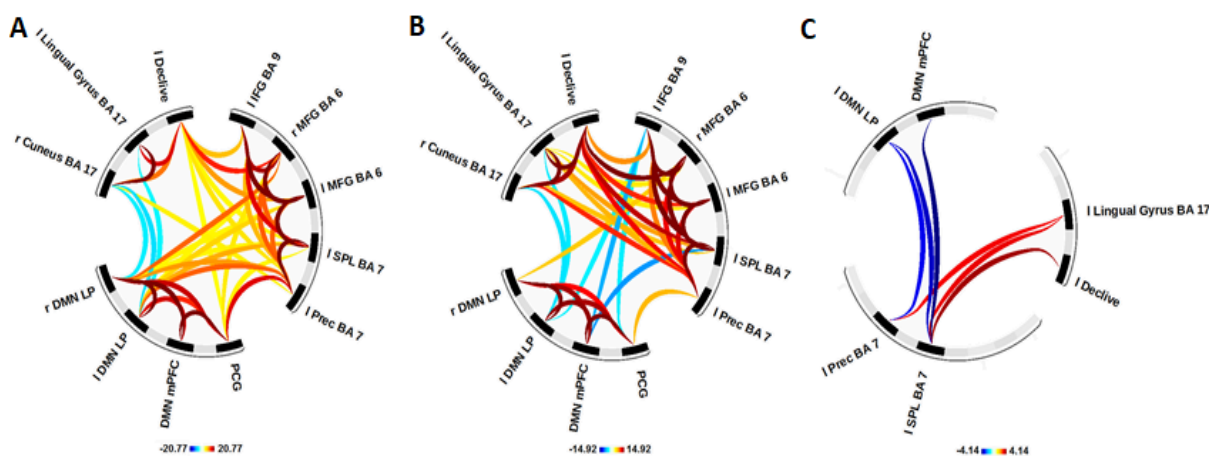
Figure 8 – Functional connectomes for the group during the (A) resting-state, (B) SDMT performance, and (C) when comparing SDMT performance with the resting-state condition (p-FDR < 0.05). The color bars represent t-values. l: left; r: right; IFG: inferior frontal gyrus; MFG: middle frontal gyrus; SPL: superior parietal lobule; Prec: precuneus; PCG: posterior cingulate gyrus; DMN: default mode network; mPFC: medial prefrontal cortex; LP: lateral parietal.

associated with focusing attention on external stimuli, and the frontoparietal control network, related to executive, top-down cognitive control processes (29); and one task-negatively related system, formed by the DMN. It is hypothesized that the antagonistic relationship between control systems and the DMN occurs due to the competition for the use of sensory computational resources and the positive coupling with brain networks involved in cognitive control (96). Therefore, efficient deactivation of the DMN is considered a reliable predictor of the ability to change from a self-referential state to a task demanding external focus, suggesting an essential role for such a network in healthy cognitive functioning. The lack of optimal DMN suppression is evident in several psychiatry conditions such as schizophrenia (138) and remitted depression (139).

In the DMN-LP node, the angular gyrus has been associated with a spatial visual shift of attention toward salient stimuli (140). Temporary impairment due to magnetic stimulation on the left angular gyrus has been linked to reduced accuracy in distinguishing left from right, especially when verbal labeling is required (114). In our study, functional localization findings suggest increased activity of the left angular gyrus during the task. Due to the small region, we did not divide it, requiring future studies to further investigating such a region. The suppression of ventral mPFC activation during the performance of goal-directed tasks was previously demonstrated (109). A positron emission tomography (PET) study about the emotional interferences with attention showed a decrease of relative cerebral flow of the inferior mPFC with higher attentional loads (141). It corroborates previous findings regarding the role of this region in the selection processes of competitive inputs from several brain regions, which can be linked to the theory of a default mode of brain function (109). This

theory suggests that the decrease of oxygen extraction fraction from the baseline in some regions during specific goal-directed behaviors means that there is an organized, baseline default mode of brain function that is suspended during these behaviors (109).

However, parts of the DMN-PCC node were positively related to the performance of the SDMT task. A previous neuroimaging study reported the precuneus as a centerpiece in the human brain, essential for supporting complex cognition and behavior (94). Although part of the precuneus is considered a portion of the DMN-PCC node, its functional connectivity with task-positive networks increases during goal-directed tasks. On the other hand, during the resting state and specific functions as episodic and autobiographical memory, its functional connectivity increases with other DMN nodes (142).

Moreover, Margulies and colleagues showed connectivity-based subdivisions within the precuneus using RS-FC analysis (87). They found three distinct patterns: (i) the anterior precuneus with a sensorimotor function; (ii) the central precuneus with a cognitive/associative function; and (iii) the posterior precuneus connected with cortical visual regions. Our results are consistent with such findings since we observed that the precuneus is connected to (i) superior parietal lobule, involved in top-down goal-directed attention; (ii) inferior frontal gyrus and bilateral middle frontal gyri, related with convergence areas for stimulus-driven and top-down control, and (iii) lingual gyrus and cuneus, associated with visual perception and processing. Even during attentional task performance, the precuneus showed a multimodal integrative role, and then considered a heterogeneous structure. Our results also suggest that the FC pattern of the precuneus is state-dependent. As previously reported, it had increased FC with the control network during task performance when compared to RS, but the FC with other DMN nodes increased at rest (94).

Additionally, the precuneus and neighboring PCG are differentiated from each other once the latter is linked to limbic structures (87). The PCG is the most ventral part of the DMN-PCC node, and during task performance, the PCG was positively correlated with DMN regions. Previously, the ventral part of the PCG was also linked to the DMN and responsible for internally directed cognition, such as memory retrieval and planning. In contrast, the dorsal PCG has been connected to the prefrontal cortex, controlling attentional focus (95).

Our primary motivation to split the DMN-PCC into two regions was to show that this large DMN portion comprises regions with different functional roles and connectivity behaviors. In summary, our results showed that the left precuneus (BA 7), during the performance of the SDMT adapted to an fMRI experiment, is positively correlated with the IPS task-positive network and anticorrelated with the DMN nodes, differently from the classical antagonistic models (131, 143). In contrast, the remaining DMN-PCC subarea, the PCG, presented the classical pattern of connectivity during the task. Once the anatomical boundary of the DMN is not clear, our results provide some evidence that the left precuneus (BA 7) belongs partially to the DMN-PCC region and is an adjacent context-dependent modulatory region that works

as a transient in-between hub connecting the idling DMN to task-positive areas.

Moreover, recent studies have reported that the dorsal part of the precuneus is more related with the dorsal attention network than with the DMN (144, 145, 146, 147). However, although the majority of the left precuneus BA 7 ROI in our study comprises the dorsal precuneus, its anatomical template overlaps part of the anatomical DMN-PCC node, and our FC results showed that such a region is connected with both task-related and DMN regions during the resting-state. During task performance, the left precuneus was connected with the whole task-related network and with the PCG (part of the DMN-PCC node). The implications of these results are debatable: is the left precuneus part of the DMN or not? Does it depend on the task performed? Our results suggest that the left precuneus partially belongs to the DMN, a slightly different statement than the ones of the studies mentioned above. Moreover, such behavior may indicate the precuneus as a centerpiece of the DMN.

Disconnection over posterior DMN areas was related to Alzheimer's disease (148), mild cognitive impairment (149), attention deficit hyperactivity disorder (150), major depressive disorders (151), internet gaming disorder (152, 153), obstructive sleep apnea (OSA) (154) and temporal lobe epilepsy (155). More specifically, the precuneus was related to mental imagery (156, 157), episodic memory retrieval (158), and conscious processes (158, 88). Therefore, the precuneus is an essential piece to study higher cognitive function and disorders of consciousness, such as vegetative state and minimally conscious state.

Our study has some limitations. We must consider that node selection can be explored considering not only the regions obtained in a meta-analysis but also checking individual differences in statistical parametric maps. Unlike the DMN-PCC node, we did not separate the left DMN-LP node once the activated region in both contrasts was small, making a reliable separation difficult. Additionally, we must consider different tasks to check how different parts of the DMN are functionally connected to the network according to the task performed.

4.5 Conclusion

In conclusion, we found that the activation and functional connectivity of the DMN is, in general, suppressed during the information processing. However, the left precuneus BA 7 presented a context-dependent modulatory behavior, working as a transient in-between hub connecting the DMN to task-positive areas. Such findings support studies that show increased activation and excitatory functional connectivity of DMN portions during goal-directed tasks. Moreover, our results may contribute to defining more precise functional correlates of IPS deficits in a wide range of clinical and neurological diseases.

This study was already published (159).

5 Contrast-agent-free State-of-the-art Magnetic Resonance Imaging on Cerebral Small Vessel Disease: from lesions to connections and cognition.

5.1 Introduction

Cerebral small vessel disease (cSVD) is a pathological condition that affects the human cerebrovascular system by deregulating the blood circulation through the arterioles, venules, and the correspondent perfusing brain tissue at the capillary bed. It results in damaged cortical and subcortical gray matter (GM) and white matter (WM) (160, 161), is considered the most important cause of vascular cognitive impairment (VCI) (162), and is responsible for around 20% of all strokes worldwide (163). Magnetic resonance imaging (MRI) has become crucial in evaluating brain changes and predicting cSVD-related cognitive decline in clinical and research settings (161, 164).

However, reports on the association between conventional MRI measures and clinical features of cSVD are not always concordant (165). Such MRI measures cannot delineate the heterogeneity of cSVD lesions with similar appearance and can only show part of the whole-brain damage related to cSVD (166). Additionally, cSVD has been suggested as not a focal lesion disease, but it also affects remote brain areas, influencing the clinical outcome (166). It also impairs structural and functional network connectivity, disrupting efficient communication in brain networks necessary for functional performance. Such facts have motivated the use of additional MRI acquisition and analysis models, which can disentangle differential assessment of cSVD-related brain damage, its effects on connections and cognition, and future clinical outcomes (167). Moreover, contrast-agent-free state-of-the-art MRI techniques have shown subtle changes not observed with traditional imaging (168). They have also allowed assessing pathophysiological processes underlying the cSVD development (169) and the extent of the overall brain damage that leads to a disconnection syndrome (166).

The administration of gadolinium-based contrast agents (GBCAs) in MRI scans to enhance brain lesions for diagnosis is performed million times per year (170). However, it has been criticized for rare but dangerous nephrogenic systemic fibrosis in patients with impaired renal function and its deposition in many organs, including the brain (170). Then, the use and development of contrast-agent-free MRI techniques have been considered a safer alternative without loss of potential to diagnosis and prognosis.

In terms of pathophysiological processes, it is suggested that damage to functional units can cause cerebral blood flow (CBF) deregulation, affects cerebrovascular reactivity (CVR), and cause blood-brain barrier (BBB) leakage, among other effects, which together

Chapter 5. Contrast-agent-free State-of-the-art Magnetic Resonance Imaging on Cerebral Small Vessel Disease: from lesions to connections and cognition.

56

are responsible for the cSVD-related brain injuries (164). Non-contrast MRI methods have been developed to assess such parameters. A powerful tool in assessing perfusion-related alterations in cSVD comes from MRI perfusion-weighted images. In that sense, arterial spin labeling (ASL), designed to explore the water molecules in the arterial blood as an endogenous tracer, allows a noninvasive approach to measure CBF and related parameters (171). Additionally, intravoxel incoherent movement (IVIM), a diffusion-weighted imaging (DWI) technique, can describe both perfusion and diffusion-related parameters of the brain microstructure quantitatively without using an exogenous contrast agent (172).

Moreover, MRI methods have been used to analyze the cSVD burden effects on brain structural and functional networks and how the disruptions contribute to the outcome. The diffusion tensor image (DTI) has been used to evaluate cSVD due to its sensitivity to white matter damage (165), allowing quantifying the cSVD burden and assessing the integrity of the structural brain network. Similarly, functional MRI (fMRI) based on the blood oxygenation level-dependent (BOLD) contrast has been considered to study the functional brain networks in resting-state and task conditions (14, 13), and, because of its dependency on CBF, it is a reliable and reproducible method to assess cerebrovascular reactivity (CVR-BOLD) at the tissue level (173).

Therefore, we gathered a group of researchers to prepare a review focused on the applications of contrast-agent-free state-of-the-art MRI (ASL, DTI, IVIM, and BOLD-fMRI) and its additional information compared to conventional MRI for the etiology, diagnosis, and prognosis of cSVD. Considering the objectives of the present thesis, we will show the results of the systematic review regarding the DTI and BOLD-fMRI techniques.

5.2   Methods

We followed the PRISMA-P (Preferred Reporting Items for Systematic Review and Meta-Analysis Protocols) 2015 checklist: recommended items to address in a systematic review protocol guidelines (174). The review parameters were delineated using the PICOS worksheet and Search Strategy (Centre for reviews and dissemination. Systematic Reviews: CRD's Guidance for Undertaking Reviews in Health Care. York: University of York; 2006). The main question of our study was: What are the applications of contrast agent-free state-of-the-art MRI and its additional information compared to conventional MRI for the etiology, diagnosis, and prognosis of cSVD? Online searches in PubMed and Scopus were carried out considering the term "Cerebral Small Vessel Disease" combined with each one of the techniques. Inclusion criteria were original publications in English between 2000 and 2021 (last search on May 15th, 2021), and with subjects of both sex, 18 years old or more.

For the Identification, the authors independently researched the articles following the search strategy and inclusion criteria; then, they reached a consensus on which articles would

be included in the final analysis. All the records and data selected had their title, authors' names, year of publication, MRI technique, and main findings (about pathophysiology, lesions, connections, and/or clinical outcomes) extracted using a standardized data extraction form shared among the authors.

Then, duplicates were removed, and records were screened, i.e., non-full-text articles such as reviews and editorials were removed. The remaining full-text articles were assessed for eligibility. In addition to the inclusion criteria mentioned, we considered the exclusion criteria: studies with animals, text not available, methods development, no MRI technique used, another clinical group (instead of cSVD), trial presentation (description of future clinical trials), and drug use as cSVD prevention. The remaining full-text articles were included in the systematic review. The articles' details regarding Identification, Screening, Eligibility and Inclusion (PRISMA-P diagram flow) are described in Figure 9.
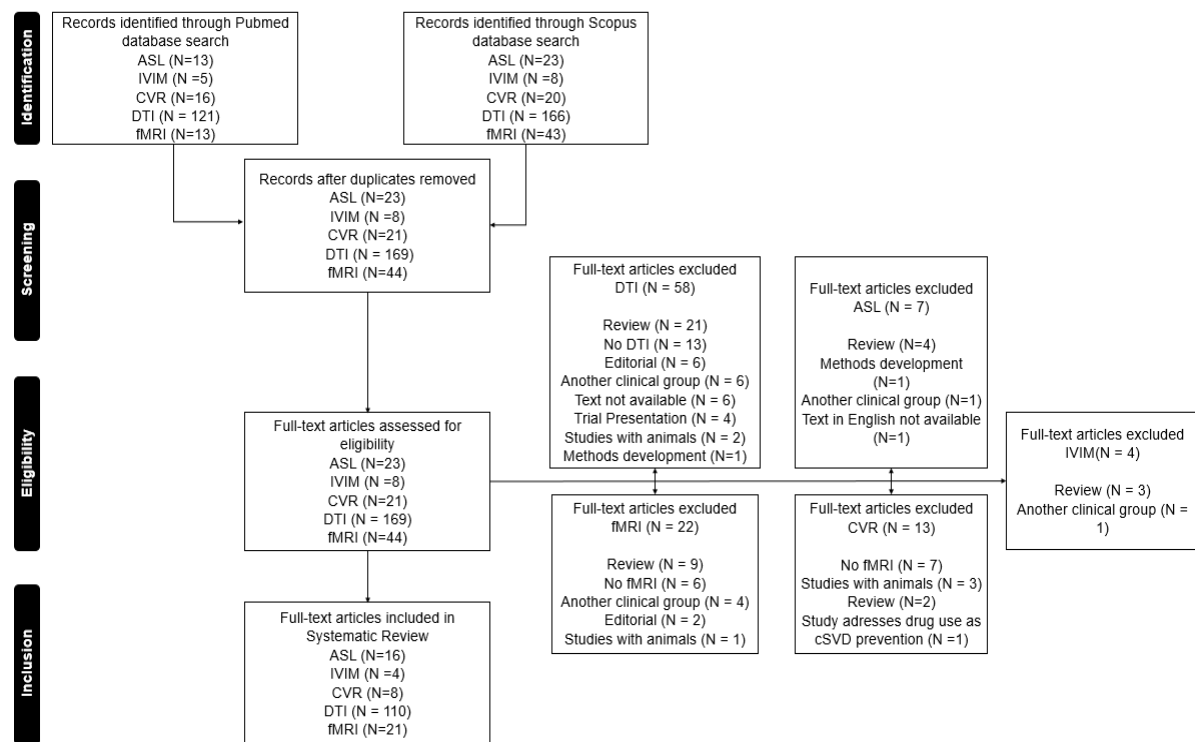
Figure 9 – Flow diagram of the selection process of the systematic review. For the article, we considered five MRI methods. For the thesis purposes, we are showing the DTI and BOLD-fMRI results.

5.3 Results

Diffusion Tensor Imaging (DTI)

Among several diffusion-weighted images (DWI) models, DTI is a proper quantitative method in assessing in vivo white matter (WM) microstructure integrity. It measures water

molecules' diffusion within WM tracts using magnetic diffusion gradients applied in at least six different directions. A diffusion tensor is then acquired, from which two quantitative measures, fractional anisotropy (FA) and mean diffusivity (MD), are obtained. High FA and low MD values usually reflect intact microstructural integrity (175, 176).

<u>DTI additional contributions in comparison to conventional MRI</u>

A cross-sectional tract-based spatial statistics (TBSS) study on the normal-appearing white matter (NAWM) of patients with mild cognitive impairment (MCI) reported that cSVD effects on WM go beyond the macrostructural damage visible through conventional MRI (Figure 10A) (177). Tractography studies showed decreased fractional anisotropy (FA) and increased mean diffusivity (MD) correlated with cognitive performance and strong association between MD, Serum neurofilament Light chain (NfL), a blood marker to neuroaxonal damage, and information processing speed (IPS) scores in cSVD patients (178, 179), which was also poorly correlated with conventional MRI markers. Better performance of DTI in comparison to conventional MRI was also observed in longitudinal studies. Changes in MD and FA of cSVD patients were detectable over a 1-year follow-up (180). Moreover, a 9-year longitudinal study showed that DTI could detect impaired WM microstructure preceding the conversion into WMH years before becoming visible on conventional neuroimaging (181).

Furthermore, while MD correlated significantly with executive function tests even after controlling for demographic variables and conventional MRI markers (182), radial diffusivity (RD) could better predict executive dysfunction in cSVD (183). Such a strong association between executive function and DTI parameters was confirmed by a multimodal MRI model containing age, gender, brain volume, FA, and premorbid intelligence quotient, which explain 74% of the variance of executive function score (180). Axial diffusivity (AxD) of the posterior frontal periventricular NAWM, right middle cingulum bundle, and mid-posterior corpus callosum also predicted cognitive impairment in cSVD patients (184). Besides, MD of WM lesions (WMH) and NAWM correlated with gait disturbances (185, 186), linked to higher morbidity and mortality (187).

In longitudinal studies, FA changes in the thalamus correlated with WMH progression among cSVD patients (188). Increased MD was also consistent with progressive degradation of WM integrity in symptomatic cSVD (189), predicted cognitive decline (190), and was one of the best predictors of mortality (191). Additionally, while the degree of baseline microstructural impairment explained clinical variability in patients with similar cSVD severity (181) and predicted incident dementia, risk of mortality, and cSVD severity (192, 193, 194), it did not correlate with CMB (195). In contrast, other studies have questioned the advantages of using DTI over conventional MRI since the former requires sophisticated computational processing, is more time-consuming, and showed similar or worse results than conventional MRI in some cases (196, 197, 198, 199, 200). However, despite the divergences, DTI has been widely

Chapter 5. Contrast-agent-free State-of-the-art Magnetic Resonance Imaging on Cerebral Small Vessel Disease: from lesions to connections and cognition.

59

used in cSVD. WMH was associated with two patterns of altered diffusion characteristics in the surrounding WM tracts. A penumbra pattern with improving diffusion characteristics was observed in lesion-free tracts distant from the WMH lesion. However, in the WMH tract, a Wallerian-type degeneration pattern was present (201). Moreover, a study investigating hemispheric asymmetry in cSVD found that the right hemisphere is more susceptible to neurodegeneration and related to cognitive decline and higher mortality (138).

Brain structural networks

Furthermore, the severity of structural disruption of brain networks in cSVD was correlated with cognitive impairment, mainly in executive functions, divided attention, IPS, psychomotor speed, episodic memory, and global cognition assessed by the Mini-Mental State Exam (MMSE) (202, 203, 204, 205). Such correlations were evident in highly connected network regions (206). Cognitive impairment has been associated with functional and structural connectivity changes within brain networks, such as the default mode network (DMN), attributed to WMH progression (207). The effect of WMH on dementia was reported to be mediated by global network efficiency and the peripheral connections' strength in the elderly with cSVD (208). The brain network measurements may be regarded as a direct and independent surrogate marker of cognitive impairment in cSVD (209). However, a recent study found WM integrity widely abnormal in non-demented cSVD patients, while structural connectivity was relatively preserved (210). Microstructural changes identified with DTI through graph-theory analysis and network-based statistical analysis can be found during the preclinical cognitive impairment (PCI) and MCI stages, suggesting that early cognitive changes are related to a disruption pattern from peripheral to central connections (211). Measures of network efficiency have been considered the best markers for cognitive performance and an essential contribution to the genesis of the cognitive decline in cSVD (212). More recently, WMH volume, structural network local efficiency, and IPS performance were interrelated, with the structural connectivity partially mediating the effects of WMH on IPS (213).

DTI-related markers of cSVD

DTI parameters, such as the peak-width skeletonized mean diffusivity (PSMD), free water (FW), and tissue compartment measures (FAt, MDt), have been recently proposed and used in the assessment of cSVD. PSMD was consistently associated with IPS in genetically defined, inherited, and sporadic cSVD cohorts and memory clinic patients, offering further advantages of a fast and fully automated marker. It also outperformed conventional MRI markers by explaining more cognitive variance in the IPS domain. In a longitudinal analysis, PSMD values changed significantly within 18 months and offered smaller sample size estimates than other imaging markers employed (214, 215). More recently, it was strongly associated with conventional cSVD markers and outperformed MD in cognition prediction

(216).

Recently, a more complex yet probably more realistic FW diffusion model has been applied in cSVD. Rather than alterations in the WM fiber organization, it was suggested that increased extracellular water is the main contributor to diffusion changes in CADASIL and sporadic cSVD patients (179). Increased FW also correlated with an IL-18-centered inflammatory network (217), was found to mediate the association between deep medullary veins (DMV) disruption and WM integrity in cSVD (218), was related to geriatric depressive symptoms (219), and presented a stronger association with cognitive deficits than conventional DTI method, showing to be a marker of cSVD–related degeneration (220).

An alternative diffusion tensor decomposition model has been developed to provide isotropic and anisotropic tensor components. Such parameters were significantly correlated with executive functions, IPS, and conversion to dementia in a 3-year longitudinal study (221, 222). Conventional DTI, multi-shell diffusion imaging, and advanced diffusion modeling were compared in cSVD patients. The multi-shell scheme and the Diffusion Kurtosis Imaging provided metrics that correlated strongly with cognitive measures and better characterized WM damage related to cSVD than traditional DTI (223).

Complications and outcomes of cSVD associated with DTI-derived metrics

Low FA and high MD in several WM areas (mainly NAWM) were associated with decreased cognitive scores in cSVD in a cross-sectional TBSS study (224). Recently, WM damage was restricted to specific segments in cSVD patients, disrupting some fibers related to many cognitive deficits (225).Conversely, a 5-year prospective study showed no relationship between baseline WM and NAWM microstructural integrity, measured using mean FA and mean MD, and declined global cognitive performance after correcting multiple comparisons. Authors suggested that other factors, rather than solely WM integrity, might be related to cognitive impairment (226). A two-year follow-up study reported that DTI measurements are the main predictor of clinical changes over time in CADASIL patients (227). Compared to healthy controls, CADASIL patients showed decreased FA and increased diffusivity in several brain areas, with these microstructural integrity changes correlated with their cognitive performance (228).

In a multicenter study with symptomatic cSVD patients, DTI outputs and the number of lacunes were independently associated with global cognition and Montreal Cognitive Assessment (MoCA) scores. DTI markers solely were also independently associated with mental flexibility and verbal fluency (229). Furthermore, working and long-term memory abilities were reduced in cSVD patients compared to controls and were partly explained by microstructural changes of the cingula and uncinated tracts, respectively (Figure 10B) (230). Finally, in the elderly with cSVD, verbal memory performance was related to DTI-derived metrics extracted from the hippocampus and cingulum, even before macrostructural changes

Chapter 5. Contrast-agent-free State-of-the-art Magnetic Resonance Imaging on Cerebral Small Vessel Disease: from lesions to connections and cognition.

61

could be detected, suggesting that DTI metrics may detect early microstructural abnormalities (231, 232).
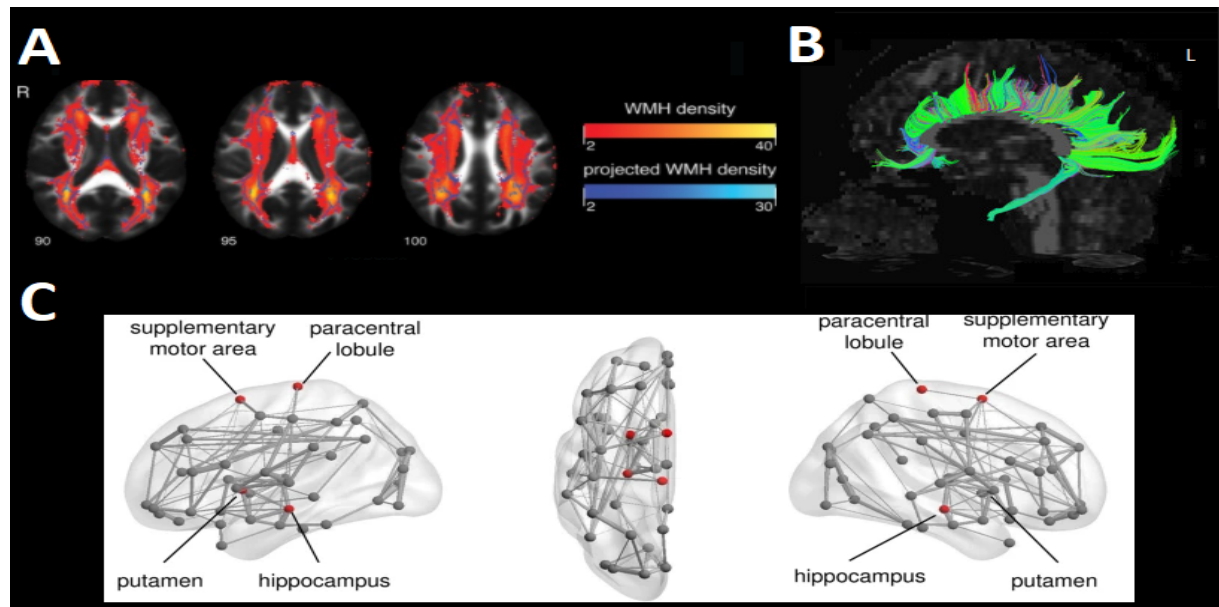
Figure 10 – Three DTI methods applied to cSVD. (A) TBSS skeleton projections on the WMH map are superimposed on the mean FA image (177). (B) Tractography representation of the cingula tract whose integrity loss explained memory performance (230). (C) Group structural brain network of patients with first TIA or ischemic stroke. In red, regions with significantly lower nodal efficiency due to the presence of cSVD. The node size and edge width are weighted by nodal efficiency and the number of connections (41)

MCI patients with cSVD showed microstructural abnormalities detected through DTI in the subcortical region, periventricular, and central semiovale WM (233) and the NAWM of the anterior corpus callosum, internal and external capsule, and periventricular WM (177). Moreover, disruption of structural connectivity has been detected even in cognitively normal cSVD patients, affecting mainly the prefrontal areas, whereas in MCI cSVD patients, networks from frontal and parietal regions were disrupted (234). Interestingly, MD and FA were more strongly associated with MoCA than MMSE scores, suggesting that the former might be more useful as a cognitive screening tool for cSVD patients (165, 235, 224). However, the T2 relaxation time of the NAWM in cSVD patients was associated with cognition, which the DTI metric of the NAWM failed to achieve (236).

Higher hippocampal MD correlated with an increased 5-year risk of dementia in the elderly with cSVD (237). A preliminary study found mean FA within periventricular WMH associated with peripheral inflammatory markers in AD patients (238). In a cross-sectional study with midlife participants, angiopoietin 2, a circulating growth factor involved in regulating vascular function, correlated with lower FA in WM tracts such as posterior thalamic radiation, middle cerebellar peduncle, and cingulum among APOE (apolipoprotein E)-ϵ4

midlife carriers (239). In a multicenter study investigating six independent samples of memory clinic patients covering the entire spectrum of AD, mixed disease, and cSVD, DTI changes were more strongly associated with cSVD than with AD markers, suggesting that DTI might be particularly sensitive to cSVD-related pathology (240).

Besides cognitive decline, gait (lower extremities) abnormalities are also a clinical feature of cSVD and have been investigated using DTI. Recently, it was shown that cSVD patients with higher WMH burdens presented worse cognitive performance and balance issues affecting their daily lives (241). One study reported that FA measured in the NAWM mediated the negative association between WMH and gait disturbances (242). Although in a 5-year longitudinal study, baseline GM volume and DTI-derived cSVD markers did not correlate with gait impairment (243), progressive changes in WM volume, MD, AxD, and FA (extracted from a skeleton of the significant WM tracts) were associated with such gait decline in another study (244). While CADASIL patients were found to have minor impairment in gait performance compared to controls, higher PSMD and MD (voxel-based) were associated with shorter single task stride length (245).

Mild parkinsonian signs, including gait and balance disturbances, have been associated with the microstructural integrity of WMHs in the elderly with cSVD, measured through FA and MD, mainly in the frontal lobe (246). Similarly, lower FA values have been found in bilateral frontal WM tracts of cSVD patients with vascular parkinsonism (247). More recently, the association between structural network efficiency assessed with DTI measures and gait in cSVD patients is mediated by cognition (248). Lower regional FA was related to worse manual dexterity (upper extremities) and increased serum ceramides in a group of asymptomatic cSVD (249).

Finally, depression in the setting of cSVD has also been the subject of investigation. Depression in cSVD patients has been associated with reduced white matter integrity measured through FA (250). Participants with cSVD and depressive symptoms showed damaged microstructural integrity, measured using FA and TBSS, mainly in fronto-subcortical WM tracts, potentially disrupting circuits involved in mood regulation (251, 252). Structural connectivity was also disrupted in cSVD patients with depression (252). In MCI patients with cSVD, decreased WM FA and increased WM MD were independently correlated with worse Geriatric Depression Scale (GDS) score (253).

Similarly, network connectivity is related to GDS in cognitively impaired patients and mediates the cSVD burden (WMH and lacunes) with GDS scores (254). Apathy in cSVD patients was also correlated with microstructural disruption of WM tracts (strongest effect in limbic association tracts) using DTI metrics, which were not associated with depression (255). Structural network disruption in premotor and cingulate regions underlies apathy, but not depression, in cSVD patients (256). Moreover, reduced efficiency in the reward network was related to increased apathy in symptomatic cSVD subjects (257).

Functional Magnetic Resonance Imaging (fMRI)

fMRI-BOLD signal reflects differences in the magnetic susceptibility of intravascular hemoglobin, depending on whether it is bound to oxygen or not. Oxyhemoglobin is diamagnetic, while deoxyhemoglobin is paramagnetic. An increase in regional CBF surpassing an increase in oxygen consumption results in a reduction of deoxyhemoglobin concentration, increasing local signal intensity in T2*-weighted images. Task-based and resting-state (RS) fMRI have been performed to identify brain regions and their correspondent functions in the normal brain and provide insights into the effects of diseases and injuries in the functional organization (258).

CSVD has been associated with motor and cognitive impairment assessed by task-based and RS fMRI. Activation in the pre-supplementary motor area (SMA), related to complex motor tasks, has been correlated with frontal WMH load in the elderly with severe WMH but not cognitive dysfunction. It suggests that the WMH load can disturb the functional motor network at the early stage of the disease, even before cognitive impairment is present (259). CSVD patients with gait impairment showed the reduced fractional amplitude of low-frequency fluctuation (fALFF) in the left SMA and increased fALFF in the right inferior frontal gyrus, the left caudate, and the left precuneus. They also presented lower RS functional connectivity in the left SMA and temporal lobe (260).

MCI patients with cSVD presented lower activation in the precuneus area for a working memory task than MCI patients without cSVD and controls. These activation differences between MCI patients with and without cSVD, which presented similar cognitive impairments, supports that cSVD can affect MCI patients cognitively (Figure 11A) (261). Furthermore, MCI patients with cSVD who underwent a cognitive rehabilitation program presented increased activation in brain circuits involved in attention and working memory (262).

In an attention-demanding test evaluated with multi-echo BOLD fMRI, subjects with WMH showed lower activation in frontoparietal regions and temporal-parietal junctions than healthy elderly. They also presented higher activation in the precuneus and posterior cingulate gyrus in an executive function contrast. These results suggest that WMH may disrupt functional brain networks that underlie salience and cognitively mediated attention (263).

CSVD patients at the initial stages of the disease presented lower resting-state functional connectivity (RS-FC) in frontoparietal networks and higher in cerebellar regions than healthy controls. Such changes correlated with WMH and cognitive impairments widely associated with the cSVD condition (264). In patients with severe WMH load, impaired functional and structural connectivity between the posterior cingulate cortex (PCC) and thalamus were independent risk factors for slower IPS. In contrast, PCC-middle frontal gyrus functional connectivity and PCC-hippocampus structural connectivity were related to memory decline (265). Resting-state whole-brain regional homogeneity of MCI patients with cSVD correlated significantly with MoCA and Stroop scores, distinctive in this clinical group (Figure 11B) (266).

Chapter 5. Contrast-agent-free State-of-the-art Magnetic Resonance Imaging on Cerebral Small Vessel Disease: from lesions to connections and cognition.

64

Both cSVD patients with and without cognitive impairment showed decreased connectivity within the DMN network and weak negative connectivity between the DMN with dorsal attention network (DAN) and frontoparietal control network (FPCN) networks. The cSVD with cognitive impairment group showed within- and between-network alterations of the FPCN correlated with its cognitive function, while the connectivity of the FPCN and the DMN correlated with deep WMH volume in cSVD subjects. These findings suggest that cognitive alterations of cSVD subjects may be mediated by the FPCN connectivity impaired by the deep WMH burden (267).

WMHs in basal ganglia (BG) have been significantly associated with vascular cognitive impairment (VCI). Patients with subcortical vascular MCI (SVMCI) presented higher WMHs, mainly in caudate regions than patients with amnestic mild cognitive impairment (aMCI) and healthy control subjects. In SVMCI patients, BG WMHs in both dorsal and ventral caudate correlated with functional connectivity and verbal episodic memory performance, while such correlations did not happen in aMCI patients. These findings suggest a relationship between structural changes due to cSVD, the functional integrity of BG circuits, and episodic memory performance in SVMCI (268). In a study with 269 elderly subjects with cSVD, the BG resting-state functional connectivity was related to gait speed, independently of locomotor risk factors such as WMH (269).

Moreover, the graph theory approach showed that MCI patients with cSVD presented changes in Executive Control Network (ECN) and DMN compared to MCI patients without cSVD. More specifically, the connectivity of the right inferior frontal gyrus of the ECN mediated the relationship between periventricular WMH and visuospatial processing in MCI patients with cSVD (267). Recently, lower global efficiency of the DMN in CADASIL patients with higher cSVD burden was reported (270). cSVD patients with lacunes on the thalamus presented subtle changes in their functional connectome when compared to those without thalamus lacunes and correlated with mild cognitive impairment in episodic memory and IPS, suggesting that lacunes on the thalamus played a vital role in mediating the functional neural changes of cSVD patients (Figure 11C) (271). In contrast, in a study comparing functional and structural networks as markers of symptomatic cSVD severity, only structural networks supported evidence to detect clinical and control differences (192).

Recent studies also used fMRI to investigate risk factors, genetic factors, and outcomes of cSVD. In middle-aged adults with type 1 diabetes mellitus, brain activation changes seem to mediate the disease with slower IPS, although it did not associate with the presence of cSVD (272). In an event-related Go/No-go task, CADASIL patients showed lower activation in the alerting network and areas involved in executive functions, probably related to the presence of cSVD (273).

In a voxel-based morphometry analysis, both the MCI with and without depressive symptoms presented decreased GM density in the left parahippocampal, right hippocampus,
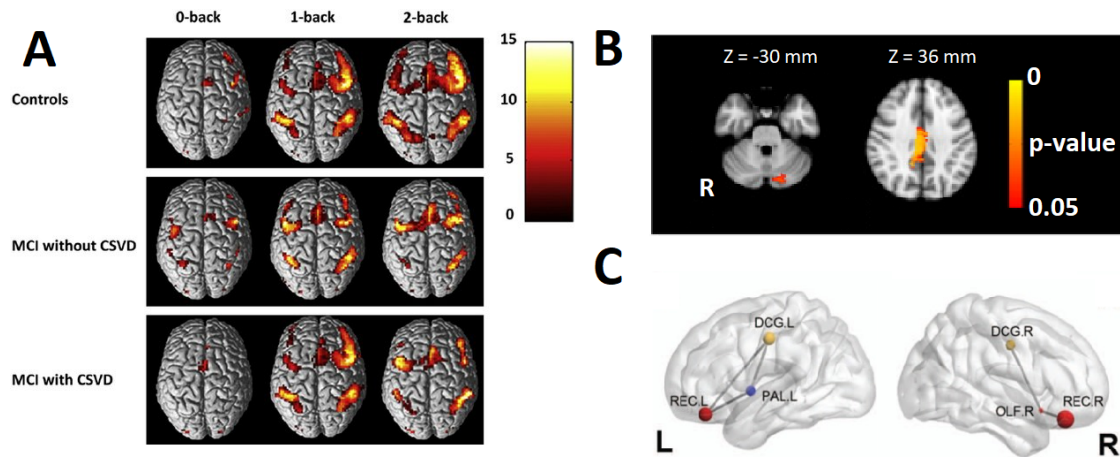
Figure 11 – Three fMRI studies applied to cSVD. (A) Group activation for different levels of working memory load (0-back versus rest; 1-back versus rest, 2-back versus rest) (p-FWE < 0.05) (261). (B) Significant associations between regional homogeneity (ReHo) and cognitive performance (p < 0.05, corrected for multiple comparisons). On the left, a negative association between ReHo and MoCA score in the left posterior cerebellum. On the right, positive association between ReHo and Stroop score in the bilateral middle cingulate cortex (266). (C) Significantly decreased brain functional connectome nodal centralities in cSVD patients with thalamus lacunes compared to healthy controls (p < 0.05, network-based statistics). Different-color nodes represent different brain regions. DCG.L: left middle cingulum, DCG.R: right middle cingulum, OLF.R: right olfactory, PAL.L: left pallidum, REC.L: left rectus, REC.R: right rectus (271).

and right middle cingulate cortex (rMCC) when compared to normal controls. The increased GM density in the rMCC correlated with rs-FC with right parahippocampal in the MCI with depressive symptoms compared to the MCI without depressive symptoms (274). In Alzheimer's disease, the emergence of amyloid plaques is followed by forming tau-containing neurofibrillary tangles correlated with neurodegeneration and dementia symptoms. In an rs-fMRI study, functional connectivity correlated with tau-PET uptake independently of the presence of dementia symptoms, amyloid deposition assessed by amyloid-PET, or cSVD, supporting the view that prion-like tau spreading is facilitated by neural activity (275).

Finally, the BOLD-fMRI physiological noise within WM measured as raw physiological noise and cardiac pulsatility showed that graded increases in cardiac pulsations in NAWM are related to both age and the presence of cSVD, independently. These measures are suggested as a complementary dynamic measure of WM integrity to the static FLAIR anatomical images (276). A correlation between ultrasound and fMRI measures of cerebrovascular pulsatility was also shown. This association provided insight into the transmission of pulsatile energy from large basal arteries at the Circle of Willis to downstream cerebrovascular beds and has implications for the utility of cardiac-related pulsatility as a potential marker for cSVD (277).

5.4 Discussion

DWI and, more specifically, DTI is the most used technique for the diffusion assessment in cSVD. The first DTI studies showed whether DTI-derived metrics such as MD and FA could be sensitive to WM damage and correlate better with cognitive function than conventional MRI imaging. MD and FA were already considered sensitive to measure WM damage and better markers for cognitive impairment in cSVD compared to traditional MRI measures (278, 279). Issues such as the role in the clinical management of microbleeds present in a significant proportion of cSVD patients arose (278). Additionally, the full impact of tractography techniques on cSVD has not been performed (279).

DTI-derived markers have been correlated with cardiovascular risk factors, with several other MRI markers, with clinical features, including cognitive impairment. Additionally, longitudinal findings support the hypothesis that conventional MRI markers of cSVD (e.g., WMH, lacunes, and microbleeds) cause cognitive decline and dementia via disruption of structural brain networks (280, 192). Therefore, DTI has provided new insights into understanding the mechanisms of the main clinical consequences of cSVD, particularly by evaluating the structural integrity of the cerebral WM architecture. Moreover, DTI may furnish reliable surrogate markers to be applied in future clinical trials, investigating potential therapeutic interventions. However, the pathophysiology underlying WM abnormalities remains incompletely understood. While the interpretation that the increased MD and reduced FA result from microstructural tissue damage is notable and cSVD has a significant role in losses of microstructural WM integrity (281), mechanisms other than cSVD must also be considered. WM microstructural abnormalities can be caused by ischemic damage due to cSVD and indirect effects of cSVD, such as Wallerian degeneration. Future studies must be considered to address this issue.

fMRI can also be a valuable tool for investigating cSVD, providing insights into the functional networks disruption related to cSVD and cognitive decline, dementia, and mortality. Findings reported task-based activation changes in motor (259), working memory (261, 262), and attentional (263) brain functions in cSVD patients. RS-FC studies (264, 268, 267) indicated the DAN, ECN, FPN, and DMN functional connectivity as essential markers of cSVD functional changes. Joint analysis with structural findings (274), tau-PET intake (275), and novel approaches (276, 277) with BOLD-fMRI also showed brain changes associated with the occurrence of cSVD. However, only structural networks supported evidence to detect clinical and control differences (192). Future studies must also include massive testing of the associations among fMRI metrics and WMH, lacunes, microbleeds, and other conventional markers and risk factors of cSVD. Finally, longitudinal studies are desirable to look for causal relationships between functional network disruption and cSVD.

In addition to the individual contribution of each technique, it is possible to see how they could be used together for an integrated cSVD assessment (Figure 12). The contribution

of risk factors such as age, diabetes, hypertension, and physical inactivity in developing the disease can be studied not only with DTI, but also ASL, CVR, and IVIM. The effects of protective factors can also be considered with such methods. Once these conditions can lead to small vessel impairments, affecting CBF, vasoreactivity, and BBB permeability, ASL, CVR, and IVIM can contribute mainly to the pathophysiology study. In contrast, DTI can contribute to the understanding of lesions.

However, whether all the above imaging markers are independently associated with cSVD outcomes or have combined effects is still an open question. Regarding mediation effects, brain structural connectivity disruption has been suggested to mediate WMH and cognition in cSVD patients. More specifically, it has been suggested that structural network local efficiency partially mediates the effects of WMH volume on information processing speed (213). Global network efficiency and the peripheral connections' strength in the elderly with cSVD mediates the effect of WMH on dementia (282). Additionally, it has been shown that WMH areas present altered CVR but not CBF (283), proposing more studies, mainly longitudinal, to explain the cSVD development and the relationship between these metrics and the underlying mechanisms of the cSVD. Although the literature has not demonstrated the definitive way to assess the effects of the disease on brain structure, focal lesions in the network of structural and functional connections seem to have an essential contribution to the patient's clinical outcome. However, some questions remain regarding the vascular-related changes being consequences or contributing to cSVD and their relation with cognition; whether the DTI changes mediate the effects of traditional cSVD markers in cognition; and if the functional changes are due to impaired flow or impaired metabolism, and their implications.

5.5   Conclusion

Although cSVD is still a challenging research topic with many open questions, contrast-free MRI methods have been a valuable tool for addressing some of the main questions. Such MRI methods and their related quantitative parameters are promising tools for evaluating risk factors and applying prevention strategies, especially concerning modifiable risk factors. It has also been applied to study pathophysiological mechanisms underlying WM damage and promote markers for evaluating therapies. Finally, it has been used to assess damage to structural and functional brain connectivity, the first being suggested as a mediator of the effects of structural damage on cognition. New developments and ongoing studies are essential to delineate more accurate MRI measures for the diagnosis, prognosis, and prediction of cSVD.

This study was already published (284).
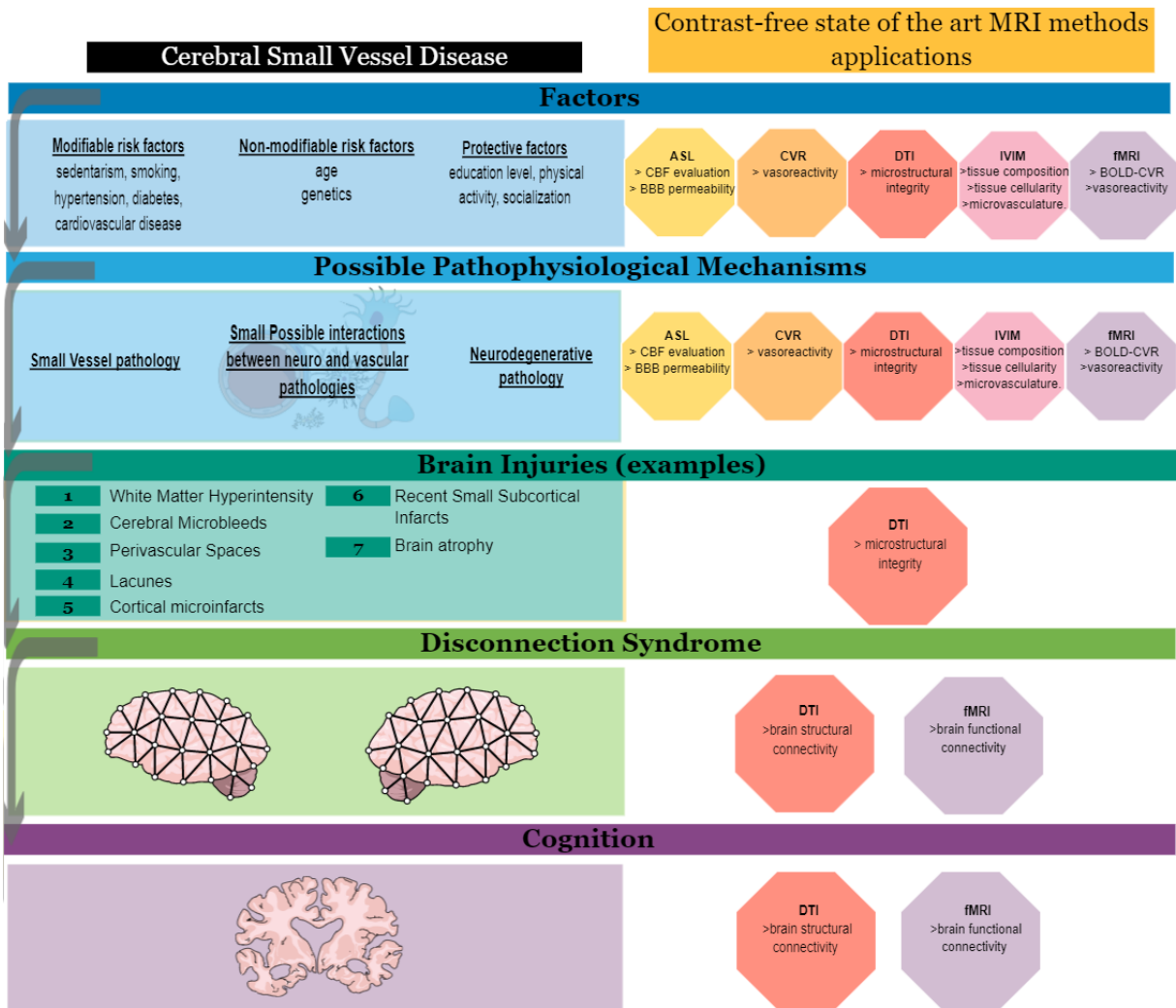
Figure 12 – Application of contrast agent-free MRI methods in cerebral small vessel disease (cSVD). Left box: description of research topics in cSVD. From top to bottom: risk and protective factors that may, respectively, contribute to the onset of the disease or to protect against it, followed by possible pathophysiological mechanisms not yet fully elucidated, including small vessel, neurodegenerative and mixed pathology, which translate into damage to the brain tissue, the most famous being WMH. The damage is said to have "distant" effects, impacting brain networks, making the disease a disconnect syndrome, which would help to understand the heterogeneity in terms of cognitive deficits presented by patients. Right box: description of contrast agent-free MRI techniques applied for each research topic mentioned in the left box. Each colored octagon represents an MRI technique previously applied and revised in the present paper, and the items represent which variables the technique may assess regarding the disease. ASL: arterial spin labeling. BBB: blood-brain barrier. BOLD: blood oxygen level-dependent. CBF: cerebral blood flow. CVR: cerebrovascular reactivity. DTI: diffusion tensor imaging. fMRI: functional magnetic resonance imaging. IVIM: intravoxel incoherent motion. MRI: magnetic resonance imaging. WMH: white matter hyperintensity. Figure created in the Mind the Graph platform <www.mindthegraph.com>.

6 WMH effects on Cortical Thickness, Brain Networks, and Information Processing Speed in non-demented Small Vessel Disease patients: A mediation study

6.1 Introduction

Cerebral small vessel disease (SVD) is the major contributor to vascular cognitive impairment (VCI) and dementia (162). White matter hyperintensities of presumed vascular origin (WMH), the most common imaging feature of SVD (37), are associated with cognitive impairment (285), especially processing speed deficits. However, these associations are generally weak and some studies showed no association with cognition. Therefore, it is unclear if and how WMH can impact cognition. Recent studies showed more precise quantification of micro-scale degeneration of white and gray matter, and functional and structural brain connectivity in cSVD. Such alterations have been associated with cognitive impairment (286, 180, 264). Several factors can justify it, including the location of the lesions (161), cortical thinning (287, 288), and brain network disruption (289, 213, 290, 291).

WMH foci can be divided topographically in several ways. A categorization that has been gaining strength divides WMH into deep (DWMH) and periventricular WMH (PVWMH) (292). Studies indicate that different risk factors (293) and genetic variants (294) are associated with specific patterns of WMH distribution. Periventricular foci seem to have a greater association with cognitive outcomes, including the digit symbol test (295) and other attention and executive function tests (296).

Gray matter atrophy has been proposed as a possible explanation for the link between cognitive deterioration and WMH in SVD patients (297, 298, 286). Cortical thinning has been shown to mediate the relationship between WMHs and cognitive decline (288, 299, 300). It is hypothesized that cortical atrophy is a distant effect of WMH (301, 302, 303), suggesting that such alteration should be studied together with vascular pathology in cSVD.

Recent analysis of topological networks of brain circuits suggests that modular and hierarchical structural networks are particularly suited to the functional integration of local (functionally specialized) neuronal operations underlying cognition. Complex network theory is particularly attractive when applied to the study of clinical neuroscience, where many cognitive and emotional disorders have been characterized as "disconnectivity" syndromes, as indicated by abnormal profiles of anatomical or functional connectivity between brain regions (2). Disruptions in structural and functional brain networks have provided important novel insights regarding the cognitive decline mechanisms in cSVD, and a recent review suggests the disease as a disconnection syndrome (166).

A systematic review with functional magnetic resonance imaging (fMRI) and electroencephalography (EEG) studies in cSVD suggests that damage of frontal-subcortical circuits and cholinergic fibers disrupts the connectivity among the Default Mode Network (DMN), FrontoParietal Control Network (FPCN), and Dorsal Attention Network (DAN), which are related to attentional control processes. It leads to deficits in IPS (291). Evidence also suggests that cortical atrophy must be considered in future studies to address its influence on the relationship between WMH and cognitive decline in cSVD.

Delayed IPS underlies attention deficits in many conditions and is one of the earliest cognitive impairments in cSVD patients. In an age-related cSVD group, it was shown that damage to frontal interhemispheric and thalamic projection fiber tracts underlying frontal-subcortical neuronal circuits was a predictor for processing speed performance (304). In another study, the effects of WMH on IPS were shown to be mediated by local network efficiency (213). Cortical atrophy was shown to mediate the effects of ischemic lesion on processing speed in cSVD patients (287).

In this study, we have three objectives. First, we investigated the relationship between WMH and cognition, by characterizing the effect of WMH distribution on IPS measures. Second, we aimed to better understand the relationship between WMH and cortical thickness and brain connectivity based on functional and structural networks. Third, we assessed whether the association between WMH and cognition is mediated by cortical thickness and/or brain connectivity. To this end, we used the RUN-DMC (Radboud University Nijmegen Diffusion tensor and Magnetic resonance imaging Cohort) databank consisting of 503 cSVD patients (305) .

6.2   Methods

Study sample

The study sample was drawn from the RUN DMC (Radboud University Nijmegen Diffusion tensor and Magnetic resonance imaging Cohort) study (305). 389 non-demented elderly, aged between 50-85 years, with cSVD were included. Participants underwent a structured questionnaire on demographics and vascular risk factors, a cognitive and motor assessment, followed by an MRI protocol including conventional MRI, DTI, and resting-state fMRI. The rationale and methodology have been described previously in detail (305).

MRI acquisition

Scans were acquired in a 1.5-Tesla Magnetom scanner (Siemens, Erlangen, Germany). A whole-brain 3D T1W imaging was performed using a magnetization-prepared rapid gradient-echo (MPRAGE) sequence (TR/TE/TI = 2250/3.68/850 ms; flip angle = 15°; voxel size = $1.0 \times 1.0 \times 1.0$ mm³). T2-weighted Fluid Attenuated Inversion Recovery (FLAIR)

sequence was used with the following parameters: TR/TE/TI = 9000/84/2200 ms; voxel size = 1.0 × 1.2 × 6.0 mm³ (including slice gap of 1 mm). DTI was acquired with the following parameters: TR/TE = 10100/93 ms; voxel size = 2.5 × 2.5 × 2.5 mm³; 4 unweighted scans, 30 diffusion-weighted scans, with a non-collinear orientation of the diffusion-weighting gradient, and b value = 900 s/mm²). Resting-state fMRI was acquired using a gradient-echo EPI sequence (TR/TE = 2400/40 ms; voxel size = 3.5 × 3.5 × 4.4 mm² (including slice gap of 0.4 mm)). During resting state, participants were told not to concentrate on any particular subject but to relax with their eyes closed. The complete scanning protocol took 31 minutes.

Neuropsychological assessment

Measurement of global cognitive function was assessed by the Mini-Mental State Examination (MMSE) (306). Information processing speed was evaluated with the Letter-Digit Substitution Task (LDST), a modified version of the Symbol Digit Modalities Test (SDMT) (20). The higher the LDST score, the better the information processing speed performance.

WMH segmentation

T1-weighted and FLAIR scans were processed with UBO Detector <https://cheba.unsw.edu.au/group/neuroimaging-pipeline> to segment WMH regions (307). Briefly, FLAIR images were registered to T1, and then warped to Diffeomorphic Anatomical Registration Through Exponentiated Lie Algebra (DARTEL) space. After non-brain tissue removal, FMRIB's Automated Segmentation Tool (FAST) was applied to FLAIR data to generate candidate clusters. A supervised learning algorithm, k-nearest neighbours (k-NN), was used to determine WMH clusters. Default settings with k = 5 and a probability threshold of 0.7 were used. Results were manually checked for segmentation quality. WMH was quantified as global volume, number of incidences (punctuate, focal, medium, and confluent), lobar volume, and lobar volume by hemisphere.

WMH mapping to strategic WM tracts

TOPMAL is a toolbox to map cSVD-related lesions to brain atlases, including John Hopkins University (JHU) WM Tractography Atlas (308) and Harvard-Oxford Subcortical Structural Atlas (309). The output can be directly used for the region of interest (ROI) LSM analyses (310). TOPMAL was developed as an extension of UBO Detector <https://cheba.unsw.edu.au/group/neuroimaging-pipeline>, an automated pipeline for WMH extraction. We used TOPMAL to map WMH to JHU WM atlas. The WMH masks from UBO Detector were in standard space (DARTEL space) (311), which enables further analyses regarding the lesion location. Flow field map was applied to JHU WM atlas to bring it to DARTEL space, and the resultant atlas was then applied to WMH maps derived from UBO Detector. The obtained image contained WMH regions overlapped with strategic WM tracts on the JHU WM atlas.

Total GM and WM volumes

Gray matter (GM), white matter (WM), cerebrospinal fluid (CSF) were automatically segmented on structure T1W images using the Statistical Parametric Mapping 12 <https://www.fil.ion.ucl.ac.uk/spm/> and CAT12 toolbox <https://www.neuro.uni-jena.de/vbm/>, and surface and thickness estimation for ROI analysis in the writing options. Total intracranial volume (TIV) was computed as the sum of GM, WM, and CSF volumes. Region-based Morphometry (RBM) analysis was performed by extracting the mean cortical thickness values for 68 ROIs defined by the Desikan-Killiany (DK) atlas (309) using standard procedures for ROI extraction. Data were entered in a statistical model to perform a multiple linear regression analysis by defining the association between WMH volume by territory or LDST with regional cortical thickness after controlling for age, sex and education. Statistical thresholds were set to p ≤ 0.01 (p-Holm Bonferroni corrected).

DTI analysis

A total of 389 diffusion MRI scans were included in the connectometry database. The accuracy of b-table orientation was examined by comparing fiber orientations with those of a population-averaged template (74). Affine distortion in our diffusion-weighted images from residual eddy-currents was minimized during MR acquisition and did not require further correction using post-processing methodology (312). The diffusion data were reconstructed in the MNI space using q-space diffeomorphic reconstruction (53) to obtain the spin distribution function (65). A diffusion sampling length ratio of 1.25 was used. The output resolution in diffeomorphic reconstruction was 2 mm isotropic. The restricted diffusion was quantified using restricted diffusion imaging (66). The tensor metrics were calculated. The Fractional Anisotropy (FA) values were used in the connectometry analysis.

Connectometry analysis

Diffusion MRI connectometry (313) was used to derive the correlational tractography that has FA correlated with WMH volumes by territory and LDST scores. Firstly, a nonparametric Spearman partial correlation was used to derive the correlation and the effect of age, sex, and education. A total of 389 subjects were included in the analysis. A t-score threshold ranging from 2 to 5 with steps of 1 was assigned and tracked using a deterministic fiber tracking algorithm (72) to obtain correlational tractography. A seed region was placed on the whole brain. The tracks were filtered by topology-informed pruning (314) with four iterations. An FDR threshold of 0.05 was used to select tracks. 4000 randomized permutations were applied to the group label to obtain the null distribution of the track length and estimate the false discovery rate.

Resting-state fMRI analysis

Resting-state fMRI signals were preprocessed using the CONN toolbox version 20b <https://www.nitrc.org/projects/conn>. Preprocessing steps included a standard pipeline (realignment and unwarp, slice-timing correction, structural unified segmentation and normalization, functional normalization, outlier detection, and smoothing with a 10-mm FWHM Gaussian kernel). The ART algorithm <http://www.nitrc.org/projects/artifact_detect/> was applied to detect motion during the functional scan. Time points in subjects' images were marked as outliers if the global signal exceeded five standard deviations from the mean or if scan-to-scan motion deviation exceeded 0.9 mm. Those outliers, in addition to the linear and polynomial trends of six head motion parameters, WM and CSF signal were included as nuisance regressors during the denoising procedure in the CONN toolbox. Data were also band-pass filtered at 0.008–0.09 Hz.

We performed seven seed-to-voxel analyses, each one corresponding to a resting-state network (RSN) from the CONN network cortical ROIs (HCP-ICA) (60): Default Mode Network (DMN), Sensorimotor Network (SMN), Salience Network, Dorsal Attention Network (DAN), Fronto-parietal Network (FPN), Language Network (LAN), and Cerebellar Network. Table 3 shows the details regarding the seeds from each RSN.

Single-subject seed-to-voxel correlation maps were calculated by extracting the residual BOLD time course from each seed and computing Pearson's correlation coefficients between that time course and the ones of all other voxels in the brain. Correlation coefficients were normalized to z-values via Fisher's z-transformation. We implemented a multiple linear regression analysis for each seed at group level by defining the association between WMH volume by territory or LDST with functional connectivity after controlling for age, sex and education. Statistical thresholds were set to $p < 0.001$ (uncorrected) at single voxel level, and the resulting cluster(s) were thresholded to a cluster-level Family-wise error (FWE) $p < 0.05$.

Statistical analyses

A hierarchical multiple regression analysis was performed to examine the unique contribution of global (total WMH, PVWMH, and DWMH) and regional (lobes, lobes by hemisphere, and WMH loadings on strategic WM tracts) structural measures in the prediction of LDST scores. An LDST score was the dependent variable in each instance, and a global volume or regional structural measure was the independent variable. Age, sex, and education were considered in the regression model as control variables. Firstly, we entered LDST scores as the dependent variables and the control variables as independent variables (Model 1). Then, we added global or regional structural volume as the independent variable (Model 2). The independent variables were examined for collinearity before the hierarchical multiple regression analysis was performed. The variance inflation factor (all less than 10.0) and collinearity tolerance (all greater than 0.7) suggest that the estimated betas are well established in the following regression model. Changes in R^2 and the corresponding p-values were reported

Chapter 6. WMH effects on Cortical Thickness, Brain Networks, and Information Processing Speed in non-demented Small Vessel Disease patients: A mediation study

74

Table 3 – Resting-state networks (RSNs) from the CONN network cortical ROIs (HCP-ICA) atlas, its seeds, and coordinates.[1]

Resting-state Network (RSN)	Seeds (Coordinates)
Default Mode Network (DMN)	DefaultMode.MPFC (1,55,-3)
	DefaultMode.LP (L) (-39,-77,33)
	DefaultMode.LP (R) (47,-67,29)
	DefaultMode.PCC (1,-61,38)
SensoriMotor Network (SMN)	SensoriMotor.Lateral (L) (-55,-12,29)
	SensoriMotor.Lateral (R) (56,-10,29)
	SensoriMotor.Superior (0,-31,67)
Visual Network	Visual.Medial (2,-79,12)
	Visual.Occipital (0,-93,-4)
	Visual.Lateral (L) (-37,-79,10)
	Visual.Lateral (R) (38,-72,13)
Salience Network	Salience.ACC (0,22,35)
	Salience.AInsula (L) (-44,13,1)
	Salience.AInsula (R) (47,14,0)
	Salience.RPFC (L) (-32,45,27)
	Salience.RPFC (R) (32,46,27)
	Salience.SMG (L) (-60,-39,31)
	Salience.SMG (R) (62,-35,32)
Dorsal Attention Network (DAN)	DorsalAttention.FEF (L) (-27,-9,64)
	DorsalAttention.FEF (R) (30,-6,64)
	DorsalAttention.IPS (L) (-39,-43,52)
	DorsalAttention.IPS (R) (39,-42,54)
FrontoParietal Network (FPN)	FrontoParietal.LPFC (L) (-43,33,28)
	FrontoParietal.PPC (L) (-46,-58,49)
	FrontoParietal.LPFC (R) (41,38,30)
	FrontoParietal.PPC (R) (52,-52,45)
Language Network (LAN)	Language.IFG (L) (-51,26,2)
	Language.IFG (R) (54,28,1)
	Language.pSTG (L) (-57,-47,15)
	Language.pSTG (R) (59,-42,13)
Cerebellar Network	Cerebellar.Anterior (0,-63,-30)
	Cerebellar.Posterior (0,-79,-32)

Medial prefrontal cortex (MPFC), precuneus/posterior cingulate cortex (PCC), lateral parietal (LP); anterior cingulate cortex (ACC), anterior insula (AInsula), rostral prefrontal cortex (RPFC), and supramarginal gyrus (SMG), frontal eye field (FEF), intraparietal sulcus (IPS), lateral prefrontal cortex (LPFC), posterior parietal cortex (PPC), inferior frontal gyrus (IFG), posterior superior temporal gyrus (pSTG).

for comparison. All results were reported in raw p-values, and the ones that survived the Bonferroni correction for multiple tests were marked.

A mediation analysis was used to test whether alterations in cortical thickness, structural or functional connectivity are on the potential causal pathway of the association between WMH volume and IPS (Figure 13). We used bootstrapping (5000 samples) to calculate bias-corrected 95% Confidence Interval (CI) with the PROCESS statistical package for SPSS (315). Analyses were conducted using PROCESS model 4, N = 389. Age, sex, and education were used as covariates. Total WMH (cited as WMH from now on), PVWMH, and DWMH volumes were the independent variable; LDST scores, the dependent variable. Mediators were regional cortical thickness, fractional anisotropy, and functional connectivity, which were statistically significant in our previous steps. Firstly, we tested the direct association between WMH/PVWMH/DWMH volume and LDST scores (path c). Then, we tested the association between WMH/PVWMH/DWMH volume and the mediator (path a) and the association between WMH/PVWMH/DWMH volume and LDST scores adjusting for the mediator (path c').

Finally, we tested the association between the mediator and LDST adjusted for the effect of WMH/PVWMH/DWMH on LDST scores (path b). Standardized regression coefficients were reported when significant ($p \leq 0.05$).
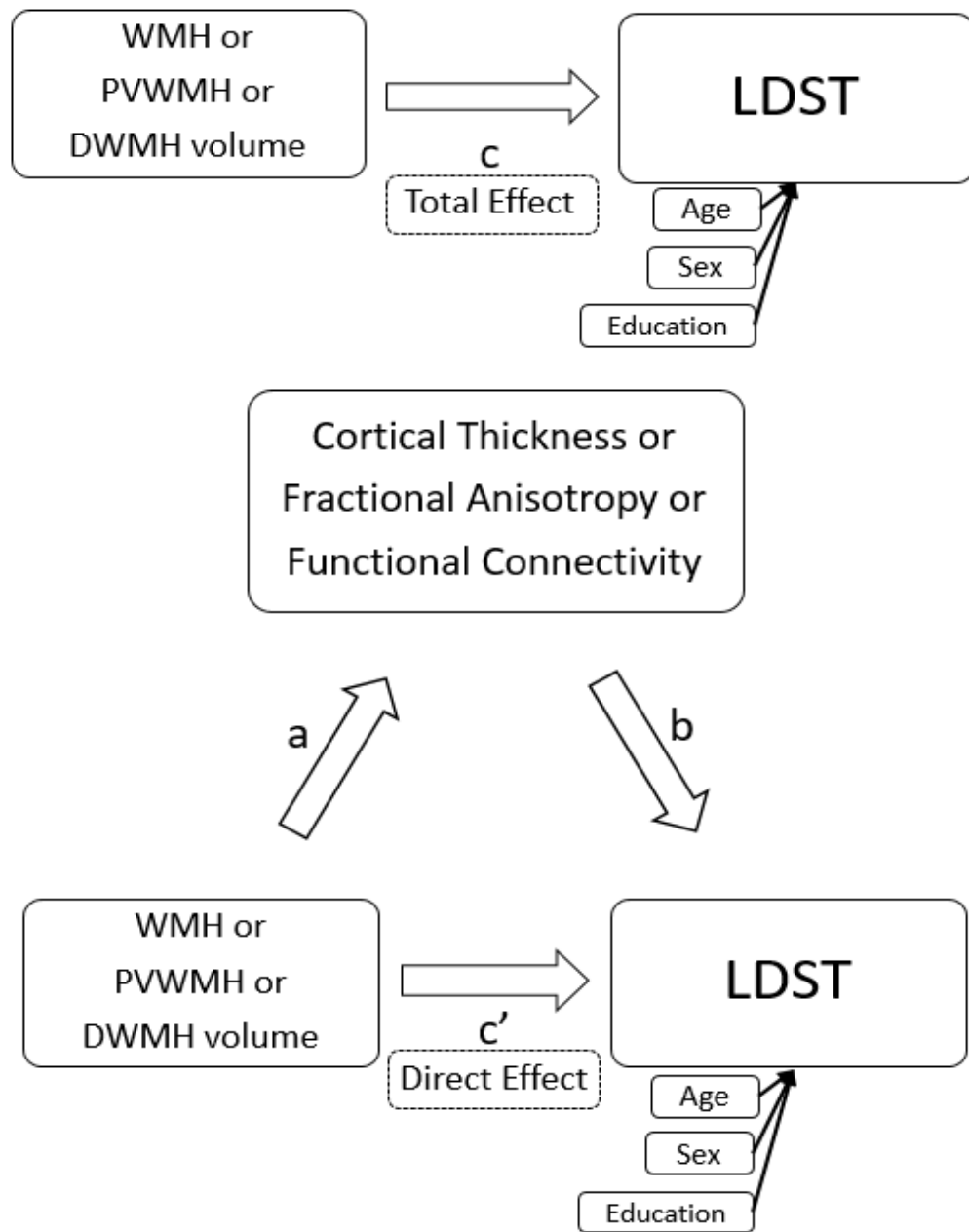
Figure 13 – Simple Mediation Model. a = the association between WMH/PVWMH/DWMH volume and MRI metric. b = the association between MRI metric (Cortical Thickness or Fractional Anisotropy or Functional Connectivity) and LDST adjusted for the effect of WMH/PVWMH/DWMH on LDST scores. c' = the association between WMH/PVWMH/DWMH volume and LDST scores adjusting for MRI metric. c = the direct association between WMH/PVWMH/DWMH volume and MRI metric. Age, sex, and education were included as confounders. WMH: white matter hyperintensity. PVWMH: periventricular WMH. DWMH: deep WMH.

6.3   Results

Study population

Table 4 shows the general characteristics of the sample, which consisted of 389 individuals with a mean age of 65.33 ± 8.72 years; 179 of the 389 participants (46%) were women, 279 (72%) had hypertension, and 42 (11%) had diabetes.

Table 4 – General characteristics of the study population. WMH = white matter hyperintensity.

Characteristic	Value (n =389)	Min-Max
Demographics		
Age (years)[1]	65.33 ± 8.72	49.67-85.39
Number of women (%)	179 (46%)	
Number of women (%)	179 (46%)	
Cardiovascular risk factors		
Hypertension (%)	279 (72%)	
Diabetes (%)	42 (11%)	
Smoking (%)	263 (68%)	
Hypercholesterolemia (%)	176 (45%)	
Cardiovascular morbidity (%)	180 (46%)	
Malignancy baseline (%)	41 (11%)	
Body-mass index (kg/m²)[1]	27 ± 4	17.7-43.4
Lifestyle fators		
Cardiovascular morbidity (%)		
Never (%)	126 (32%)	
Former (%)	207 (53%)	
Current (%)	56 (14.4%)	
Cognitive scores		
Mini-mental state examination total score[1]	28.20 ± 1.63	22 to 30
Letter-digit substitution test[1]	27.54 ± 9.68	7 to 55
Cognitive index[1]	0.029 ± 0.702	-1.57 to 1.61
Cerebral small vessel disease characteristics		
Total WMH volume (mm³)[1]	9979.65 ± 12530.76	30.38-77878.81
Periventricular WMH volume (mm³)[1]	6701.59 ± 7933.47	20.25-36088.88
Deep WMH volume (mm³)[1]	3212.98 ± 5377.02	0-47651.63

[1] Means ± standard deviations are shown.

WMH associations with cortical thickness

WMH, PVWMH and DWMH volumes were negatively and significantly associated with the cortical thickness of frontal, temporal, and occipital areas after controlling for age, sex, and education ($p < 0.01$, Holm Bonferroni corrected) (Figure 14 and Table 5). The spatial distribution pattern of associations was similar for WMH, PVWMH and DWMH volumes (Figure 14). The cortical thickness and volume of the left transverse temporal region was the most significantly associated with WMH, PVWMH and DWMH volumes. The number of regions whose PVWMH volume was significantly associated with the cortical thickness was almost double (n = 12) than that obtained with the DWMH volume (n = 7). Associations were similar when considering the regions by hemisphere and the number of regions (Table 5).

Figure 14 – Multiple linear regression analysis results define the association between WMH volume by territory (independent variable) and regional cortical thickness (dependent variable) after controlling for age, sex, and education. Statistical thresholds were set to $p < 0.01$ (p-Holm Bonferroni corrected). WMH: white matter hyperintensity. PVWMH: periventricular WMH. DWMH: deep WMH.

Table 5 – T and p-values of the associations between WMH/PVWMH/DWMH volume with regional cortical thickness after controlling for age, sex, and education (p < 0.01, Holm Bonferroni corrected).

WMH territory	Desikan Killiany atlas (309) region	t-value	p-value
WMH	Transverse temporal L	-7.06	0.000000
	Pars opercularis L	-5.01	0.00002
	Superior temporal L	-4.03	0.002
	Lingual L	-3.93	0.001
	Supramarginal L	-3.56	0.01
	Pars orbitalis L	-3.31	0.01
	Pars triangularis L	-3.09	0.05
	Transverse temporal R	-5.02	0.00003
	Pars opercularis R	-4.83	0.00002
	Lingual R	-4.18	0.001
	Supramarginal R	-3.51	0.003
	Pars triangularis R	-3.45	0.0015
	Pericalcarine R	-3.13	0.006
	Superior temporal R	-2.65	0.004
PVWMH	Transverse temporal L	-6.70	0.000000
	Pars opercularis L	-5.64	0.000000
	Superior temporal L	-4.30	0.001
	Lingual L	-4.14	0.001
	Pars triangularis L	-3.53	0.01
	Supramarginal L	-3.29	0.03
	Transverse temporal R	-4.88	0.00003
	Pars opercularis R	-4.77	0.00003
	Lingual R	-4.23	0.0002
	Pericalcarine R	-3.61	0.005
	Pars triangularis R	-3.49	0.02
	Supramarginal R	-3.46	0.01
DWMH	Transverse temporal L	-6.12	0.000000
	Supramarginal L	-3.23	0.03
	Pars opercularis L	-3.19	0.040
	Superior temporal L	-2.87	0.002
	Transverse temporal R	-4.25	0.00025
	Pars opercularis R	-3.96	0.002
	Lingual R	-3.33	0.01

WMH associations with fractional anisotropy

The connectometry analysis found many tracts showing FA positively correlated with WMH, PVWMH, or DWMH volumes (p-FDR ≤ 0.05) after regressing out the effects of age, sex, and education for T = 2, T = 3, T= 4 and T = 5 (Figure 15). No significant result was found in tracks with FA negatively correlated with WMH, PVWMH and DWMH (p-FDR ≤ 0.05).
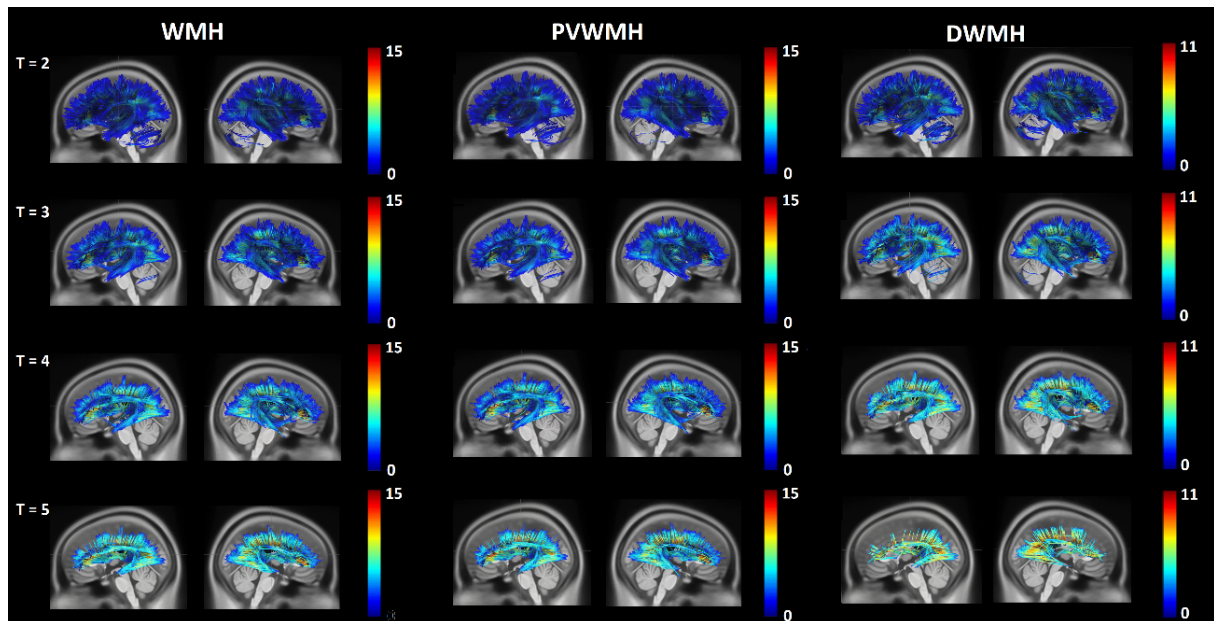
Figure 15 – Tracks with FA positively correlated with WMH, PVWMH and DWMH volumes, respectively at T = 2, T = 3, T = 4 and T =5 (p-FDR ≤ 0.05). A nonparametric Spearman partial correlation was used to derive the correlation, and the effect of sex, age, and education was removed using a multiple regression model. FA: Fractional Anisotropy. WMH: white matter hyperintensity. PVWMH: periventricular WMH. DWMH: deep WMH.

For T = 2, the Corpus Callosum Body has the most significant percentage of the number of tracts (p-FDR ≤ 0.05) for the associations between FA and WMH, PVWMH and DWMH (Table 6). The right Inferior Longitudinal Fasciculus and left Superior Corticostriatal complete the top three. For T = 3, the Corpus Callosum Body remains as the first regarding the number of tracts. The main change is substituting the right Inferior Longitudinal Fasciculus for the right Posterior Thalamic Radiation to complete the top three. While the T becomes higher and the analysis more specific, the Corpus Callosum loses the top position for the right Thalamic Radiation Posterior. The Corpus Callosum and the left Posterior Thalamic Radiation remain at the top three. Another finding is that, while the T becomes more restrictive, the top three are responsible for a greater percentage of the total number of tracts. As an example, for WMH associations with FA, the top three corresponds to 22.85% of the number of tracts at T = 2, while it increases to 45.64% for T = 5. For associations between PVWMH and FA, the top three corresponds to 23.29% of the tracts at T =2, while it increases to 40.63% for T = 5. For associations between DWMH and FA, the top three corresponds to 23.42% of the tracts at T

=2, while it increases to 62.37% for T = 5.

Table 6 – The three tracks with the biggest percentage (%) of the number of tracts identified in the associations between FA and LDST scores, respectively at T = 2, T = 3, T = 4, and T = 5 (p-FDR ≤ 0.05). A nonparametric Spearman partial correlation was used to derive the correlation, and the effects of sex, age, and education were removed using a multiple regression model. FA: Fractional Anisotropy. LDST: Letter-Digit Substituion Test. L: left. R: right.

	WMH	PVWMH	DWMH
T = 2	9.24% Corpus Callosum Body 7.03% Inferior Longitudinal Fasciculus R 6.58% Corticostriatal Tract Superior R	9.76% Corpus Callosum Body 6.94% Inferior Longitudinal Fasciculus R 6.59% Corticostriatal Tract Superior R	9.48% Corpus Callosum Body 7.65% Corticostriatal Tract Superior R 6.29% Inferior Longitudinal Fasciculus R
T = 3	12.30% Corpus Callosum Body 7.66% Corticostriatal Tract Superior R 7.18% Thalamic Radiation Posterior R	12.48% Corpus Callosum Body 8.11% Thalamic Radiation Posterior R 7.13% Corticostriatal Tract Superior R	12.54% Corpus Callosum Body 8.95% Corticostriatal Tract Superior R 8.49% Thalamic Radiation Posterior R
T = 4	15.39% Corpus Callosum Body 11.15% Thalamic Radiation Posterior R 8.62% Thalamic Radiation Posterior L	14.42% Corpus Callosum Body 11.38% Thalamic Radiation Posterior R 8.26% Thalamic Radiation Posterior L	16.43% Thalamic Radiation Posterior R 14.06% Corpus Callosum Body 12.06% Thalamic Radiation Posterior L
T = 5	18.72% Thalamic Radiation Posterior R 15.88% Corpus Callosum Body 11.04% Thalamic Radiation Posterior L	17.13% Thalamic Radiation Posterior R 14.14% Corpus Callosum Body 9.36% Thalamic Radiation Posterior L	34.57% Thalamic Radiation Posterior R 17.21% Thalamic Radiation Posterior L 10.59% Corpus Callosum Body

WMH associations with resting-state functional connectivity

Functional connectivity from the SMN, DMN, Visual, FPN, and DAN networks was significantly associated with the WMH burden (Figure 16). Functional connectivity from the SMN, Salience, Visual, DAN, FPN, and Cerebellar networks was significantly associated with PWMH burden (Figure 16). Functional connectivity from the SMN, DMN, FPN, and DAN was associated with DWMH burden (Figure 16). The number of RSN associated with lesion burden was the biggest for the PVWMH (n = 6), followed by WMH (n = 5) and DWMH (n = 4).

Figure 16 – Statistical maps from the associations between seed-to-voxel functional connectivity and LDST scores after controlling for age, sex, and education. Results were thresholded at p-uncorrected < 0.001 (voxel level) and then corrected at the cluster level using a family-wise error (FWE) of p < 0.05. WMH: white matter hyperintensity. PVWMH: periventricular WMH. DWMH: deep WMH.

Hierarchical multiple regression

The global structural volumes were significantly associated with LDST scores (Table 7). No significant association was found between the number of incidences (punctuate, focal, medium, or confluent) and LDST scores (Table 7). The associations with WMH, PVWMH, and DWMH were negative, with total WMH volume being the most significant one (ß = -0.116, p = 0.009). Regarding regional structural volumes, when considering lobar WMH, an association was found only between parietal WMH volume and LDST scores (p = 0.05, Bonferroni corrected). Associations were statistically significant for bilateral parietal volume (p = 0.05, Bonferroni corrected) when considering lobar WMH by hemisphere. When considering the associations of WMH loadings on strategic white matter fiber tracts with LDST scores, only the WMH loading on the left corticospinal tract survived the statistical threshold (p < 0.05, Bonferroni corrected).

Table 7 – Associations of global measures (volume and number) with LDST scores. WMH: white matter hyperintensity. PVWMH: periventricular WMH. DWMH: deep WMH. LDST: Letter-Digit Substitution Test

Global structural measure	β	ΔR^2	R^2	p
WMH volume (cm³)[1]	-0.116	1.1%	39.1%	**0.009**
PVWMH volume (cm³)[2]	-0.106	0.9%	38.9%	**0.019**
DWMH volume (cm³)[2]	-0.106	1.0%	39.0%	**0.013**
Total number of WMH incidences[1]	-0.010	0.0%	38.0%	0.825
Number of punctuate incidences[1]	-0.045	0.2%	38.2%	0.278
Number of focal incidences*[1]	0.002	0.0%	38.0%	0.968
Number of medium incidences[1]	-0.001	0.0%	38.0%	0.987
Number of confluent incidences[1]	-0.15	0.0%	38.0%	0.747

[1] After regressing out effects of age, sex, and education level. In bold associations are statistically significant (p < 0.05).
[2] After regressing out effects of age, sex, and education level. In bold associations are statistically significant after Bonferroni correction (p < 0.025).

LDST associations with cortical thickness

Cortical thickness values from frontal, temporal, and cingulate areas were positively and significantly associated with LDST scores after controlling for age, sex, and education (p < 0.01, Holm Bonferroni corrected) (Figure 17 and Table 8).
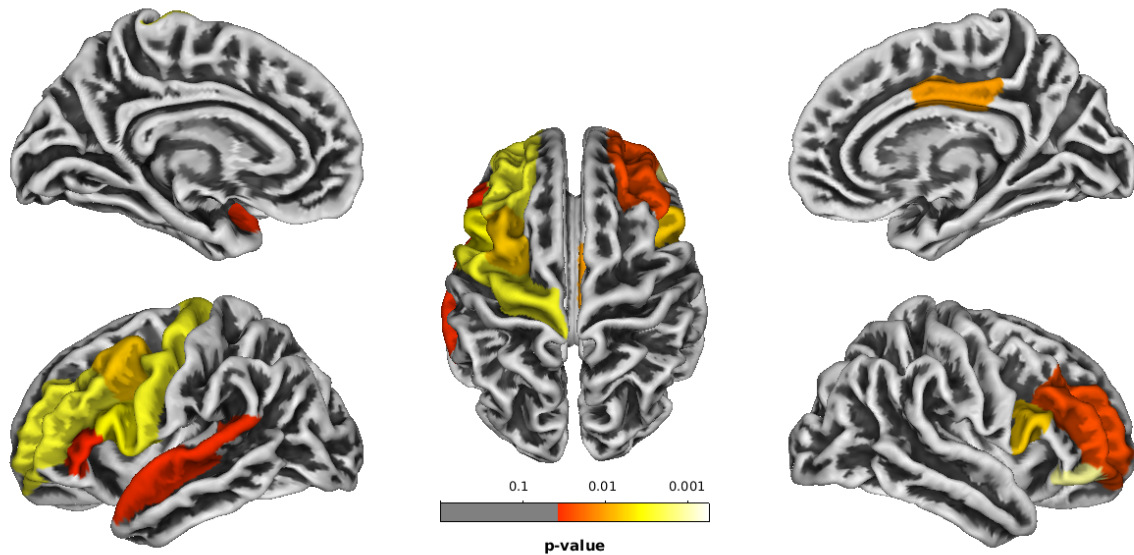
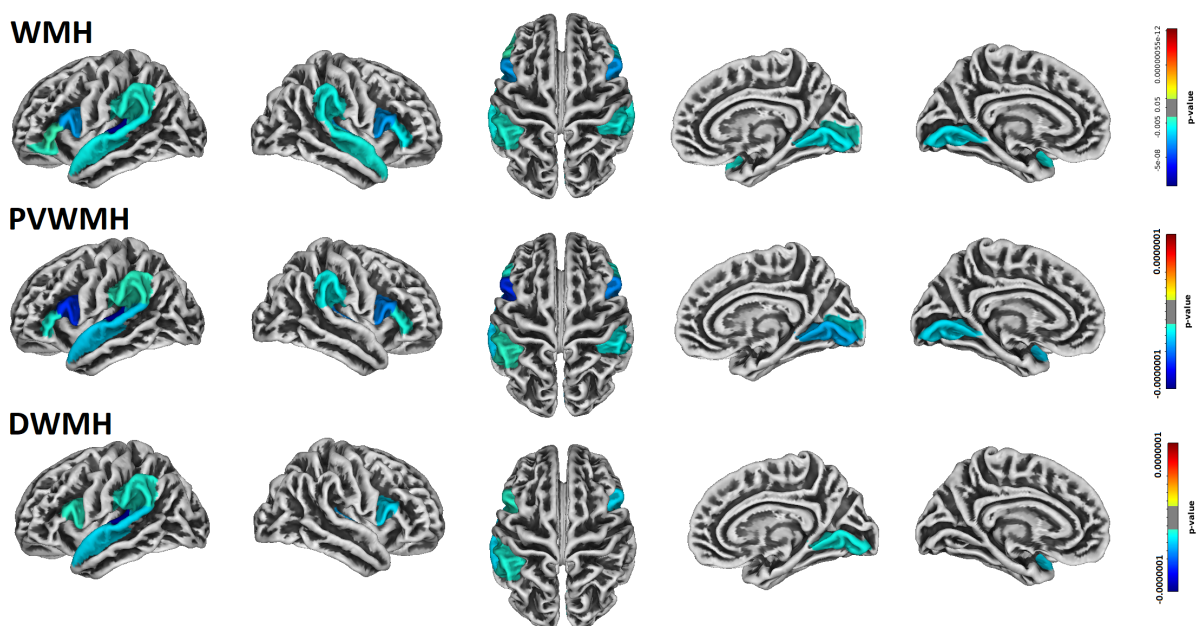Figure 17 – Multiple linear regression analysis results define the association between LDST scores (independent variable) and regional cortical thickness (dependent variable) after controlling for age, sex, and education. Statistical thresholds were set to p < 0.01 (p-Holm Bonferroni corrected). LDST: Letter-Digit Substitution Test.

Table 8 – T and p-values of the associations between LDST scores with regional cortical thickness after controlling for age, sex, and education (p < 0.01, Holm Bonferroni corrected). LDST: Letter-Digit Substitution Test.

Hemisphere	Desikan Killiany atlas (309) region	t	p
Left	Pars opercularis	3.60	0.0037
	Rostral middle frontal	3.42	0.0024
	Caudal middle frontal	3.40	0.006
	Pars triangularis	3.18	0.037
	Superior temporal	3.16	0.034
	Precentral	3.15	0.003
Right	Pars orbitalis	4.17	0.001
	Pars opercularis	3.63	0.006
	Posterior cingulate	3.62	0.01
	Rostral middle frontal	3.36	0.02

LDST Associations with fractional anisotropy

The connectometry analysis found many tracts showing FA positively correlated with LDST (p-FDR ≤ 0.05) after regressing the effects of age, sex, and education for T = 2, T = 3, T = 4, and T = 5 (Figure 18). No significant result was found in tracks with FA negatively correlated with LDST (p-FDR ≤ 0.05).
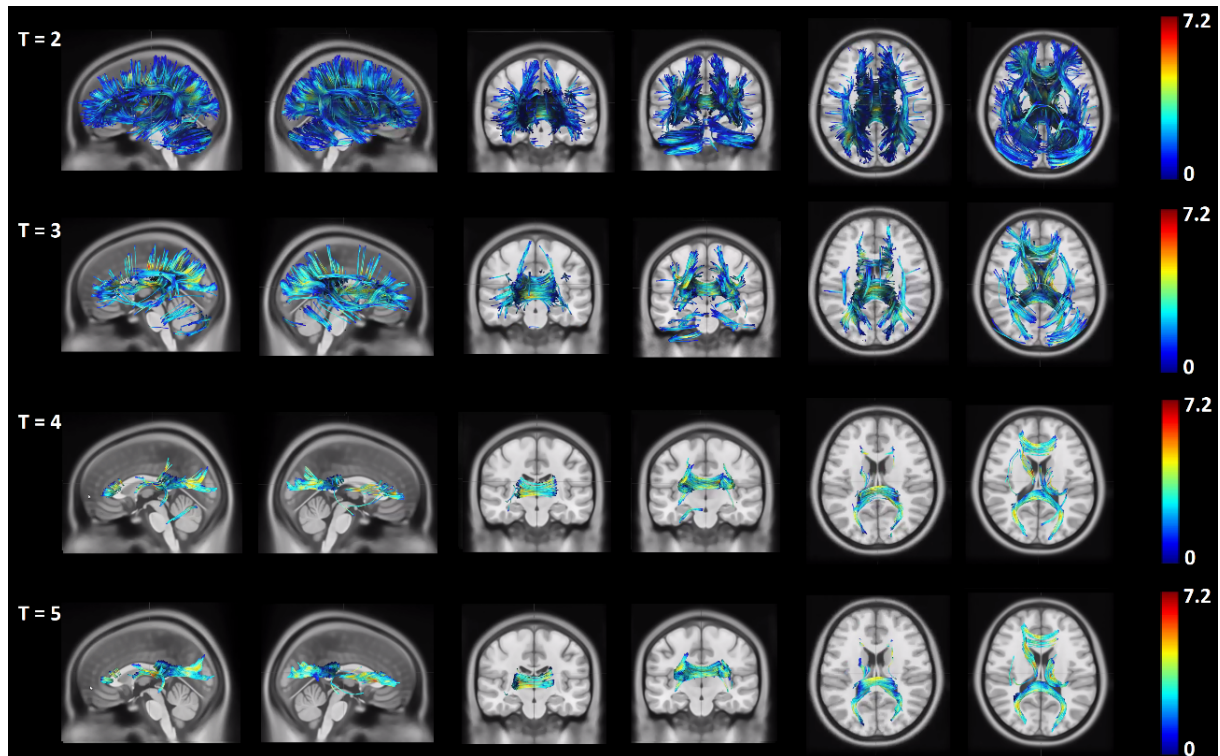
Figure 18 – Tracks with FA positively correlated with LDST (p-FDR ≤ 0.05). A nonparametric Spearman partial correlation was used to derive the correlation, and the effect of sex, age, and education was removed using a multiple regression model. FA: Fractional Anisotropy. LDST: Letter-Digit Substitution Test.

For T = 2, the corpus callosum major forceps showed the biggest percentage of the number of tracts (p-FDR ≤ 0.05) for the associations between FA and LDST scores (Table 9). Bilateral thalamic radiation posterior, right anterior corticostriatal tract, and corpus callosum body complete the top five. For T = 3, the right thalamic radiation posterior became the one with the biggest percentage of the tracts. While the T became higher and the analysis more specific, the left thalamic radiation posterior assumed the top position. The top five were entirely composed of thalamic radiation and callosal tracts. Another finding is that, while the T was becoming more restrictive, the top five became responsible for a bigger percentage of the tracts. For example, for LDST associations with FA, the top five corresponded to 52.3% of the tracts at T = 2; it increased to 94.4% at T = 5. For T = 5, the remaining volume of tracts was composed by 2.5% of right thalamic radiation anterior, 1.1% of right corticostriatal tract anterior, 0.9% of right Acoustic Radiation, 0.5% of left thalamic radiation superior, 0.3% of

corpus callosum minor forceps, 0.2% of left superior longitudinal fasciculus, 0.06% of left cingulum parahippocampal parietal, and 0.04% of corpus callosum tapetum.

Table 9 – The three tracks with the biggest percentage (%) of the number of tracts identified in the associations between FA and LDST scores, respectively at T = 2, T = 3, T = 4, and T = 5 (p-FDR ≤ 0.05). A nonparametric Spearman partial correlation was used to derive the correlation, and the effects of sex, age, and education were removed using a multiple regression model. FA: Fractional Anisotropy. LDST: Letter-Digit Substitution Test. L: left. R: right.

T = 2	T = 3	T = 4	T = 5
15.6% Corpus Callosum Forceps Major	22.8% Thalamic Radiation Posterior R	33.5% Thalamic Radiation Posterior R	39.9% Thalamic Radiation Posterior L
11.2% Thalamic Radiation Posterior R	18.8% Corpus Callosum Forceps Major	32.0% Thalamic Radiation Posterior L	37.1% Thalamic Radiation Posterior R
9.2% Corticostriatal Tract Anterior R	18.7% Thalamic Radiation Posterior L	12.8% Corpus Callosum Forceps Major	10.4% Corpus Callosum Body
9.0% Thalamic Radiation Posterior L	8.4% Corpus Callosum Body	10.2% Corpus Callosum Body	4.2% Corpus Callosum Forceps Major
7.3% Corpus Callosum Body	6.6% Corticostriatal Tract Anterior R	4.2% Corpus Callosum Forceps Minor	2.8% Thalamic Radiation Superior R

Chapter 6. WMH effects on Cortical Thickness, Brain Networks, and Information Processing Speed in non-demented Small Vessel Disease patients: A mediation study

88

LDST associations with Resting-state fMRI

Functional connectivity from the SMN, DMN, Language, Visual, and FPN Networks was significantly associated with LDST scores (Figure 19, Table 10).
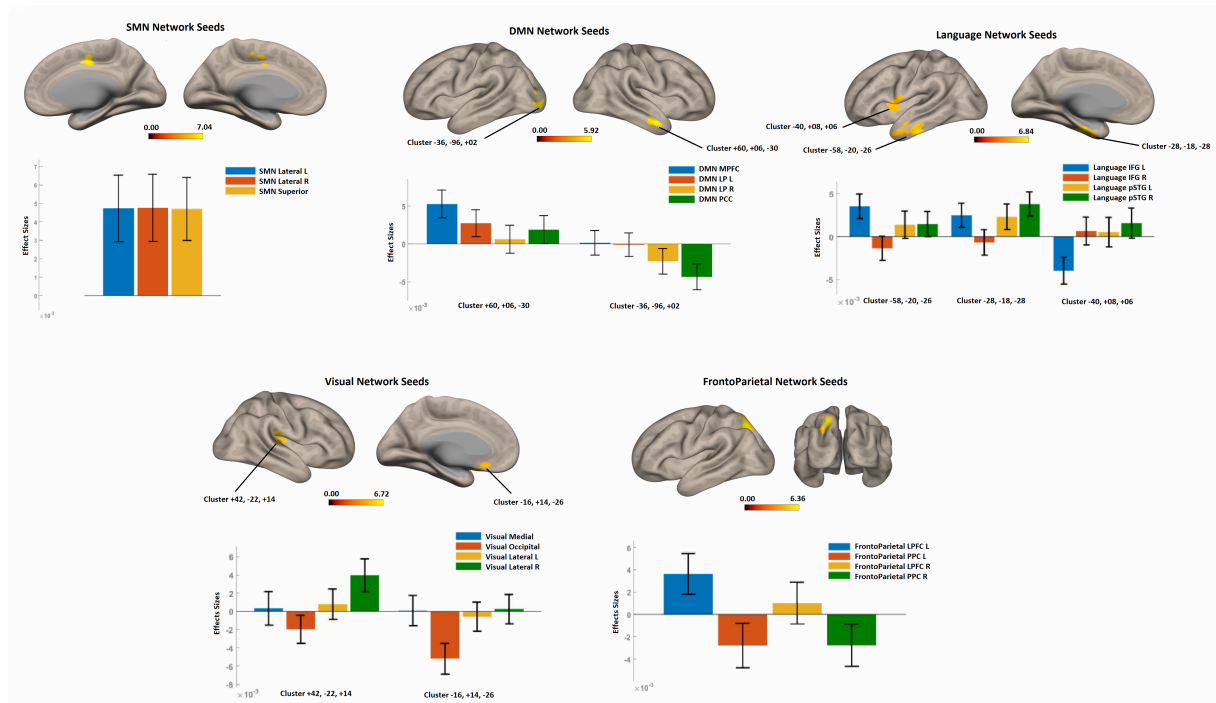
Figure 19 – Statistical maps and Effect Size from the associations between seed to voxel functional connectivity and LDST scores after controlling for age, sex and education in one sample with 389 small vessel disease patients without dementia. Note : Results show connectivity between the each network seeds and the voxels from whole-brain associated with LDST scores after controlling for age, sex and education. Results are thresholded at the voxel-level at p uncorrected < 0.001 and then corrected at the cluster-level using a family-wise error (FWE) of p < 0.05. LDST: Letter-Digit Substitution Test.

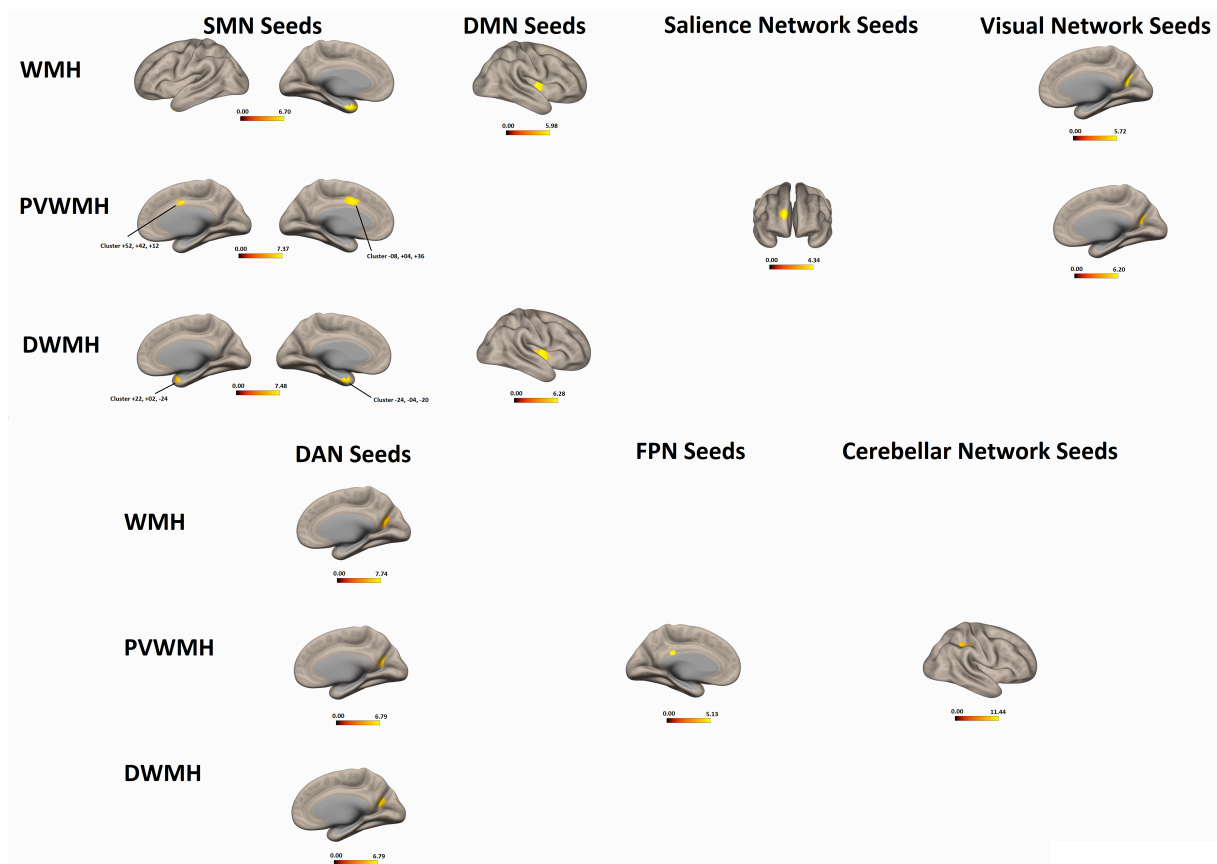**Table 10 – Composition of the clusters from the association between seed-to-voxel functional connectivity and LDST scores after controlling for age, sex, and education level.[1]**

	Cluster (x, y, z)	size	size p-FWE	peak p-uncorrected	Composition of the cluster
SMN Seeds	+12, -08, +40	140	0.033	0.00002	51 voxels (36%) covering 2% of atlas.AC (Cingulate Gyrus, anterior division) 25 voxels (18%) covering 4% of atlas.SMA r (Juxtapositional Lobule Cortex -formerly Supplementary Motor Cortex- Right) 13 voxels (9%) covering 2% of atlas.SMA L (Juxtapositional Lobule Cortex -formerly Supplementary Motor Cortex- Left) 3 voxels (2%) covering 0% of atlas.PreCG r (Precentral Gyrus Right) 2 voxels (1%) covering 0% of atlas.PreCG l (Precentral Gyrus Left) 2 voxels (1%) covering 0% of atlas.PC (Cingulate Gyrus, posterior division) 44 voxels (31%) covering 0% of atlas.not-labeled
DMN Seeds	+60, +06, -30	138	0.026	0.000011	86 voxels (62%) covering 21% of atlas.aMTG r (Middle Temporal Gyrus, anterior division Right) 30 voxels (22%) covering 1% of atlas.TP r (Temporal Pole Right) 2 voxels (1%) covering 0% of atlas.pMTG r (Middle Temporal Gyrus, posterior division Right) 20 voxels (14%) covering 0% of atlas.not-labeled
	-36, -96, +02	120	0.0475	0.000007	95 voxels (79%) covering 4% of atlas.OP l (Occipital Pole Left) 16 voxels (13%) covering 1% of atlas.iLOC l (Lateral Occipital Cortex, inferior division Left) 9 voxels (8%) covering 0% of atlas.not-labeled
Language Network Seeds	-58, -20, -26	358	0.000038	0.000001	141 voxels (39%) covering 14% of atlas.pITG l (Inferior Temporal Gyrus, posterior division Left) 80 voxels (22%) covering 3% of atlas.TP l (Temporal Pole Left) 36 voxels (10%) covering 3% of atlas.pMTG l (Middle Temporal Gyrus, posterior division Left) 27 voxels (8%) covering 6% of atlas.aMTG l (Middle Temporal Gyrus, anterior division Left) 11 voxels (3%) covering 3% of atlas.aITG l (Inferior Temporal Gyrus, anterior division Left) 63 voxels (18%) covering 0% of atlas.not-labeled
	-28, -18, -28	246	0.000753	0.000001	169 voxels (69%) covering 29% of atlas.aPaHC l (Parahippocampal Gyrus, anterior division Left) 29 voxels (12%) covering 4% of atlas.Hippocampus l 17 voxels (7%) covering 5% of atlas.aTFusC l (Temporal Fusiform Cortex, anterior division Left) 3 voxels (1%) covering 0% of atlas.pTFusC l (Temporal Fusiform Cortex, posterior division Left) 1 voxels (0%) covering 0% of atlas.pPaHC l (Parahippocampal Gyrus, posterior division Left) 27 voxels (11%) covering 0% of atlas.not-labeled
	-40, +08, +06	153	0.012941	0.000076	52 voxels (34%) covering 5% of atlas.CO l (Central Opercular Cortex Left) 37 voxels (24%) covering 1% of atlas.PreCG l (Precentral Gyrus Left) 32 voxels (21%) covering 2% of atlas.IC l (Insular Cortex Left) 13 voxels (8%) covering 4% of atlas.FO l (Frontal Operculum Cortex Left) 8 voxels (5%) covering 1% of atlas.IFG oper l (Inferior Frontal Gyrus, pars opercularis Left) 11 voxels (7%) covering 0% of atlas.not-labeled
Visual Network Seeds	+42, -22, +14	198	0.004780	0.000001	77 voxels (39%) covering 14% of atlas.PO r (Parietal Operculum Cortex Right) 59 voxels (30%) covering 21% of atlas.HG r (Heschl's Gyrus Right) 39 voxels (20%) covering 4% of atlas.CO r (Central Opercular Cortex Right) 15 voxels (8%) covering 1% of atlas.IC r (Insular Cortex Right) 4 voxels (2%) covering 1% of atlas.PT r (Planum Temporale Right) 4 voxels (2%) covering 0% of atlas.not-labeled
	-16, +14, -26	133	0.034675	0.000006	83 voxels (62%) covering 5% of atlas.FOrb l (Frontal Orbital Cortex Left) 23 voxels (17%) covering 2% of atlas.SubCalC (Subcallosal Cortex) 27 voxels (20%) covering 0% of atlas.not-labeled
FrontoParietal Seeds	-20, -64, +50	272	0.000398	0.000016	224 voxels (82%) covering 5% of atlas.sLOC l (Lateral Occipital Cortex, superior division Left) 1 voxels (0%) covering 0% of atlas.SPL l (Superior Parietal Lobule Left) 47 voxels (17%) covering 0% of atlas.not-labeled

Note: Results show connectivity between the each network seeds and the voxels from whole-brain associated with LDST scores after controlling for age, sex and education. Results are thresholded at the voxel level at p-uncorrected < 0.001 and then corrected at the cluster level using a family-wise error (FWE) of $p < 0.05$. SMN: sensorio-motor network. DMN: default mode network. LDST: Letter-Digit Substitution Test.

Mediation Analysis

Table 11 presents the direct (path c), path a, path b, path c', and indirect (mediation) effects of WMH/PVWMH/DWMH and regional cortical thickness on LDST scores. The higher the volume of lesion, the lower the LDST scores (direct effect). The higher the lesion volume, the lower the regional cortical thickness (path a). The higher the regional cortical thickness, the higher the LDST scores (path b). The indirect (mediation) effect of WMH and PVWMH volumes on LDST scores was significantly mediated by the regional cortical thickness of the bilateral pars opercularis, left pars triangularis, bilateral middle rostral frontal cortex, left superior temporal cortex, and right posterior cingulate. The indirect effect of DWMH volume on LDST scores was significantly mediated by the regional cortical thickness of the bilateral pars opercularis and left superior temporal cortex.

Table 11 – Direct, path a, path b, path c', and indirect (mediation) effects of WMH/PVWMH/DWMH and regional cortical thickness on LDST scores.[1]

	WM tract	Direct effect (c path)	a	b	c'	Indirect (mediation) effects 95% BCI - a*b
WMH	Pars opercularis L	-0.12^2	-0.24^2	0.13^2	-0.08	[-0.060 -0.0091]
	Pars opercularis R	-0.12^2	-0.23^2	0.13^2	-0.08	[-0.06 -0.01]
	Pars triangularis L	-0.12^2	-0.14^2	0.12^2	-0.10^2	[-0.04 -0.002]
	Rostral middle frontal L	-0.12^2	-0.12^2	0.13^2	-0.10^2	[-0.04 -0.003]
	Rostral middle frontal R	-0.12^2	-0.13^2	0.13^2	-0.10^2	[-0.04 -0.003]
	Superior temporal L	-0.12^2	-0.21^2	0.10^2	-0.10^2	[-0.05 -0.003]
	Posterior cingulate R	-0.12^2	-0.16^2	0.09^2	-0.10^2	[-0.04 -0.0002]
PVWMH	Pars opercularis L	-0.11^2	-0.27^2	0.14^2	-0.07	[-0.07 -0.01]
	Pars opercularis R	-0.11^2	-0.24^2	0.13^2	-0.07	[-0.06 -0.01]
	Pars triangularis L	-0.11^2	-0.17^2	0.12^2	-0.08	[-0.045 -0.0035]
	Rostral middle frontal L	-0.11^2	-0.15^2	0.13^2	-0.09	[-0.043 -0.004]
	Rostral middle frontal R	-0.11^2	-0.15^2	0.13^2	-0.09	[-0.04 -0.0035]
	Superior temporal L	-0.11^2	-0.24^2	0.10^2	-0.08	[-0.05 -0.004]
	Posterior cingulate R	-0.11^2	-0.17^2	0.09^2	-0.09^2	[-0.04 -0.0001]
DWMH	Pars opercularis L	-0.11^2	-0.14^2	0.14^2	-0.09^2	[-0.04 -0.004]
	Pars opercularis R	-0.11^2	-0.17^2	0.14^2	-0.08	[-0.05 -0.008]
	Superior temporal L	-0.11^2	-0.14^2	0.11^2	-0.09^2	[-0.03 -0.002]

Analyses conducted using PROCESS model 4, N = 389. Sex was dummy coded (1 = female and 0 = male). Standardized regression coefficients are presented; a = the association between WMH/PVWMH/DWMH volume and regional cortical thickness. b = the association between regional cortical thickness and LDST adjusted for the effect of WMH/PVWMH/DWMH on LDST scores. c' = the association between WMH/PVWMH/DWMH volume and LDST scores adjusting for cortical thickness. c = the direct association between WMH/PVWMH/DWMH volume and regional cortical thickness. Standardized regression coefficients are also presented for the mediation (a*b) effects. *p < 0.05. BCI = Bias corrected confidence interval (bootstrap). WMH: white matter hyperintensity. PVWMH: periventricular WMH. DWMH: deep WMH. L: left. R : right.

Table 12 presents the direct (path c), path a, path b, path c', and indirect (mediation) effects of WMH/PVWMH/DWMH and FA on LDST scores. The higher the lesion volume, the lower the LDST scores (direct effect). The higher the lesion volume, the lower the fractional anisotropy (path a). The higher the fractional anisotropy, the higher the LDST scores (path b). The indirect effects of WMH, PVWMH, and DWMH volumes on LDST scores were significantly mediated by the left cingulum parahippocampal parietal, left superior longitudinal fasciculus1, right acoustic radiation, right corticostriatal tract anterior, bilateral anterior and

Chapter 6. WMH effects on Cortical Thickness, Brain Networks, and Information Processing Speed in non-demented Small Vessel Disease patients: A mediation study

91

posterior thalamic radiation, and corpus callosum (body, tapetum, minor forceps, and major forceps).

Table 12 – Direct, path a, path b, path c', and indirect (mediation) effects of WMH/PVWMH/DWMH and fractional anisotropy on LDST scores.[1]

	WM tract	Direct effect (c path)	a	b	c'	Indirect (mediation) effects 95% BCI - a*b
WMH	Cingulum Parahippocampal Parietal L	-0.12[2]	-0.48[2]	0.22[2]	-0.013	[-0.16 -0.053]
	Superior Longitudinal Fasciculus1 L	-0.12[2]	-0.36[2]	0.14[2]	-0.01	[-0.09 -0.01]
	Acoustic Radiation R	-0.12[2]	-0.40[2]	0.14[2]	-0.06	[-0.098 -0.019]
	Corticostriatal Tract Anterior R	-0.12[2]	-0.40[2]	0.24[2]	-0.02	[-0.14 -0.05]
	Thalamic Radiation Anterior R	-0.12[2]	-0.41[2]	0.24[2]	-0.015	[-0.15 -0.05]
	Thalamic Radiation Posterior L	-0.12[2]	-0.52[2]	0.22[2]	-0.0007	[-0.18 -0.06]
	Thalamic Radiation Posterior R	-0.12[2]	-0.49[2]	0.21[2]	-0.01	[-0.16 -0.055]
	Thalamic Radiation Superior L	-0.12[2]	-0.39[2]	0.17[2]	-0.05	[-0.11 -0.02]
	Thalamic Radiation Superior R	-0.12[2]	-0.39[2]	0.22[2]	-0.03	[-0.135 -0.045]
	Corpus Callosum Forceps Minor	-0.12[2]	-0.32[2]	0.17[2]	-0.06	[-0.09 -0.024]
	Corpus Callosum Body	-0.12[2]	-0.36[2]	0.15[2]	-0.06	[-0.09 -0.02]
	Corpus Callosum Tapetum	-0.12[2]	-0.395[2]	0.14[2]	-0.06	[-0.095 -0.017]
	Corpus Callosum Forceps Major	-0.12[2]	-0.49[2]	0.21[2]	-0.013	[-0.16 -0.05]
PVWMH	Cingulum Parahippocampal Parietal L	-0.11[2]	-0.42[2]	0.22[2]	-0.014	[-0.14 -0.05]
	Superior Longitudinal Fasciculus1 L	-0.11[2]	-0.37[2]	0.14[2]	-0.05	[-0.098 -0.01]
	Acoustic Radiation R	-0.11[2]	-0.36[2]	0.15[2]	-0.05	[-0.09 -0.02]
	Corticostriatal Tract Anterior R	-0.11[2]	-0.42[2]	0.25[2]	-0.001	[-0.15 -0.06]
	Thalamic Radiation Anterior R	-0.11[2]	-0.42[2]	0.25[2]	-0.001	[-0.15 -0.06]
	Thalamic Radiation Posterior L	-0.11[2]	-0.48[2]	0.22[2]	-0.0004	[-0.16 -0.05]
	Thalamic Radiation Posterior R	-0.11[2]	-0.45[2]	0.215[2]	-0.008	[-0.15 -0.05]
	Thalamic Radiation Superior L	-0.11[2]	-0.38[2]	0.18[2]	-0.04	[-0.115 -0.024]
	Thalamic Radiation Superior R	-0.11[2]	-0.39[2]	0.23[2]	-0.02	[-0.13 -0.045]
	Corpus Callosum Forceps Minor	-0.11[2]	-0.34[2]	0.18[2]	-0.045	[-0.10 -0.03]
	Corpus Callosum Body	-0.11[2]	-0.36[2]	0.15[2]	-0.05	[-0.095 -0.02]
	Corpus Callosum Tapetum	-0.11[2]	-0.35[2]	0.14[2]	-0.055	[-0.09 -0.02]
	Corpus Callosum Forceps Major	-0.11[2]	-0.44[2]	0.21[2]	-0.013	[-0.14 -0.05]
DWMH	Cingulum Parahippocampal Parietal L	-0.11[2]	-0.45[2]	0.22[2]	-0.007	[-0.15 -0.05]
	Superior Longitudinal Fasciculus1 L	-0.11[2]	-0.27[2]	0.14[2]	-0.07	[-0.07 -0.009]
	Acoustic Radiation R	-0.11[2]	-0.37[2]	0.14[2]	-0.05	[-0.09 -0.02]
	Corticostriatal Tract Anterior R	-0.11[2]	-0.29[2]	0.23[2]	-0.04	[-0.01 -0.04]
	Thalamic Radiation Anterior R	-0.11[2]	-0.33[2]	0.24[2]	-0.03	[-0.12 -0.04]
	Thalamic Radiation Posterior L	-0.11[2]	-0.48[2]	0.22[2]	-0.0003	[-0.16 -0.055]
	Thalamic Radiation Posterior R	-0.11[2]	-0.45[2]	0.21[2]	-0.01	[-0.14 -0.05]
	Thalamic Radiation Superior L	-0.11[2]	-0.31[2]	0.17[2]	-0.05	[-0.09 -0.02]
	Thalamic Radiation Superior R	-0.11[2]	-0.32[2]	0.22[2]	-0.04	[-0.11 -0.04]
	Corpus Callosum Forceps Minor	-0.11[2]	-0.21[2]	0.18[2]	-0.07	[-0.07 -0.02]
	Corpus Callosum Body	-0.11[2]	-0.29[2]	0.15[2]	-0.06	[-0.08 -0.02]
	Corpus Callosum Tapetum	-0.11[2]	-0.37[2]	0.14[2]	-0.05	[-0.09 -0.02]
	Corpus Callosum Forceps Major	-0.11[2]	-0.46[2]	0.21[2]	-0.009	[-0.15 -0.05]

Analyses conducted using PROCESS model 4, N = 389. Sex was dummy coded (1 = female and 0 = male). Standardized regression coefficients are presented; a = the association between WMH/PVWMH/DWMH volume and fractional anisotropy. b = the association between fractional anisotropy and LDST adjusted for the effect of WMH/PVWMH/DWMH on LDST scores. c' = the association between WMH/PVWMH/DWMH volume and LDST scores adjusting for fractional anisotropy. c = the direct association between WMH/PVWMH/DWMH volume and fractional anisotropy. Standardized regression coefficients are also presented for the mediation (a*b) effects. BCI = Bias corrected confidence interval (bootstrap). WMH: white matter hyperintensity. PVWMH: periventricular WMH. DWMH: deep WMH. L: left. R : right. [2] Significant at $p < 0.05$.

Table 13 presents the direct (path c), path a, path b, path c', and indirect (mediation) effects of WMH/PVWMH/DWMH and functional connectivity on LDST scores. The higher the WMH and PVWMH volumes, the lower the LDST scores (direct effect). The higher the lesion volume, the lower the functional connectivity (path a). The higher the functional connectivity,

the higher the LDST scores (path b). The indirect effects of WMH and PVWMH volumes on LDST scores were significantly mediated by the seed-to-voxel functional connectivity of the right lateral SMN seed.

Table 13 – Direct, path a, path b, path c', and indirect (mediation) effects of WMH/PVWMH/DWMH and regional cortical thickness on LDST scores.[1]

	Network	Direct effect (c path)	a	b	c'	Indirect (mediation) effects 95% BCI - a*b
WMH	Right Lateral (SMN)	-0.12[2]	-0.135[2]	0.15[2]	-0.09[2]	[-0.04 -0.002]
PVWMH	Right Lateral (SMN)	-0.11[2]	-0.13[2]	0.15[2]	-0.08	[-0.04 -0.003]

Analyses conducted using PROCESS model 4, N = 389. Sex was dummy coded (1 = female and 0 = male). Standardized regression coefficients are presented; a = the association between WMH/PVWMH/DWMH volume and regional cortical thickness. b = the association between regional cortical thickness and LDST adjusted for the effect of WMH/PVWMH/DWMH on LDST scores. c' = the association between WMH/PVWMH/DWMH volume and LDST scores adjusting for cortical thickness. c = the direct association between WMH/PVWMH/DWMH volume and regional cortical thickness. Standardized regression coefficients are also presented for the mediation (a*b) effects. BCI = Bias corrected confidence interval (bootstrap). WMH: white matter hyperintensity. PVWMH: periventricular WMH. DWMH: deep WMH. L: left. R : right.
[2] Significant at p < 0.05.

6.4 Discussion

Our results showed associations of WMH burden and location with cortical thickness, brain connectivity, and LDST performance in a group of cSVD patients without dementia. Additionally, cortical thickness and brain connectivity were shown to mediate the association of WMH burden and location with LDST scores.

Gray matter atrophy has been suggested as a possible mechanism to explain the association between cognitive decline and WMH in cSVD patients ([297], [298], [286]). Cortical thinning was shown to mediate this association ([288], [299], [300]). Firstly, regarding the spatial pattern of WMH volume and cortical thickness associations, we found it mainly in frontal, temporal, and occipital areas. Previously, associations were found bilaterally in the dorsolateral prefrontal, parietal and posterior-superior temporal cortices in CADASIL patients ([297]) and predominantly in frontal areas in memory clinic patients with SVD ([298]). Using the same database from the present study, WMH load was negatively correlated with cortical thickness in bilateral frontotemporal regions, whereas WMH load was positively correlated with cortical thickness in the paracentral regions ([300]). The prominence of frontal areas in our study and the mentioned ones is hypothesized to be related to the increased susceptibility of axons in these areas to impaired cerebral perfusion and vascular injury, leading to partial frontal lobe disconnection ([316]).

Another mechanism to explain the heterogeneity of clinical outcomes is the disruption of brain networks by WMH. MRI techniques such DTI and BOLD-fMRI are expected to contribute to understanding the pathophysiology of WM lesions (and of cSVD in general) and their clinical correlates ([317]) through studies of structural and functional brain connectivity.

We found associations between callosal tracts and projection tracts with lesion volume concerning the structural brain networks. A graph analysis study showed that structural brain networks are disturbed in cSVD patients associated with the disease severity. It also showed the most impairment in the interhemispheric and prefrontal connections ([203]). We also found the association of projection, callosal, association, and limbic system tracts with LDST scores. Similarly, a study with non-demented and stroke-free participants showed a positive and significant association of tract-specific FA with LDST scores involving the anterior and posterior thalamic radiation (projection tracts), superior, inferior, and inferior fronto-occipital fasciculus (association tracts), cingulate gyrus (limbic system tracts) and major and minor forceps (callosal tracts) ([318]). When adjusted for global FA, the association remained for the posterior thalamic radiation, inferior and inferior fronto-occipital fasciculus, and minor forceps (callosal tract).

The mechanism behind the indirect effects of WMH on LDST through WM microstructural impairment is still unclear. One possibility is the cortex atrophy due to disconnection of WM tracts caused by WMH due to disease, a process called secondary degeneration

(301, 302, 303). The strongest associations involving the posterior thalamic radiation, which connects the thalamus with the posterior parietal and occipital lobes (319), and have a key role in connecting visual and motor processes, suggest that IPS assessed with LDST relies on the processes supported by this tract.

On the other hand, we found associations between SMN, DMN, salience, DAN, FPN, cerebellar and visual networks functional connectivity with lesion volume. LDST scores were associated with SMN, DMN, language, visual and FPN functional connectivity. Neuroimaging studies reported reduced functional connectivity in distributed networks. Three networks that are commonly affected are the DMN, DAN, and FPCN, which all play an important role in attention directed by goals and executive functions (291, 320). Disturbed functional connectivity within the FPCN, DAN, and DMN has been linked to a higher level of cognitive impairment (321, 264, 322). More specifically, cSVD causes disruptions in the frontal-subcortical circuits and long association fibers that, in turn, impair communication between crucial neural networks responsible for cognitive control or attention, such as DMN, FPCN, and DAN (320).

However, functional connectivity from SMN right lateral seed was the only one to mediate the association of WMH and PVWMH volumes. Previously, functional connectivity from the right cingulate motor area, left posterior insula, and left ventral premotor area showed attenuated functional connectivity in leukoaraiosis patients, and the degree of attenuation was associated with disease severity (323). The functional connectivity disruptions in the right cingulate motor area were associated with sensorimotor integration performance. CSVD is considered the most likely cause in 69% of sensorimotor stroke patients (323). Complementary, in our analysis of associations between WMH loading on specific WM tracts with LDST scores, the only tract that survived the statistical threshold was the left corticospinal tract, which originates from many brain areas, such as motor, premotor, and somatosensory cortices (324), parietal lobe, and cingulate gyrus (325). It suggests that disruptions in functional connectivity of sensorimotor areas are associated with PVWMH burden and LDST performance, mediating the relationship between them and suggesting another functional network also affected in cSVD patients without dementia, in addition to the traditional DMN, FPN, and DAN. The mechanism behind the indirect effects of WMH on LDST scores through functional connectivity remains unclear, once it can be due to changes in neural activation or neurovascular coupling (326). The neurobiological significance of different changes in resting-state functional connectivity is also unclear (327), with white matter disruptions, gray matter atrophy, and amyloid deposition as possible contributors (328).

In addition to WMH load, the WMH location (periventricular and deep) was also associated with LDST scores, although the associations were statistically similar. The interesting findings were concerning the indirect effects. Only the association between PVWMH and LDST was mediated by functional connectivity. Almost double the cortical areas mediated the association between PVWMH and LDST scores compared to the number of cortical areas

mediating the DWMH-LDST relationship. We hypothesize that PVWMH may disturb long cortico-subcortical association fibers (329), and may be adjacent to ascending cholinergic fibers (330, 291). More specifically, the frontal subcortical circuit plays a crucial role in executive functions and attention due to the involvement of particular areas, such as the thalamus (331), allowing the control of motor, cognitive, and behavioral abilities (332). The integrity of the cholinergic system was shown to play a critical role in cognitive decline in both normal aging and neurological disorders, including Alzheimer's disease and vascular cognitive impairment (333). The lateral pathway of the cholinergic system was tracked, and the external capsule division was successfully tracked to the inferior frontal cortex through the uncinate fasciculus, and parietal and temporal cortices via posterior thalamic radiation (which was an important tract in our study) and internal capsule.

A limitation of the present study includes considering only WMH, while other traditional cSVD are also crucial to the cognitive outcome. The contribution of neurodegenerative pathologies other than SVD, the influence of cardiovascular risk factors, the associations with other cognitive domains, the interaction with compensatory mechanisms, the value of rs-fMRI in cSVD studies as fMRI relies on intact neurovascular coupling, which is impaired in cSVD, and the findings in groups with dementia and other symptoms should also be considered in future studies.

6.5   Conclusion

In conclusion, because the conventionally known focal lesions (WMH) affect distant brain areas, structural and functional networks, and relate to IPS performance evaluated with the LDST, we suggest that cSVD should be regarded as a global rather than a localized syndrome. We also point out the role of the sensorimotor network as another important functional network disrupted in this clinical group.

7 The neural substrates of information processing speed deficits in cerebral small vessel disease patients without dementia: a brain disconnectome mapping study

7.1 Introduction

Cerebral small vessel diseases (cSVD) manisfest with clinical, imaging and pathological findings secondary to the dysfunction of arterioles, capillaries, and venules of the brain, causing significant impact on public health worldwide (334). cSVD is commonly associated with aging, stroke, cognitive decline, dementia, impaired gait, and mood disorders, but may also present with few or no symptoms. Up to 45% of dementia cases, virtually all hemorrhagic and about 20% of ischemic strokes worldwide are caused by cSVDs (160).

cSVD often coexists with neurodegenerative diseases and can exacerbate physical and cognitive deficits, particularly in information processing speed and executive functions (335, 336). Given the difficulty in visualizing cSVD-related pathologies in vivo, the diagnosis of cSVD has been heavily based on neuroimaging, mainly in white matter hyperintensity (WMH) (160). WMH has been shown to relate to cognitive decline (336). In addition to WMH burden, WMH location may also explain the lesion impact on cognition. A commonly used topographic categorization of WMH divides the lesions in deep (DWMH) and periventricular WMH (PVWMH), according to the distance from the ventricles' margins (292), and reflecting different functional, aetiological and histopathological characteristics (337).

Brain lesion studies are critical to understanding the mechanisms behind human brain functioning. Traditionally, lesion-symptom mapping has considered that a patient's symptoms are caused by visible and physically affected locations (338, 339), regarded as the neural substrate for the function affected. However, evidence suggests that brain lesions may also lead to neurological deficits indirectly, by disrupting intricate structural and functional connections, without necessarily affecting eloquent cortical areas (340, 341). In fact, studies indicate that WM disconnectivity can be a better predictor of brain dysfunction and recovery when compared to the lesion location itself (342, 343).

cSVD has been considered a dysconnectome syndrome (166), with the WMH disrupting structural brain networks and affecting cognitive performance (289). Evidence suggests that cognitive impairments due to cerebral cSVD (mainly by WMH) result from disruption of frontal-subcortical circuits and long association fibers. Such a disruption impairs communication among crucial neural networks responsible for cognitive control or attention, such as Default Mode Network (DMN), FrontoParietal Control Network (FPCN), and Dorsal Attention Network (DAN) (320). However, the relationship between brain disconnection due to brain

lesions and dysfunction remains limited.

A review of lesion-symptom mapping studies found associations between WMH burden in the anterior thalamic radiation and minor forceps and decline in processing speed in Cerebral Autosomal Dominant Arteriopathy with Subcortical Infarcts and Leukoencephalopathy (CADASIL) and mixed dementia patients (310). The cingulum, major forceps, and left corticospinal tracts were similarly linked to processing speed in CADASIL. However, it was not replicated in subsequent research (310). Moreover, the relationship between brain disconnection due to brain lesions and dysfunction remains limited.

In the face of disconnection, a region deprived of its inputs and outputs will undergo transneuronal degeneration leading to apoptosis. The effects of disconnections on brain structure and function must also be analyzed. Therefore, using the BCBToolkit (344), we investigated WMH lesion anatomy that results in impaired IPS, one of the earliest and most common cognitive impairments in the cSVD population, in a large dataset (n = 195) of cerebral SVD patients without dementia (van Norden et al. 2011).

The BCBToolkit approach, an advanced lesion analysis tool, creates a probabilistic map of disconnections from each patient's brain lesion map to find the disconnections linked to cognitive abnormalities at the group level and have been successfully applied in stroke patients (345, 346, 347, 348). Then, measurements of indirect disconnections caused by the lesion with functional connectivity analysis were performed to identify the complete functional network related to IPS. We also compared the disconnectome maps and functional connectivity results with the cortical thickness associations with IPS scores findings to explore possible structural changes related to lesion disconnections.

7.2   Methods

Patients and neuropsychological assessment

The study sample was drawn from the RUN DMC (Radboud University Nijmegen Diffusion tensor and Magnetic resonance imaging Cohort) study (305). We included 195 non-demented elderly, aged between 50-85 years, with cSVD. Participants underwent a structured questionnaire on demographics and vascular risk factors, cognitive and motor assessments, and an MRI protocol including conventional MRI, DTI, and resting-state functional MRI (fMRI). The rationale and methodology have been described previously in details (305). Measurement of global cognitive function was assessed by the Mini-mental State Examination (MMSE) (306). Information processing speed (IPS) was evaluated with the Letter-Digit Substitution Task (LDST) (30), a modified version of the Symbol Digit Modalities Test (SDMT) (20). The higher the LDST score, the better the information processing speed performance.

MRI acquisition

Scans were acquired in a 1.5-Tesla Magnetom scanner (Siemens, Erlangen, Germany). A whole-brain 3D T1 was acquired using a magnetization-prepared rapid gradient-echo (MPRAGE) sequence (TR/TE/TI = 2250/3.68/850 ms, flip angle = 15°, voxel size = 1.0 × 1.0 × 1.0 mm³). T2-weighted Fluid Attenuated Inversion Recovery (FLAIR) sequence was used with the following parameters: TR/TE/TI = 9000/84/2200 ms, voxel size = 1.0 × 1.2 × 6.0 mm³ (including slice gap of 1 mm). Diffusion Tensor Imaging (DTI) was acquired with the following parameters: TR/TE = 10100/93 ms, voxel size = 2.5 × 2.5 × 2.5 mm³, four unweighted scans, 30 diffusion-weighted scans, with non-collinear orientation of the diffusion-weighting gradient, and b value = 900 s/mm2. Resting-state fMRI was acquired using a gradient-echo EPI sequence (TR/TE = 2400/40 ms; voxel size = 3.5 × 3.5 × 4.4 mm², including slice gap of 0.4 mm). During resting state, subjects were told not to concentrate on any particular subject but to relax with their eyes closed. The complete scanning protocol takes 31 minutes.

Lesion segmentation and normalization

T1-weighted (T1W) and FLAIR scans were processed with UBO Detector <https://cheba.unsw.edu.au/group/neuroimaging-pipeline> to segment WMH regions. The algorithm has been described previously (307). Briefly, FLAIR images were registered to T1W images and then warped to Diffeomorphic Anatomical Registration Through Exponentiated Lie Algebra (DARTEL) space. After non-brain tissue removal, FMRIB's Automated Segmentation Tool (FAST) was applied to FLAIR data to generate candidate clusters. A supervised learning algorithm, k-nearest neighbors (k-NN), was used to determine WMH clusters. We used the default settings (k = 5, probability threshold = 0.7) and manually checked the results for segmentation quality. Registrations of patients' T1W MRI were performed using BCBtoolkit (344). The skull stripping was performed using the ANTs brain extraction algorithm <http://stnava.github.io/ANTs/>. T1W images were registered to the template (MNI152) using affine and diffeomorphic deformations (349, 350).

Disconnectome analysis

We mapped the lesion from each patient onto tractography reconstructions of white matter pathways obtained from a group of healthy controls (351). We quantified disconnection severity, measuring the tract probability to be disconnected (352) using Tractotron software as part of the BCBtoolkit (344) <http://www.toolkit.bcblab.com>. Disconnectome maps were calculated using BCBtoolkit (344), using a set of 10 diffusion-weighted imaging datasets of healthy controls (351) to track fibers passing through each lesion. For each participant, tractography was estimated as indicated in Thiebaut de Schotten et al. (353). Patients' lesions in the MNI152 space were registered to each control native space using affine and diffeomorphic deformations (349, 350) and subsequently used as seed for the tractography in Trackvis (Trackvis, <http://trackvis.org/>). Tractography from the lesions was transformed in

visitation maps (354), binarised, and brought to the MNI152 using the inverse of precedent deformations. Finally, we produced a percentage overlap map by summing the normalized visitation map of each healthy subject at each point in the MNI space. Hence, each voxel value considered the interindividual variability of tract reconstructions in controls and indicated a probability of disconnection from 0 to 100% for a given lesion (355).

Statistical analysis

We performed a permuted (n = 5000) multiple regression with LDST scores as the independent variable and the probability of disconnection of each voxel in the disconnectome map as dependent variables while controlling for age, sex, and education. Threshold-Free Clusters Enhancement option was applied to boost cluster-like structures of voxels. Results that survived 5000 permutations were controlled for a family-wise error rate (p > 0.95). This analysis was performed using the function Randomise (356) from the software package FSL <https://fsl.fmrib.ox.ac.uk/fsl,version5.0>.We compared the involvement of the anatomical structures emerging from the regression analysis with the probability maps of the Harvard-Oxford Atlas (309). The comparison was also performed visually overlapping each region from the atlas to the regression maps once it was a possible check for laterality. Then, the common ROIs, which appeared in disconnectome maps from total, periventricular and deep WMH, were used in the following functional connectivity analysis. We used an atlas of human brain connections, the ICBM-DTI-81 white-matter labels atlas (357), to confirm the identity of the white matter tracts disconnected.

Functional connectivity analysis

Resting-state fMRI was preprocessed using the CONN toolbox version 20b <https://www.nitrc.org/projects/conn>. Preprocessing steps included a standard pipeline (realignment and unwarping, slice-timing correction, structural unified segmentation and normalization, functional normalization, outlier detection, and smoothing with a 10 mm FWHM Gaussian kernel). The Artifact Detection Tool (ART) algorithm <http://www.nitrc.org/projects/artifact_detect/> was applied to detect motion during the resting-state fMRI scan. Time points in subjects' images were marked as outliers if the global signal exceeded five standard deviations from the mean or if scan-to-scan motion deviation exceeded 0.9 mm. Those outliers, in addition to the linear and polynomial trends of six head motion parameters, WM and cerebrospinal fluid (CSF) signal were included as nuisance regressors during the denoising procedure in the CONN toolbox. Data were also band-pass filtered at 0.008–0.09 Hz. The ROIs mentioned in the previous subsection were used as seeds. Single-subject seed-to-voxel correlation maps were calculated by extracting the residual blood oxygen level dependent (BOLD) time course from each seed and computing Pearson's correlation coefficients between that time course and the time course of all other voxels in the brain. Correlation coefficients

were normalized to z-values via Fisher's z-transformation. We implemented a multiple linear regression analysis for each seed at the group level by defining the association between LDST with functional connectivity after controlling for age, sex, and education. Statistical thresholds were set to p < 0.001 (uncorrected) at a single voxel level, and the resulting clusters were thresholded to a cluster-level Family-wise error (FWE) p < 0.05.

Cortical thickness analysis

The gray matter (GM), white matter (WM), cerebrospinal fluid (CSF) were automatically segmented on structure T1W images using SPM12 <https://www.fil.ion.ucl.ac.uk/spm/> and CAT12 toolbox <https://www.neuro.uni-jena.de/vbm/> using surface and thickness estimation for ROI analysis in the writing options. Total intracranial volume (TIV) was computed as the sum of GM, WM, and CSF volumes. Region-based Morphometry (RBM) analysis was performed by extracting the mean cortical thickness values for 34 ROIs defined by the Desikan-Killiany (DK) atlas (309) using standard procedures for ROI extraction. Data were entered in a statistical model to perform a multiple linear regression analysis by defining the association of LDST with regional cortical thickness, controlling for age, sex, and education. Statistical thresholds were set to p < 0.05 (p-Holm Bonferroni corrected).

7.3   Results

Patients' description

The mean age was 65.0 ± 8.6 years old (min-max: 49.7-85.4 years). One hundred and twenty-two (63%) were women. The mean LDST score was 26.48 ± 9.15 (min-max: 7 – 51), while the mean MMSE was 28.16 ± 1.60 (min-max: 23-30).

Lesion maps

The binary maps of WMH, PVWMH, and DWMH lesions for the group are displayed in Figure 20. The total WMH and DWMH were negatively and significantly associated with LDST scores after controlling for age, sex, and education (Table 14). No association of lesion volume in specific tracts with LDST survived after multiple comparison corrections (p-Bonferroni = 0.05).

Disconnectome Maps

Figure 21 shows the mean disconnectome maps from WMH, PVWMH, and DWMH. The highest probabilities were identified in WM territories, decreasing in cortical areas. Figure 22 shows the group voxelwise statistical maps of disconnectome probability associated with LDST scores, regressing the effects of age, sex, and education. The associations of the voxel
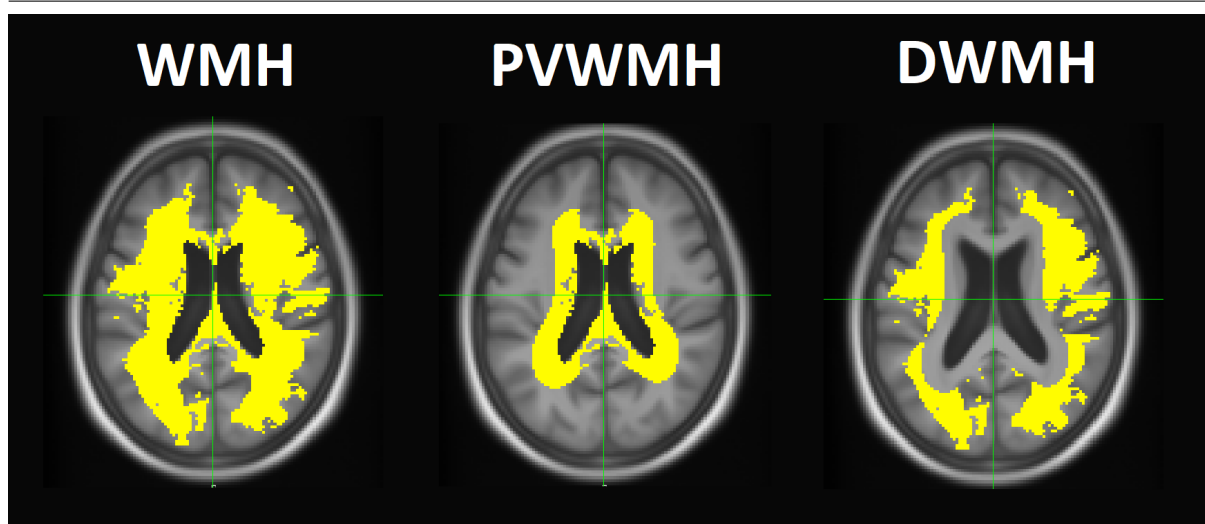
Figure 20 – Binary maps in yellow displaying (from left to right) WMH, PVWMH, and DWMH lesions for the group. WMH = white matter hyperintensity. PVWMH = periventricular WMH. DWMH = deep WMH.

Table 14 – Associations of global measures with LDST scores. LDST = Letter Digit Substitution Test. WMH = white matter hyperintensity. PVWMH = periventricular WMH. DWMH = deep WMH.

Global structural measure	beta	ΔR^2	R^2	p
WMH volume (cm³)[1]	-0.145	1.7%	38.4%	**0.021**
PVWMH volume (cm³)[2]	-0.111	1.0%	37.6%	0.081
DWMH volume (cm³)[2]	-0.158	2.2%	38.9%	**0.009**

[1] After regressing out effects of age, sex, and education level. In bold association statistically significant ($p < 0.05$).
[2] After regressing out effects of age, sex, and education level. In bold associations statistically significant after Bonferroni correction ($p < 0.025$).

disconnectivity probability maps obtained from WMH, PVWMH, and DWMH with the LDST scores indicated distinct topographic distributions. Then, we compared the regression results from Figure 22 with cortical, subcortical (Table 15), and WM atlases (Table 16).

The connections between LDST scores and disconnetome maps from WMH lesions were topographically distributed mainly in the right hemisphere. More specifically, they were in the parietal lobe, thalamus, and the following tracts: body of corpus callosum, right superior longitudinal fasciculus, right anterior corona radiata, and genu of the corpus callosum.

The connections with LDST in disconnetome maps from PVWMH lesions were seen in the right hemisphere, involving the frontal, parietal, temporal, and occipital lobes, thalamus and right superior longitudinal fasciculus, right anterior corona radiata, right anterior and

posterior limbs of the internal capsule, and right superior corona radiata.

Finally, for the disconnectome maps from DWMH lesions, the associations were found in both hemispheres while still prominent in the right hemisphere. They were in the parietal, temporal, and occipital lobes, subcortical areas, and WM tracts such as the body of corpus callosum, right posterior corona radiata, right superior corona radiata, splenium of the corpus callosum, right superior longitudinal fasciculus.

More detailed information can be seen in Table 15 and Table 16.

WMH
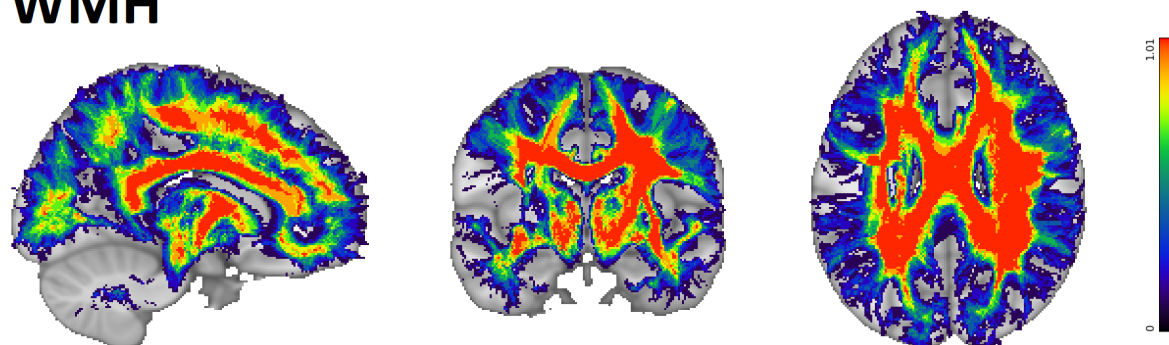
PVWMH
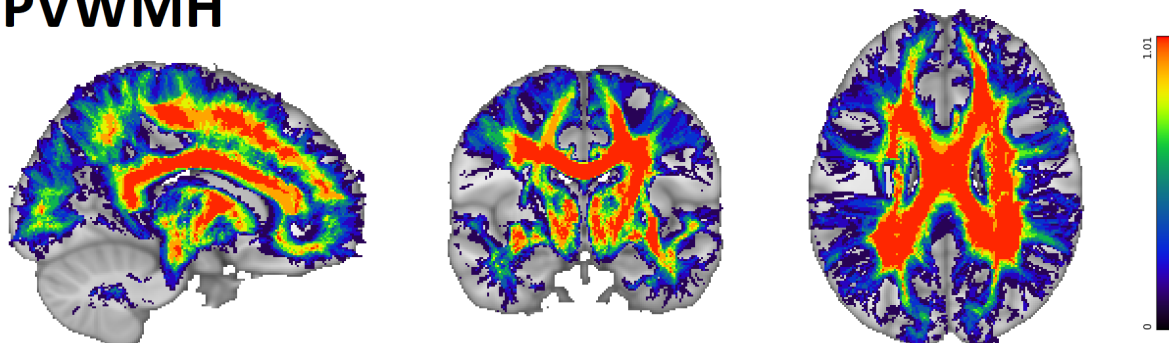
DWMH
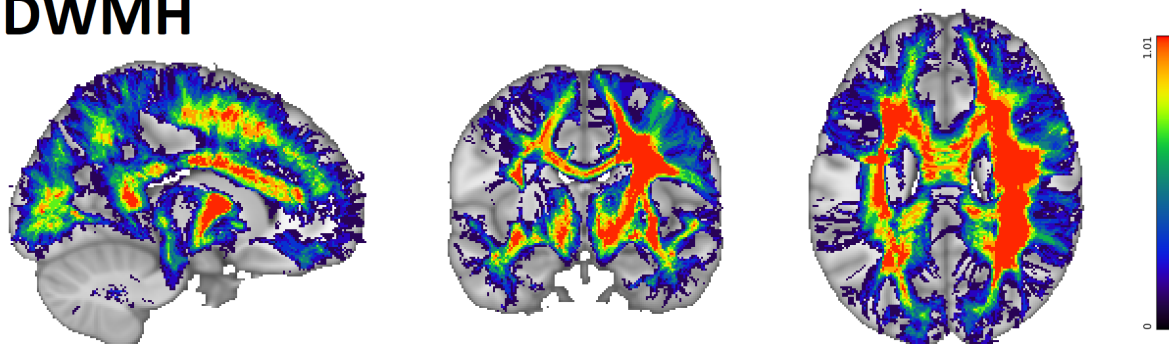
Figure 21 – Group disconnectome maps. Probability for disconnection ranges from 0 (blue) to 1 (red). A disconnectome probability of 0 means that the voxel has no chance of being affected by the lesion. In contrast, a disconnectome probability of 1 means that the voxel has a 100% chance of being affected by the lesion. WMH = white matter hyperintensity. PVWMH = periventricular WMH. DWMH = deep WMH.
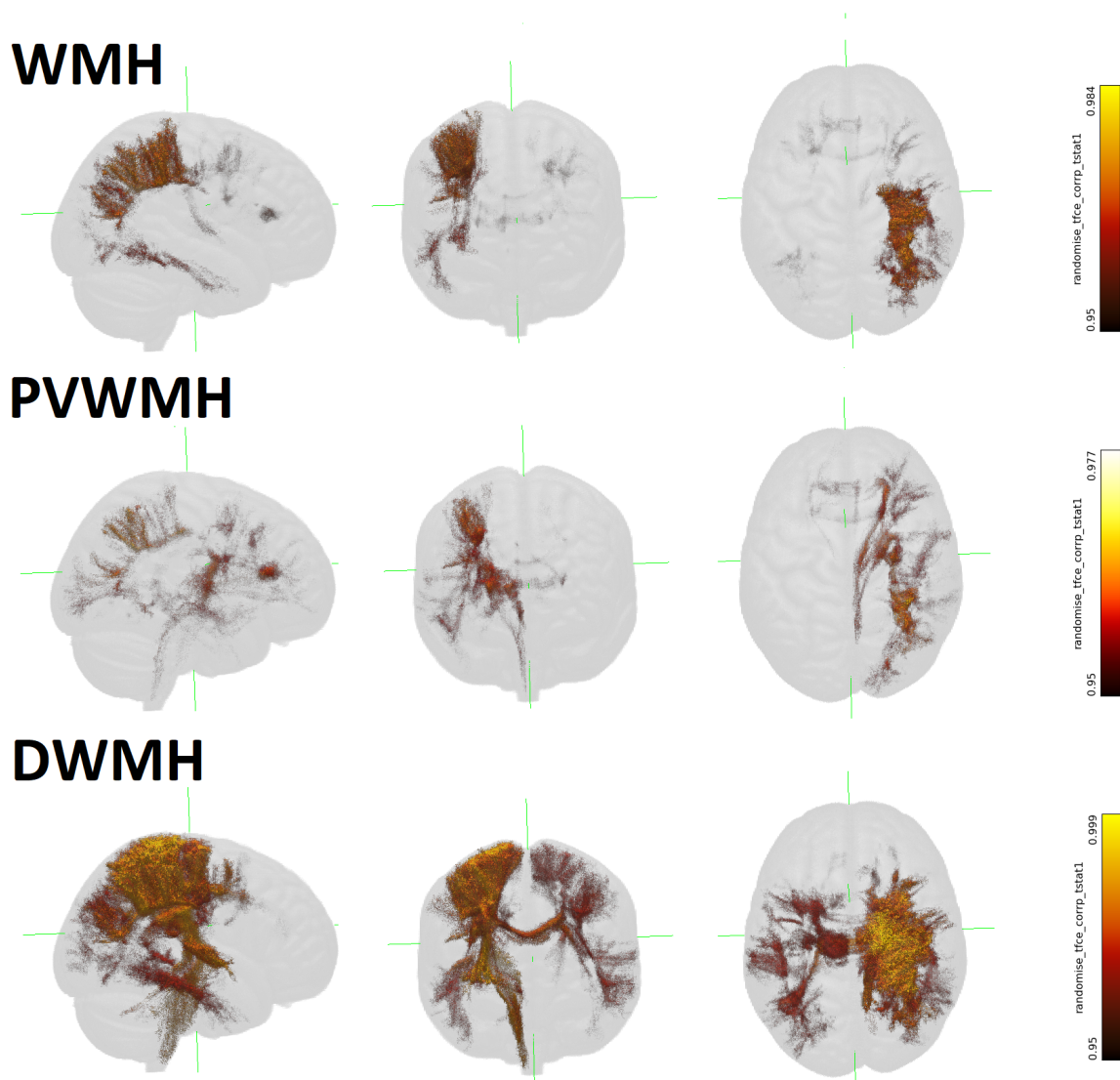
Figure 22 – Group voxelwise statistical maps of disconnectome probability associated with Letter Digit Substitution Test (LDST) scores regressing the effects of age, sex, and education. The results survived 5000 permutations testing and were controlled for a family-wise error rate (p > 0.95). Color bars represent p-values. WMH = white matter hyperintensity. PVWMH = periventricular WMH. DWMH = deep WMH.

Table 15 – Resulting regions from group voxelwise statistical maps of disconnectome probability associated with LDST scores, regressing the effects of age, sex, and education when compared to Cortical and Subcortical Harvard-Oxford structural atlas. LDST = Letter Digit Substitution Test. WMH = white matter hyperintensity. PVWMH = periventricular WMH. DWMH = deep WMH.

Disconnectome map	Cortical Harvard-Oxford structural atlas	Subcortical Harvard-Oxford structural atlas
WMH	Left superior frontal gyrus, bilateral middle frontal gyrus, right inferior temporal gyrus (temporooccipital part), right inferior temporal gyrus (posterior division), bilateral lateral occipital cortex (inferior division), right postcentral gyrus, bilateral lateral occipital cortex (superior division), right superior parietal lobule, bilateral frontal pole	Right thalamus
PVWMH	Right occipital pole, right lateral occipital (superior division), right superior parietal lobule, right postcentral gyrus, right middle frontal gyrus, bilateral frontal pole, right superior temporal gyrus, right inferior temporal gyrus (temporooccipital part), right lateral occipital cortex (inferior division), left superior frontal gyrus, right inferior temporal gyrus (temporooccipital part)	Right thalamus
DWMH	Bilateral lateral occipital cortex (superior division), bilateral lateral occipital cortex (inferior division), bilateral superior parietal lobule, bilateral postcentral gyrus, bilateral precentral gyrus, right inferior temporal gyrus (temporooccipital part), left superior frontal gyrus, right inferior temporal gyrus (posterior division), left middle temporal gyrus (posterior division), left middle temporal gyrus (anterior division), right planum polare	Bilateral thalamus, bilateral lateral ventricle, and bilateral putamen

Table 16 – Resulting white matter tracts and it percentage from group voxelwise statistical maps of disconnectome probability associated with LDST scores, regressing the effects of age, sex, and education when compared to JHU ICBM-DTI-81 WM Labels atlas. LDST = Letter Digit Substitution Test. WMH = white matter hyperintensity. PVWMH = periventricular WMH. DWMH = deep WMH.

Disconnectome map	JHU ICBM-DTI-81 WM Labels atlas
WMH	Body of corpus callosum (12.80%), right superior longitudinal fasciculus (12.13%), right anterior corona radiata (10.61%), genu of corpus callosum (10.41%), right anterior limb of internal capsule (8.84%), left anterior corona radiate (8.12%), right superior corona radiata (5.78%), right external capsule (5.78%), left superior corona radiata (5.72%), right posterior limb of internal capsule (4.43%)
PVWMH	Right superior longitudinal fasciculus (11.77%), right anterior corona radiata (10.75%), right anterior limb of internal capsule (9.85%), right posterior limb of internal capsule (9.49%), right superior corona radiata (7.92%), body of corpus callosum (5.94%), genu of corpus callosum (5.82%), posterior thalamic radiation (include optic radiation) (5.58%), right external capsule (5.52%)
DWMH	Body of corpus callosum (11.61%), right posterior corona radiata (10.39%), right superior corona radiata (8.66%), splenium of corpus callosum (7.83%), right superior longitudinal fasciculus (7.76%), right posterior limb of internal capsule (5.51%), right external capsule (4.95%), left superior corona radiata (4.92%)

Resting-state fMRI Analysis

The following ROIs were inserted as seeds in the seed-to-voxel functional connectivity analysis: left superior frontal gyrus (SFG), right temporooccipital inferior temporal gyrus (toITG), right posterior cingulate gyrus (PostCG), right superior parietal lobule (SPL), right superior and inferior lateral occipital cortices (sLOC, iLOC), and right thalamus.

They were the common ROIs in the disconnectome probability (WMH, PVWMH, and

Chapter 7. The neural substrates of information processing speed deficits in cerebral small vessel disease patients without dementia: a brain disconnectome mapping study

106

DWMH) associations with LDST scores. A cluster with 120 voxels (Figure 23), with 74% of its composition covering the right frontal pole, survived the statistical threshold.
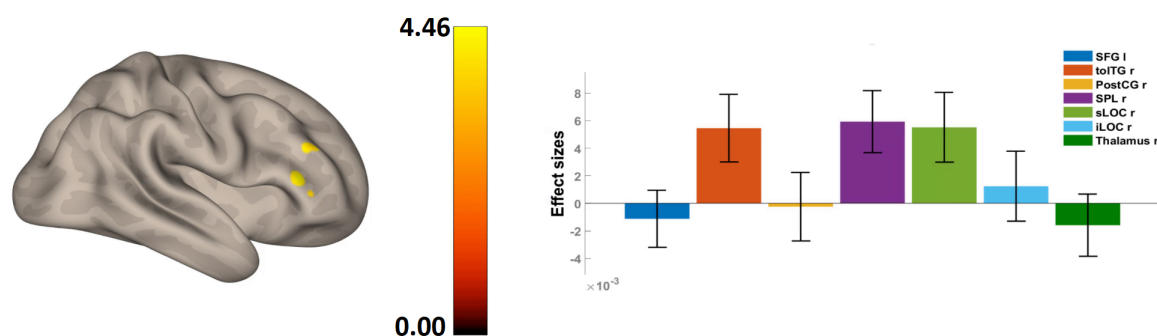
Figure 23 – Statistical map (left) and effect sizes (right) from the associations between seed-to-voxel functional connectivity and LDST scores after controlling for age, sex, and education. Results are thresholded at the voxel level at p-uncorrected < 0.001 and then corrected at the cluster level using a family-wise error (FWE) of p < 0.05. SFG: Superior Frontal Gyrus. toITG: temporooccipital Inferior Temporal Gyrus. PostCG: posterior Cingulate Gyrus. SPL: Superior Parietal Lobule. sLOC: superior Lateral Occipital Cortex. iLOC: inferior Lateral Occipital Cortex. L: left. R: right.

Cortical Thickness

The cortical thickness mainly from frontal areas, followed by temporal and parietal areas were positively and significantly associated with the LDST scores after controlling for age, sex, and education (p < 0.05, Holm Bonferroni corrected) (Figure 24 and Table 17).

When comparing the results of Table 17 with disconnectivity (Table 15) and functional connectivity results (Figure 23), it was found similar regions such as the superior frontal cortex, precentral cortex, middle frontal cortex, and precuneus (part of the superior parietal lobule).
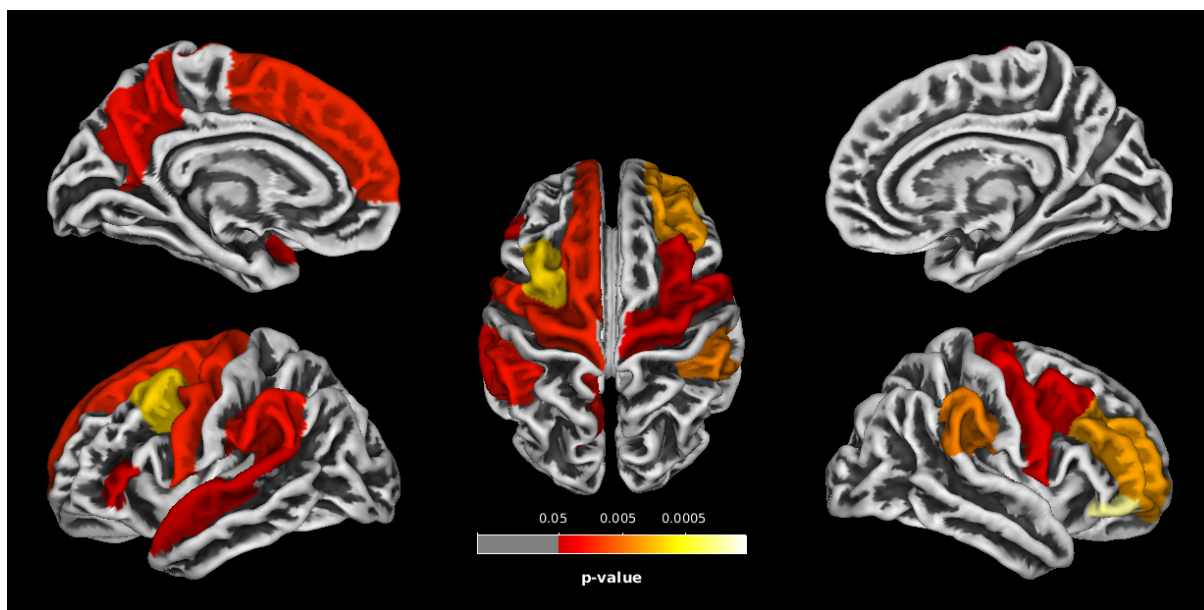
Figure 24 – Multiple linear regression analysis shows the association between Letter Digit Substitution Test (LDST) scores and regional cortical thickness after controlling for age, sex, and education. Statistical thresholds were set to p < 0.05 (p-Holm Bonferroni corrected).

Table 17 – T and p-values of the associations between LDST scores with regional cortical thickness after controlling for age, sex, and education (p < 0.05, Holm Bonferroni corrected). LDST: Letter-Digit Substitution Test.

Desikan Killiany atlas (309) region	T-value	p-value
left caudal middle frontal	4.07	0.0011
left superior frontal	3.58	0.0133
left precentral	3.49	0.0145
left supramarginal	3.38	0.0188
left superior temporal	3.23	0.0498
left pars triangularis	3.21	0.0439
left precuneus	2.78	0.0206
right pars orbitalis	4.63	0.0001
right rostral middle frontal	3.09	0.0023
right caudal middle frontal	2.86	0.0406
right supramarginal	2.72	0.0036
right precentral	2.49	0.0332

7.4   Discussion

This study investigated the anatomic basis of IPS deficits in small vessel disease patients without dementia. We analyzed the disconnections related to WMH burden and location and their relationship with IPS performance, obtaining three main findings. First, global (and not local) measures of WMH were associated with IPS performance. Secondly, the disconnection maps revealed the involvement of callosal tracts, association and projection fibers, and widespread cortical brain areas. Thirdly, functional connectivity analysis's indirect effects of lesion disconnections showed an association of frontal, parietal, temporal, occipital, and subcortical regions with the LDST. Finally, the associations between cortical thickness and LDST scores were topographically distributed mainly in the frontal lobe, followed by parietal and temporal lobes, matching areas from direct and indirect disconnections caused by WMH lesions.

Despite the associations of WMH global measures with LDST scores, it is known that this clinical group presents a significant heterogeneity of clinical outcomes. So, it is suggested that cerebral cSVD be evaluated in terms of the global effects of its lesions (166). Brain disconnectome mapping provides a unique opportunity to assess the global impact of the WMH lesions. More than that, it was possible to evaluate the effect of WMH burden and location once its topography was also associated with different functional, microstructural correlates, and clinical outcomes (358).

Our research found that callosal, association, and projection tracts had disconnectivity probability significantly associated with LDST scores. Previously, a research including cerebral cSVD patients without stroke and dementia found a positive and significant relationship between LDST scores and FA from projection, association, callosal and limbic system tracts (318). When adjusted for global FA, the association remained for projection, association, and callosal tracts. Integrative evidence suggests that cerebral cSVD causes damage mainly in frontosubcortical circuits (329) and cholinergic fibers tracts (uncinated fasciculus, posterior thalamic radiation, and internal capsule) (333), which are related to attention, promoting IPS deficits (291) The corona radiata is one of the places where the subcortical motor pathway is affected by ischemic stroke (359). Disruption mainly in the WMH penumbra of the body of the corpus callosum was suggested to contribute to the cognitive deficits associated with subcortical ischemic vascular disease (SIVD) caused by cerebral cSVD (360). These findings suggest that the varied symptomatology of patients with cSVD could partly be explained by damage to different WM tracts.

We found widespread brain areas involving cortical and subcortical regions from which disconnectivity probability was associated with LDST scores. LDST was shown to rely upon many cognitive processes (30), which can be expressed in the widespread brain areas found in our study. The simultaneous involvement of multiple distinct brain regions associated with specific functions in a symbol digit substitution test has been previously

demonstrated. A systematic review (27) of functional studies using the SDMT, from which the LDST was adapted, shows the involvement of frontal, parietal, cerebellar, and occipital brain areas. In connectivity studies (23, 93), two systems were shown to interact during SDMT performance: the regulation of goal-directed selection (bottom-up) for stimuli and response linked to the frontoparietal and frontooccipital networks and attention guided by stimuli in the brain related with the inferior temporal-parietal and frontal cortices. Our findings suggest the LDST can detect the WMH widespread effect due to its dependence on many systems involving several brain areas.

The functional connectivity analysis with cortical-subcortical disconnected areas as seeds revealed a functional network comprised of the frontal pole, superior frontal gyrus, temporooccipital inferior temporal gyrus, posterior cingulate gyrus, superior parietal lobule, superior and inferior lateral occipital cortices, and thalamus, associated with LDST scores in cSVD patients. The inferior temporal gyrus and lateral occipital cortex are probably related to letter strings and numbers (digits) visual recognition during LDST performance. It was found in a group of healthy participants that the inferior temporal gyri were more activated by letters than numbers during the performance of an fMRI task. In contrast, the latter activated a right lateral occipital part of the brain more than the letter (361). The superior frontal gyrus is involved in working memory performance (362). Working memory is a set of processes ongoing during a temporal buffer created by the lateral prefrontal cortex in decoupling perception from action that allows voluntary and goal-directed behavior to be generated considering internal guidance (363). The posterior cingulate gyrus is part of the Default Mode Network (DMN). DMN deactivation was found during SDMT performance inside the MRI environment in a group of healthy controls (23). This task-negative network presents a suppressed behavior during goal-directed tasks (96). This area has been associated with internally directed cognition and attentional focus control (95).

The superior parietal lobule linked to the precuneus has been associated with top-down goal-directed attention (87) and was also activated in SDMT task-based fMRI studies (27, 93). Neuroimaging studies point out the frontal pole ventromedial role in monitoring outcomes expected from the ongoing course of action (364, 365). Finally, the thalamus has been suggested to mediate complex cognitive function in goal-directed behavior (366).

Cortical thickness associated with LDST scores indicated similar areas from the areas of direct and indirect effects from disconnectivity caused by lesions. Previously, WMH load was negatively correlated with cortical thickness in bilateral frontotemporal regions and positively associated with cortical thickness in the paracentral regions (300) in a study with the RUN-DMC database. It is not possible to affirm that these matched areas reflect that cortical thickness is a distant effect of the lesion disconnections in the present study. Anyway, we can hypothesize that the prominence of frontal regions may reflect the higher susceptibility of axons in these areas to alter brain perfusion and vascular impairments, which causes partial

frontal lobe disconnection (316).

Interestingly, while PVWMH has been usually associated with cognitive deficits (367), only our global measures of DWMH correlated significantly with LDST scores, in line with previous studies (368, 369, 370) . It is suggested that DWMH predominantly disrupts short connections, affecting cognitive ability supported by a particular brain area. In contrast, PVWMH disrupts longer connections, impairing many cognitive domains, mainly executive and processing speed. Once the performance of the LDST relies on multiple processes (30), our findings suggests that damage to specific brain areas by DWMH affects the whole circuitry related to IPS performance. Disconnectome mapping approach provided associations between WMH burden and location and LDST scores. It shows that cSVD is a dysconnectome syndrome, so one should address the distant effects of focal lesions to understand the clinical outcomes better.

Strengths of the study include providing information on the direct and indirect impacts of WMH (considering both load and topographic distribution) locating key regions of these impacts in a large database. Weaknesses include the absence of the effect of other structural damage associated with the disease, the disregard of the impact of depression, anxiety, and cardiovascular risk factors, and the absence of quantitative associations between the disconnectivity and cortical thickness measurements.

7.5   Conclusion

Brain disconnectome mapping was a useful tool to evaluate the disconnectivity caused by the WMH lesions and its relationship with LDST scores, with functional connectivity and regional cortical thickness analysis complementing the findings. In conclusion, IPS deficits assessed with LDST involve widespread brain areas in non-demented cSVD patients, and it is affected differently by WMH burden and topographic distribution through disconnection of brain structural and functional networks.

8 General Conclusion and Future Steps

The relationship between brain structure and function is paradoxical, as a relatively fixed structure allows for a wide variety of functions. The concept of brain connectivity has been applied to explore this question. In addition to demonstrating that structural networks are optimized for brain functioning and constrain (but not determine) patterns of functional connectivity, alterations in brain connectivity have been associated with several diseases, called disconnection syndrome. Through quantitative measurements by magnetic resonance imaging, it is possible to assess the structural and functional connectivity of the brain and its relationship with cognition, in an effort to clarify the brain structure-function relationship. In the present thesis, we evaluated the brain structure-function relationship associated with performance on processing speed tests in healthy participants and in patients with cerebral small vessel brain disease using neuroimaging, sophisticated computational processing, and neuropsychological assessment.

In the first part of the thesis, entitled "Brain structural and functional networks: from connections to cognition", we evaluated the patterns of structural and functional connectivity in healthy and young participants and the relationship with SDMT scores. The study builds on the findings of two previous studies on the functional mapping of areas associated with SDMT performance in the magnetic resonance environment and its functional and effective connectivity pattern and complements it with structural connectivity analyses. The study started from metrics obtained with the Dynamic Causal Modeling (DCM) effective connectivity model to explore associations with structural connectivity metrics. The justification is based on previous studies that used functional connectivity metrics and, in the face of unsatisfactory results, suggested approaching models of functional brain connectivity that were more biologically plausible and that incorporated causality. Among these suggestions, the DCM was chosen to explore the relationship between brain structure and function. In fact, it was possible to find statistically significant associations, with the findings suggesting that structural network constrains but does not determine IPS functional network. This is the first original contribution of this thesis.

Furthermore, still in the first part of the thesis, we explored the functional network pattern during the performance of SDMT considering the DMN and its portions. This was due to the strong association of DMN functional patterns with cognitive health and suggestions that its classically accepted behavior in goal-directed tasks is not homogeneous across the network. In fact, in our study it was observed that in general, the activation and functional connectivity of the DMN is suppressed during the information processing test performance. However, the left precuneus (BA 7) presented a context-dependent modulatory behavior, working as a transient in-between hub connecting the DMN to task positive areas. A more

precise definition of functional correlates is useful for better identification of functional changes in clinical settings.

In the second part of the thesis, "A study applied in cerebral small vessel disease", it was originally supposed to perform the methods used in the first part of the thesis in a group of cSVD patients. However, due to COVID-19 pandemic, it was not possible to acquire the data. Then, we used the RUN-DMC data and slightly changed the objective from to evaluate structure-function-cognition relationship to find the disruptions patterns in both structural and functional connectivity associated with the LDST, that is based on the SDMT. Also called a dysconectome syndrome, cSVD presents heterogeneity in clinical outcomes, and brain connectivity is suggested as a possible explanation for this question.

Evaluating the associations between structural and functional connectivity with LDST scores, the findings suggested that cSVD should be regarded as a global rather than a localized syndrome. The mediation effects of the functional connectivity of the sensorimotor network between the lesion and LDST scores point out the role of this network as another important functional network disrupted in this clinical group, in addition the DMN, FPCN and DAN. Using a lesion-symptom mapping approach called "Brain disconnectome mapping", it was found that the associations between disconnectivity probability and LDST scores involved widespread brain areas in non-demented cSVD patients, and it is affected differently by WMH burden and topographic distribution through disconnection of brain structural and functional networks. Both studies, although with different methodologies, points outs to the general finding that cSVD is a dysconnectome syndrome, so one should address the distant effects of focal lesions to understand the clinical outcomes better.

Limitations include the sample size in our first two studies, the absence of the effect of other structural damage associated with the cSVD such as lacunes of vascular presumed origin and microbleeds, the disregard of the impact of depression, anxiety, and cardiovascular risk factors, and the absence of quantitative associations between the disconnectivity and cortical thickness measurements in the disconnectome mapping study.

Therefore, with the development of this work, we investigated the dynamics of functional networks, their relationship with structural networks and cognitive performance in IPS in healthy individuals and the connectivity disruptions related to IPS performance in a clinical group with cSVD, from empirical data obtained with multimodal magnetic resonance imaging and neuropsychological assessment.

Future steps include the evaluation of other traditional cSVD markers than WMH such as microbleeds and lacunes of presumed vascular origin. The contribution of neurodegenerative pathologies other than SVD, the influence of cardiovascular risk factors, the associations with other cognitive domains, the interaction with compensatory mechanisms, and the findings in groups with dementia and other symptoms should also be considered in future studies.

Bibliography

1   MEUNIER, D.; LAMBIOTTE, R.; BULLMORE, E. T. Modular and hierarchically modular organization of brain networks. *Frontiers in Neuroscience*, Frontiers, v. 4, n. DEC, p. 200, 2010. ISSN 16624548. Cited in page 21.

2   BULLMORE, E. et al. Complex brain networks: graph theoretical analysis of structural and functional systems. *Nature reviews. Neuroscience*, v. 10, n. maRcH, p. 186–98, 2009. ISSN 1471-0048. Cited 3 times in pages 21, 27, and 69.

3   VENKADESH, S.; Van Horn, J. D. Integrative Models of Brain Structure and Dynamics: Concepts, Challenges, and Methods. *Frontiers in Neuroscience*, Frontiers Media SA, v. 15, oct 2021. ISSN 1662453X. Disponível em: </pmc/articles/PMC8585845//pmc/articles/PMC8585845/?report=abstracthttps://www.ncbi.nlm.nih.gov/pmc/articles/PMC8585845/>. Cited in page 21.

4   PARK, H.-J.; FRISTON, K. Structural and functional brain networks: from connections to cognition. *Science*, American Association for the Advancement of Science, v. 342, n. 6158, 2013. Cited 2 times in pages 21 and 27.

5   FAN, X.; MARKRAM, H. A Brief History of Simulation Neuroscience. *Frontiers in Neuroinformatics*, Frontiers Media SA, v. 13, apr 2019. ISSN 16625196. Disponível em: </pmc/articles/PMC6513977//pmc/articles/PMC6513977/?report=abstracthttps://www.ncbi.nlm.nih.gov/pmc/articles/PMC6513977/>. Cited in page 21.

6   SPORNS, O. Structure and function of complex brain networks. *Dialogues in Clinical Neuroscience*, v. 15, n. 3, p. 247–262, 2013. ISSN 12948322. Cited in page 21.

7   FALLANI, F. de V. et al. Graph analysis of functional brain networks: practical issues in translational neuroscience. *Philosophical Transactions of the Royal Society B: Biological Sciences*, The Royal Society, v. 369, n. 1653, p. 20130521, 2014. Cited in page 21.

8   WANG, Z. et al. Understanding structural-functional relationships in the human brain: a large-scale network perspective. *Neuroscientist*, v. 21, n. 3, p. 290–305, 2015. ISSN 1073-8584. Cited in page 21.

9   HAGMANN, P. et al. Understanding diffusion mr imaging techniques: from scalar diffusion-weighted imaging to diffusion tensor imaging and beyond. *Radiographics*, Radiological Society of North America, v. 26, n. suppl_1, p. S205–S223, 2006. Cited in page 21.

10   XIAO, H. et al. Structural and functional connectivity in traumatic brain injury. *Neural regeneration research*, Wolters Kluwer–Medknow Publications, v. 10, n. 12, p. 2062, 2015. Cited 2 times in pages 22 and 27.

11   BISWAL, B. et al. - Functional connectivity in the motor cortex of resting human brain using. *Magn Reson Med*, v. 34, n. 9, p. 537–541, 1995. ISSN 0740-3194. Cited 2 times in pages 22 and 27.

12   Van De Ven, V. G. et al. Functional connectivity as revealed by spatial independent component analysis of fMRI measurements during rest. *Human Brain Mapping*, v. 22, n. 3, p. 165–178, 2004. ISSN 10659471. Cited in page 22.

13   LOGOTHETIS, N. K. et al. Neurophysiological investigation of the basis of the fmri signal. *nature*, Nature Publishing Group, v. 412, n. 6843, p. 150–157, 2001. Cited 3 times in pages 22, 27, and 56.

14   OGAWA, S. et al. Brain magnetic resonance imaging with contrast dependent on blood oxygenation. *Proceedings of the National Academy of Sciences of the United States of America*, v. 87, n. 24, p. 9868–72, 1990. ISSN 0027-8424. Disponível em: <http://www.pubmedcentral.nih.gov/articlerender.fcgi?artid=55275&tool=pmcentrez&rendertype=abstract>. Cited 3 times in pages 22, 28, and 56.

15   DETRE, J. A.; WANG, J. *Technical aspects and utility of fMRI using BOLD and ASL*. 2002. 621–634 p. Cited 2 times in pages 22 and 28.

16   COLE, M. W. et al. Activity flow over resting-state networks shapes cognitive task activations. *Nature Neuroscience*, v. 19, n. 12, p. 1718–1726, 2016. ISSN 1098-6596. Cited in page 22.

17   FRISTON, K. J. Functional and effective connectivity in neuroimaging: A synthesis. *Human Brain Mapping*, v. 2, n. 1-2, p. 56–78, 1994. ISSN 10970193. Cited 2 times in pages 22 and 28.

18   CHIARAVALLOTI, N. D.; GENOVA, H. M.; DELUCA, J. Cognitive rehabilitation in multiple sclerosis: the role of plasticity. *Frontiers in Neurology*, Frontiers, v. 6, p. 67, 2015. Cited 2 times in pages 22 and 28.

19   CHIARAVALLOTI, N. D.; STOJANOVIC-RADIC, J.; DELUCA, J. The role of speed versus working memory in predicting learning new information in multiple sclerosis. *Journal of Clinical and Experimental Neuropsychology*, Routledge, v. 35, n. 2, p. 180–191, 2013. PMID: 23350959. Cited 2 times in pages 23 and 45.

20   SMITH, A. The Symbol-Digit Modalities Test: A neuropsychologic test for economic screening of learning and other cerebral disorders. *Learning Disorders*, v. 3, p. 83–91, 1968. Cited 7 times in pages 23, 28, 29, 45, 46, 71, and 97.

21   FORN, C. et al. A Symbol Digit Modalities Test version suitable for functional MRI studies. *Neuroscience Letters*, v. 456, n. 1, p. 11–14, 2009. ISSN 03043940. Cited in page 23.

22   FORN, C. et al. Task-load manipulation in the Symbol Digit Modalities Test: An alternative measure of information processing speed. *Brain and Cognition*, v. 82, n. 2, p. 152–160, 2013. ISSN 02782626. Cited 2 times in pages 23 and 45.

23   SILVA, P. et al. Symbol Digit Modalities Test adaptation for Magnetic Resonance Imaging environment: A systematic review and meta-analysis. *Multiple Sclerosis and Related Disorders*, v. 20, 2018. ISSN 22110356. Cited 7 times in pages 23, 28, 30, 45, 46, 47, and 109.

24   RYPMA, B.; PRABHAKARAN, V. When less is more and when more is more: The mediating roles of capacity and speed in brain-behavior efficiency. *Intelligence*, 2009. ISSN 01602896. Cited in page 23.

25   PATEL, V. P.; WALKER, L. A.; FEINSTEIN, A. Deconstructing the symbol digit modalities test in multiple sclerosis: The role of memory. *Multiple Sclerosis and Related Disorders*, 2017. ISSN 22110356. Cited in page 23.

26 BENEDICT, R. H. et al. *Validity of the Symbol Digit Modalities Test as a cognition performance outcome measure for multiple sclerosis.* 2017. Cited 2 times in pages 23 and 45.

27 SILVA, P. H. R. et al. Brain functional and effective connectivity underlying the information processing speed assessed by the Symbol Digit Modalities Test. *NeuroImage*, 2018. ISSN 1095-9572. Disponível em: <https://linkinghub.elsevier.com/retrieve/pii/ S1053811918319529%0Ahttp://www.ncbi.nlm.nih.gov/pubmed/30292813>. Cited 5 times in pages 23, 28, 44, 45, and 109.

28 HOPFINGER, J. B.; BUONOCORE, M. H.; MANGUN, G. R. The neural mechanisms of top-down attentional control. *Nature neuroscience*, Nature Publishing Group, v. 3, n. 3, p. 284–291, 2000. Cited in page 23.

29 CORBETTA, M.; SHULMAN, G. L. Control of goal-directed and stimulus-driven attention in the brain. *Nature Reviews Neuroscience*, v. 3, n. 3, p. 201–215, 2002. ISSN 14710048. Cited 3 times in pages 23, 39, and 52.

30 JOLLES, J. et al. The Maastricht Aging Study: Determinants of cognitive aging. Disponível em: <http://www.np.unimaas.nl/maas>. Cited 4 times in pages 23, 97, 108, and 110.

31 WECHSLER, D. *Manual for the Wechsler Adult Intelligence Scale.* Oxford, England: Psychological Corp., 1955. vi, 110–vi, 110 p. Cited in page 23.

32 PRINS, N. D. et al. Cerebral small-vessel disease and decline in information processing speed, executive function and memory. *Brain*, Oxford Academic, v. 128, n. 9, p. 2034–2041, sep 2005. ISSN 0006-8950. Disponível em: <https://academic.oup.com/brain/article/128/9/ 2034/365950>. Cited in page 24.

33 NORDEN, A. G. van et al. Causes and consequences of cerebral small vessel disease. The RUN DMC study: A prospective cohort study. Study rationale and protocol. *BMC Neurology*, 2011. ISSN 14712377. Cited in page 24.

34 SHI, Y.; WARDLAW, J. M. Update on cerebral small vessel disease: a dynamic whole-brain disease. *BMJ*, v. 1, n. 3, p. 83–92, 2016. ISSN 2059-8688. Disponível em: <http://svn.bmj.com/cgi/doi/10.1136/svn-2016-000035>. Cited in page 24.

35 PANTONI, L. *Cerebral small vessel disease: from pathogenesis and clinical characteristics to therapeutic challenges.* 2010. Cited in page 24.

36 LAWRENCE, A. J. et al. *Pattern and rate of cognitive decline in cerebral small vessel disease: A prospective study.* 2015. Cited in page 24.

37 PANTONI, L.; POGGESI, A.; INZITARI, D. *The relation between white-matter lesions and cognition.* 2007. 390–397 p. Cited 2 times in pages 24 and 69.

38 CAPLAN, L. R. Lacunar infarction and small vessel disease: pathology and pathophysiology. *Journal of stroke*, v. 17, n. 1, p. 2–6, 2015. ISSN 2287-6391. Disponível em: <http://www.pubmedcentral.nih.gov/articlerender.fcgi?artid=4325635&tool=pmcentrez& rendertype=abstract>. Cited in page 24.

39 SHOAMANESH, A. et al. Inflammatory biomarkers, cerebral microbleeds, and small vessel disease: Framingham heart study. *Neurology*, v. 84, n. 8, p. 825–832, 2015. ISSN 1526632X. Cited in page 24.

40   HURFORD, R. et al. MRI-visible perivascular spaces: Relationship to cognition and small vessel disease MRI markers in ischaemic stroke and TIA. *Journal of Neurology, Neurosurgery and Psychiatry*, v. 85, n. 5, p. 522–525, 2014. ISSN 1468330X.   Cited in page 24.

41   XU, X. et al. The effect of the total small vessel disease burden on the structural brain network. *Scientific reports*, v. 8, n. 1, p. 7442, 2018. ISSN 2045-2322. Disponível em: <http://www.nature.com/articles/s41598-018-25917-4%0Ahttp://www.ncbi.nlm.nih.gov/pubmed/29748646>.   Cited 3 times in pages 12, 24, and 61.

42   DEY, A. K. et al. Pathoconnectomics of cognitive impairment in small vessel disease: A systematic review. *Alzheimer's & Dementia*, v. 12, n. 7, p. 831–845, 2016. Disponível em: <https://alz-journals.onlinelibrary.wiley.com/doi/abs/10.1016/j.jalz.2016.01.007>.   Cited in page 24.

43   SPRENG, R. N. et al. Intrinsic Architecture Underlying the Relations among the Default, Dorsal Attention, and Frontoparietal Control Networks of the Human Brain. *Journal of Cognitive Neuroscience*, v. 25, n. 1, p. 74–86, 01 2013. ISSN 0898-929X. Disponível em: <https://doi.org/10.1162/jocn_a_00281>.   Cited in page 24.

44   SUN, Y. W. et al. Abnormal functional connectivity in patients with vascular cognitive impairment, no dementia: a resting-state functional magnetic resonance imaging study. *Behav Brain Res*, v. 223, n. 2, p. 388–394, 2011. Disponível em: <http://www.ncbi.nlm.nih.gov/pubmed/21605598>.   Cited in page 24.

45   CHENG, H.-L. et al. Impairments in cognitive function and brain connectivity in severe asymptomatic carotid stenosis. *Stroke*, v. 43, n. 10, p. 2567–2573, 2012. ISSN 1524-4628.   Cited in page 24.

46   BATISTA-GARCÍA-RAMÓ, K.; FERNÁNDEZ-VERDECIA, C. I. *What we know about the brain structure-function relationship*. 2018.   Cited in page 27.

47   RUBINOV, M. et al. Symbiotic relationship between brain structure and dynamics. *BMC Neuroscience*, 2009. ISSN 14712202.   Cited in page 27.

48   HONEY, C. J. et al. Predicting human resting-state functional connectivity from structural connectivity. *Proceedings of the National Academy of Sciences of the United States of America*, 2009. ISSN 00278424.   Cited 2 times in pages 27 and 40.

49   NAKAGAWA, T. T. et al. Bottom up modeling of the connectome: Linking structure and function in the resting brain and their changes in aging. *NeuroImage*, 2013. ISSN 10538119.   Cited in page 27.

50   PERSSON, J. et al. Structure-function correlates of cognitive decline in aging. *Cerebral Cortex*, 2006. ISSN 10473211.   Cited in page 27.

51   SKUDLARSKI, P. et al. Brain Connectivity Is Not Only Lower but Different in Schizophrenia: A Combined Anatomical and Functional Approach. *Biological Psychiatry*, 2010. ISSN 00063223.   Cited in page 27.

52   ROBINSON, J. L. et al. Characterization of Structural Connectivity of the Default Mode Network in Dogs using Diffusion Tensor Imaging. *Scientific reports*, v. 6, p. 36851, 2016. ISSN 2045-2322.   Cited in page 27.

53   YEH, F.-C.; TSENG, W.-Y. I. Ntu-90: A high angular resolution brain atlas constructed by q-space diffeomorphic reconstruction. *NeuroImage*, v. 58, n. 1, p. 91–99, 2011. ISSN 1053-8119. Disponível em: <https://www.sciencedirect.com/science/article/pii/S1053811911006392>. Cited 4 times in pages 27, 31, 41, and 72.

54   MAIER-HEIN, K. H. et al. The challenge of mapping the human connectome based on diffusion tractography. *Nature Communications*, 2017. ISSN 20411723.   Cited in page 27.

55   FRISTON, K. J.; HARRISON, L.; PENNY, W. Dynamic causal modelling. *NeuroImage*, v. 19, n. 4, p. 1273–1302, 2003. ISSN 10538119.   Cited in page 28.

56   O'BRIEN, C. P. *The CAGE questionnaire for detection of alcoholism: A remarkably useful but simple tool*. 2008. 2054–2056 p.   Cited in page 29.

57   FEYS, P. et al. *The Nine-Hole Peg Test as a manual dexterity performance measure for multiple sclerosis*. 2017.   Cited 2 times in pages 29 and 46.

58   PEIRCE, J. W. Psychopy—psychophysics software in python. *Journal of neuroscience methods*, Elsevier, v. 162, n. 1-2, p. 8–13, 2007.   Cited 2 times in pages 30 and 47.

59   MALDJIAN, J. WFU PickAtlas User Manual v2 . 4. *Human Brain Mapping*, v. 63, p. 1–13, 1994.   Cited 2 times in pages 30 and 48.

60   WHITFIELD-GABRIELI, S.; NIETO-CASTANON, A. Conn: a functional connectivity toolbox for correlated and anticorrelated brain networks. *Brain connectivity*, Mary Ann Liebert, Inc. 140 Huguenot Street, 3rd Floor New Rochelle, NY 10801 USA, v. 2, n. 3, p. 125–141, 2012.   Cited 4 times in pages 30, 44, 47, and 73.

61   COLE, M. W. et al. Task activations produce spurious but systematic inflation of task functional connectivity estimates. *NeuroImage*, Elsevier, v. 189, p. 1–18, 2019.   Cited 5 times in pages 30, 46, 48, 49, and 51.

62   BÜCHEL, C. et al. Characterizing stimulus-response functions using nonlinear regressors in parametric fMRI experiments. *NeuroImage*, v. 8, n. 2, p. 140–148, 1998. ISSN 10538119.   Cited in page 31.

63   STEPHAN, K. E. et al. Bayesian model selection for group studies. *Neuroimage*, Elsevier, v. 46, n. 4, p. 1004–1017, 2009.   Cited in page 31.

64   RIGOUX, L. et al. Bayesian model selection for group studies - Revisited. *NeuroImage*, 2014. ISSN 10959572.   Cited in page 31.

65   YEH, F.-C.; WEDEEN, V. J.; TSENG, W.-Y. I. Generalized $\{q\}$-sampling imaging. *IEEE transactions on medical imaging*, IEEE, v. 29, n. 9, p. 1626–1635, 2010.   Cited 3 times in pages 31, 32, and 72.

66   YEH, F.-C. et al. Mapping immune cell infiltration using restricted diffusion mri. *Magnetic resonance in medicine*, Wiley Online Library, v. 77, n. 2, p. 603–612, 2017.   Cited 3 times in pages 31, 32, and 72.

67   ZEIDMAN, P. et al. A tutorial on group effective connectivity analysis, part 2 : second level analysis with PEB 1 Introduction. *Arxiv*, 2019.   Cited 2 times in pages 31 and 38.

68   ZEIDMAN, P. et al. A guide to group effective connectivity analysis, part 1: First level analysis with DCM for fMRI. *NeuroImage*, 2019. ISSN 10959572. Cited in page 31.

69   ANDERSSON, J. L.; SOTIROPOULOS, S. N. An integrated approach to correction for off-resonance effects and subject movement in diffusion MR imaging. *NeuroImage*, 2016. ISSN 10959572. Cited in page 31.

70   SMITH, S. M. Fast robust automated brain extraction. *Human Brain Mapping*, 2002. ISSN 10659471. Cited in page 31.

71   JENKINSON, M. et al. Fsl. *NeuroImage*, v. 62, n. 2, p. 782–790, 2012. ISSN 10538119. Cited in page 31.

72   YEH, F.-C. et al. Deterministic diffusion fiber tracking improved by quantitative anisotropy. *PloS one*, Public Library of Science San Francisco, USA, v. 8, n. 11, p. e80713, 2013. Cited 2 times in pages 31 and 72.

73   BAUER, C. M. et al. Age-related changes in structural connectivity are improved using subject-specific thresholding. *Journal of Neuroscience Methods*, 2017. ISSN 1872678X. Cited in page 31.

74   YEH, F.-C. et al. Population-averaged atlas of the macroscale human structural connectome and its network topology. *Neuroimage*, Elsevier, v. 178, p. 57–68, 2018. Cited 2 times in pages 31 and 72.

75   LIU, Y.; YTTRI, E. A.; SNYDER, L. H. Intention and attention: Different functional roles for LIPd and LIPv. *Nature Neuroscience*, 2010. ISSN 10976256. Cited in page 39.

76   KATSUKI, F.; CONSTANTINIDIS, C. Bottom-Up and Top-Down Attention. *The Neuroscientist*, 2014. ISSN 1073-8584. Cited in page 39.

77   HUANG, H.; DING, M. Linking Functional Connectivity and Structural Connectivity Quantitatively: A Comparison of Methods. *Brain Connectivity*, 2016. ISSN 21580022. Cited in page 40.

78   TSANG, A. et al. White matter structural connectivity is not correlated to cortical resting-state functional connectivity over the healthy adult lifespan. *Frontiers in Aging Neuroscience*, 2017. ISSN 16634365. Cited 2 times in pages 40 and 41.

79   KOCEVAR, G. et al. Brain structural connectivity correlates with fluid intelligence in children: A DTI graph analysis. *Intelligence*, 2019. ISSN 01602896. Cited in page 40.

80   FRISTON, K.; MORAN, R.; SETH, A. K. *Analysing connectivity with Granger causality and dynamic causal modelling*. 2013. Cited in page 40.

81   DAUNIZEAU, J.; DAVID, O.; STEPHAN, K. E. *Dynamic causal modelling: A critical review of the biophysical and statistical foundations*. 2011. Cited in page 41.

82   TALAI, A. S. et al. Widespread diffusion changes differentiate Parkinson's disease and progressive supranuclear palsy. *NeuroImage: Clinical*, 2018. ISSN 22131582. Cited in page 41.

83   MINETT, T. et al. Longitudinal diffusion tensor imaging changes in early Parkinson's disease: ICICLE-PD study. *Journal of Neurology*, 2018. ISSN 14321459. Cited in page 41.

84   KANTARCI, K. et al. White-matter integrity on DTI and the pathologic staging of Alzheimer's disease. *Neurobiology of Aging*, 2017. ISSN 15581497. Cited in page 41.

85   CABALLERO, M. Á. A. et al. White matter diffusion alterations precede symptom onset in autosomal dominant Alzheimer's disease. *Brain*, 2018. ISSN 14602156. Cited in page 41.

86   RAIKES, A. C. et al. Diffusion Tensor Imaging (DTI) correlates of self-reported sleep quality and depression following mild traumatic brain injury. *Frontiers in Neurology*, 2018. ISSN 16642295. Cited in page 41.

87   MARGULIES, D. S. et al. Precuneus shares intrinsic functional architecture in humans and monkeys. *Proceedings of the National Academy of Sciences*, National Acad Sciences, v. 106, n. 47, p. 20069–20074, 2009. Cited 4 times in pages 42, 44, 53, and 109.

88   CAVANNA, A. E. The precuneus and consciousness. *CNS spectrums*, Cambridge University Press, v. 12, n. 7, p. 545–552, 2007. Cited 3 times in pages 42, 44, and 54.

89   DELUCA, C. et al. The cerebellum and visual perceptual learning: Evidence from a motion extrapolation task. *Cortex*, 2014. ISSN 19738102. Cited in page 42.

90   LEV, M. et al. Training improves visual processing speed and generalizes to untrained functions. *Scientific Reports*, 2014. ISSN 20452322. Cited in page 42.

91   GOULDEN, N. et al. Sample Size Estimation for Comparing Parameters Using Dynamic Causal Modeling. *Brain Connectivity*, 2012. ISSN 21580022. Cited in page 42.

92   DESMOND, J. E.; GLOVER, G. H. Estimating sample size in functional MRI (fMRI) neuroimaging studies: Statistical power analyses. *Journal of Neuroscience Methods*, 2002. ISSN 01650270. Cited in page 42.

93   SILVA, P. H. R. da et al. Brain structural-functional connectivity relationship underlying the Information Processing Speed. *Brain Connectivity*, Mary Ann Liebert, Inc., publishers, mar 2020. ISSN 2158-0014. Disponível em: <https://doi.org/10.1089/brain.2019.0726>. Cited 2 times in pages 43 and 109.

94   UTEVSKY, A. V.; SMITH, D. V.; HUETTEL, S. A. Precuneus Is a Functional Core of the Default-Mode Network. *The Journal of Neuroscience*, v. 34, n. 3, p. 932–940, 2014. ISSN 0270-6474. Disponível em: <http://www.jneurosci.org/lookup/doi/10.1523/JNEUROSCI.4227-13.2014>. Cited 2 times in pages 44 and 53.

95   LEECH, R.; SHARP, D. J. The role of the posterior cingulate cortex in cognition and disease. *Brain*, Oxford University Press, v. 137, n. 1, p. 12–32, 2014. Cited 3 times in pages 44, 53, and 109.

96   ANTICEVIC, A. et al. The role of default network deactivation in cognition and disease. *Trends in cognitive sciences*, Elsevier, v. 16, n. 12, p. 584–592, 2012. Cited 4 times in pages 44, 45, 52, and 109.

97   LEECH, R. et al. Fractionating the default mode network: Distinct contributions of the ventral and dorsal posterior cingulate cortex to cognitive control. *Journal of Neuroscience*, 2011. ISSN 02706474. Cited in page 44.

98   ELTON, A.; GAO, W. Task-positive functional connectivity of the default mode network transcends task domain. *Journal of Cognitive Neuroscience*, MIT Press One Rogers Street, Cambridge, MA 02142-1209, USA journals-info . . . , v. 27, n. 12, p. 2369–2381, 2015.   Cited in page 44.

99   GAO, W. et al. Functional connectivity of the infant human brain: plastic and modifiable. *The Neuroscientist*, Sage Publications Sage CA: Los Angeles, CA, v. 23, n. 2, p. 169–184, 2017. Cited in page 44.

100   VATANSEVER, D.; MENON, D. K.; STAMATAKIS, E. A. Default mode contributions to automated information processing. *Proceedings of the National Academy of Sciences*, National Acad Sciences, v. 114, n. 48, p. 12821–12826, 2017.   Cited in page 44.

101   LAUREYS, S. et al. Impaired effective cortical connectivity in vegetative state: preliminary investigation using pet. *Neuroimage*, Elsevier, v. 9, n. 4, p. 377–382, 1999.   Cited in page 44.

102   VANHAUDENHUYSE, A. et al. Default network connectivity reflects the level of consciousness in non-communicative brain-damaged patients. *Brain*, v. 133, n. 1, p. 161–171, 12 2009. ISSN 0006-8950. Disponível em: <https://doi.org/10.1093/brain/awp313>.   Cited in page 44.

103   COSTIGAN, A. G. et al. Neurochemical correlates of scene processing in the precuneus/posterior cingulate cortex: A multimodal fmri and 1h-mrs study. *Human brain mapping*, Wiley Online Library, v. 40, n. 10, p. 2884–2898, 2019.   Cited in page 44.

104   WANG, Z. et al. The role of the precuneus and posterior cingulate cortex in the neural routes to action. *Computer Assisted Surgery*, Taylor & Francis, v. 24, n. sup1, p. 113–120, 2019. Cited in page 44.

105   SILVA, S. et al. Disruption of posteromedial large-scale neural communication predicts recovery from coma. *Neurology*, AAN Enterprises, v. 85, n. 23, p. 2036–2044, 2015.   Cited in page 44.

106   MADDOCK, R. J.; GARRETT, A. S.; BUONOCORE, M. H. Posterior cingulate cortex activation by emotional words: fmri evidence from a valence decision task. *Human brain mapping*, Wiley Online Library, v. 18, n. 1, p. 30–41, 2003.   Cited in page 44.

107   MADDOCK, R. J.; GARRETT, A. S.; BUONOCORE, M. H. Remembering familiar people: the posterior cingulate cortex and autobiographical memory retrieval. *Neuroscience*, Elsevier, v. 104, n. 3, p. 667–676, 2001.   Cited in page 44.

108   HAYDEN, B. Y. et al. Posterior cingulate cortex mediates outcome-contingent allocation of behavior. *Neuron*, Elsevier, v. 60, n. 1, p. 19–25, 2008.   Cited in page 44.

109   RAICHLE, M. E. et al. A default mode of brain function. *Proceedings of the National Academy of Sciences*, National Acad Sciences, v. 98, n. 2, p. 676–682, 2001.   Cited 3 times in pages 44, 52, and 53.

110   CATTANEO, Z. et al. The role of the angular gyrus in the modulation of visuospatial attention by the mental number line. *Neuroimage*, Elsevier, v. 44, n. 2, p. 563–568, 2009.   Cited in page 44.

111   STUDER, B.; CEN, D.; WALSH, V. The angular gyrus and visuospatial attention in decision-making under risk. *NeuroImage*, Elsevier, v. 103, p. 75–80, 2014. Cited in page 44.

112   TANAKA, S.; KIRINO, E. Increased functional connectivity of the angular gyrus during imagined music performance. *Frontiers in human neuroscience*, Frontiers, v. 13, p. 92, 2019. Cited in page 44.

113   VIGNEAU, M. et al. Meta-analyzing left hemisphere language areas: phonology, semantics, and sentence processing. *Neuroimage*, Elsevier, v. 30, n. 4, p. 1414–1432, 2006. Cited in page 44.

114   HIRNSTEIN, M. et al. TMS over the left angular gyrus impairs the ability to discriminate left from right. *Neuropsychologia*, 2011. ISSN 00283932. Cited 2 times in pages 44 and 52.

115   LEMIERE, J. et al. Longitudinal study evaluating neuropsychological changes in so-called asymptomatic carriers of the Huntington's disease mutation after 1 year. *Acta Neurologica Scandinavica*, 2002. ISSN 00016314. Cited in page 45.

116   FELMINGHAM, K. L.; BAGULEY, I. J.; GREEN, A. M. Effects of diffuse axonal injury on speed of information processing following severe traumatic brain injury. *Neuropsychology*, American Psychological Association, v. 18, n. 3, p. 564, 2004. Cited in page 45.

117   HAWORTH, J. et al. Measuring information processing speed in mild cognitive impairment: clinical versus research dichotomy. *Journal of Alzheimer's Disease*, IOS Press, v. 51, n. 1, p. 263–275, 2016. Cited in page 45.

118   ZHANG, J. Y.; FEINSTEIN, A. Screening for cognitive impairments after traumatic brain injury: A comparison of a brief computerized battery with the montreal cognitive assessment. *Journal of Neuropsychiatry and Clinical Neurosciences*, 2016. ISSN 15457222. Cited in page 45.

119   PASCOE, M. et al. The symbol-digit modalities test in mild cognitive impairment: evidence from parkinson's disease patients. *European neurology*, Karger Publishers, v. 79, n. 3-4, p. 206–210, 2018. Cited in page 45.

120   PANTONI, L. et al. Fractal dimension of cerebral white matter: A consistent feature for prediction of the cognitive performance in patients with small vessel disease and mild cognitive impairment. *NeuroImage: Clinical*, 2019. ISSN 22131582. Cited in page 45.

121   PATEL, V. P.; FEINSTEIN, A. The link between depression and performance on the Symbol Digit Modalities Test: Mechanisms and clinical significance. *Multiple Sclerosis Journal*, 2019. ISSN 14770970. Cited in page 45.

122   SHERIDAN, L. K. et al. Normative symbol digit modalities test performance in a community-based sample. *Archives of Clinical Neuropsychology*, Elsevier, v. 21, n. 1, p. 23–28, 2006. Cited 2 times in pages 45 and 46.

123   Van Schependom, J. et al. The Symbol Digit Modalities Test as sentinel test for cognitive impairment in multiple sclerosis. *European Journal of Neurology*, 2014. ISSN 14681331. Cited in page 45.

124   ZANTO, T. P.; PA, J.; GAZZALEY, A. Reliability measures of functional magnetic resonance imaging in a longitudinal evaluation of mild cognitive impairment. *Neuroimage*, Elsevier, v. 84, p. 443–452, 2014. Cited in page 45.

125 FRISTON, K. J. et al. Characterizing dynamic brain responses with fmri: a multivariate approach. *Neuroimage*, Elsevier, v. 2, n. 2, p. 166–172, 1995. Cited in page 47.

126 ASHBURNER, J.; FRISTON, K. J. Unified segmentation. *Neuroimage*, Elsevier, v. 26, n. 3, p. 839–851, 2005. Cited in page 47.

127 POWER, J. D. et al. Spurious but systematic correlations in functional connectivity mri networks arise from subject motion. *Neuroimage*, Elsevier, v. 59, n. 3, p. 2142–2154, 2012. Cited in page 47.

128 POWER, J. D. et al. Methods to detect, characterize, and remove motion artifact in resting state fMRI. *NeuroImage*, 2014. ISSN 10538119. Cited in page 47.

129 DI, X.; BISWAL, B. B. Characterizations of resting-state modulatory interactions in the human brain. *Journal of neurophysiology*, American Physiological Society Bethesda, MD, v. 114, n. 5, p. 2785–2796, 2015. Cited in page 47.

130 TZOURIO-MAZOYER, N. et al. Automated anatomical labeling of activations in spm using a macroscopic anatomical parcellation of the mni mri single-subject brain. *Neuroimage*, Elsevier, v. 15, n. 1, p. 273–289, 2002. Cited in page 48.

131 FOX, M. D. et al. The human brain is intrinsically organized into dynamic, anticorrelated functional networks. *Proceedings of the National Academy of Sciences*, National Acad Sciences, v. 102, n. 27, p. 9673–9678, 2005. Cited 2 times in pages 48 and 53.

132 BENJAMINI, Y.; HOCHBERG, Y. Controlling the false discovery rate: a practical and powerful approach to multiple testing. *Journal of the Royal statistical society: series B (Methodological)*, Wiley Online Library, v. 57, n. 1, p. 289–300, 1995. Cited in page 48.

133 YASUNO, F. et al. Resting-state synchrony between the retrosplenial cortex and anterior medial cortical structures relates to memory complaints in subjective cognitive impairment. *Neurobiology of Aging*, 2015. ISSN 15581497. Cited in page 49.

134 LIECHTI, M. E. Modern clinical research on lsd. *Neuropsychopharmacology*, Nature Publishing Group, v. 42, n. 11, p. 2114–2127, 2017. Cited in page 49.

135 MÜLLER, F. et al. Increased thalamic resting-state connectivity as a core driver of lsd-induced hallucinations. *Acta Psychiatrica Scandinavica*, Wiley Online Library, v. 136, n. 6, p. 648–657, 2017. Cited in page 49.

136 COGET, A. et al. Transient immediate postoperative homotopic functional disconnectivity in low-grade glioma patients. *NeuroImage: Clinical*, Elsevier, v. 18, p. 656–662, 2018. Cited in page 49.

137 MATTIACCIO, L. M. et al. Frontal dysconnectivity in 22q11.2 deletion syndrome: An atlas-based functional connectivity analysis. *Behavioral and Brain Functions*, 2018. ISSN 17449081. Cited in page 49.

138 ZHOU, H.; TANG, Y.; YUAN, Z. White matter asymmetries in patients with cerebral small vessel disease. *Journal of Integrative Neuroscience*, 2018. ISSN 1757448X. Cited 2 times in pages 52 and 59.

139   BARTOVA, L. et al. Reduced default mode network suppression during a working memory task in remitted major depression. *Journal of Psychiatric Research*, 2015. ISSN 18791379. Cited in page 52.

140   SHULMAN, G. L. et al. Common blood flow changes across visual tasks: II. Decreases in cerebral cortex. *Journal of Cognitive Neuroscience*, 1997. ISSN 0898929X. Cited in page 52.

141   GEDAY, J.; GJEDDE, A. Attention, emotion, and deactivation of default activity in inferior medial prefrontal cortex. *Brain and Cognition*, 2009. ISSN 02782626. Cited in page 52.

142   LUNDSTROM, B. N.; INGVAR, M.; PETERSSON, K. M. The role of precuneus and left inferior frontal cortex during source memory episodic retrieval. *NeuroImage*, 2005. ISSN 10538119. Cited in page 53.

143   FRANSSON, P.; MARRELEC, G. The precuneus/posterior cingulate cortex plays a pivotal role in the default mode network: Evidence from a partial correlation network analysis. *NeuroImage*, 2008. ISSN 10538119. Cited in page 53.

144   Thomas Yeo, B. T. et al. The organization of the human cerebral cortex estimated by intrinsic functional connectivity. *Journal of Neurophysiology*, 2011. ISSN 00223077. Cited in page 54.

145   ZHANG, S.; LI, C. s. R. Functional connectivity mapping of the human precuneus by resting state fMRI. *NeuroImage*, 2012. ISSN 10538119. Cited in page 54.

146   GORDON, E. M. et al. Generation and Evaluation of a Cortical Area Parcellation from Resting-State Correlations. *Cerebral Cortex*, 2016. ISSN 14602199. Cited in page 54.

147   LUO, Z. et al. Functional Parcellation of Human Brain Precuneus Using Density-Based Clustering. *Cerebral Cortex*, v. 30, n. 1, p. 269–282, 2019. ISSN 1047-3211. Disponível em: <https://doi.org/10.1093/cercor/bhz086>. Cited in page 54.

148   KIM, H. J. et al. Distinctive Resting State Network Disruptions among Alzheimer's Disease, Subcortical Vascular Dementia, and Mixed Dementia Patients. *Journal of Alzheimer's Disease*, 2016. ISSN 18758908. Cited in page 54.

149   WANG, Z. et al. The baseline and longitudinal changes of PCC connectivity in mild cognitive impairment: A combined structure and resting-state fMRI study. *PLoS ONE*, 2012. ISSN 19326203. Cited in page 54.

150   CASTELLANOS, F. X. et al. Cingulate-Precuneus Interactions: A New Locus of Dysfunction in Adult Attention-Deficit/Hyperactivity Disorder. *Biological Psychiatry*, 2008. ISSN 00063223. Cited in page 54.

151   KORGAONKAR, M. S. et al. Intrinsic connectomes are a predictive biomarker of remission in major depressive disorder. *Molecular Psychiatry*, 2020. ISSN 14765578. Cited in page 54.

152   BAE, S. et al. Bupropion shows different effects on brain functional connectivity in patients with Internet-based gambling disorder and internet gaming disorder. *Frontiers in Psychiatry*, 2018. ISSN 16640640. Cited in page 54.

153   LEE, D. et al. Subregions of the anterior cingulate cortex form distinct functional connectivity patterns in young males with internet gaming disorder with comorbid depression. *Frontiers in Psychiatry*, 2018. ISSN 16640640.   Cited in page 54.

154   CHEN, L. et al. Topological reorganization of the default mode network in severe male obstructive sleep apnea. *Frontiers in Neurology*, 2018. ISSN 16642295.   Cited in page 54.

155   HANEEF, Z. et al. Network analysis of the default mode network using functional connectivity MRI in temporal lobe epilepsy. *Journal of Visualized Experiments*, 2014. ISSN 1940087X.   Cited in page 54.

156   SUCHAN, B. et al. Hemispheric dissociation of visual-pattern processing and visual rotation. *Behavioural Brain Research*, 2002. ISSN 01664328.   Cited in page 54.

157   KNAUFF, M. et al. Reasoning, models, and images: Behavioral measures and cortical activity. *Journal of Cognitive Neuroscience*, 2003. ISSN 0898929X.   Cited in page 54.

158   CAVANNA, A. E.; TRIMBLE, M. R. *The precuneus: A review of its functional anatomy and behavioural correlates*. 2006.   Cited in page 54.

159   SILVA, P. H. R. da; RONDINONI, C.; LEONI, R. F. Non-classical behavior of the default mode network regions during an information processing task. *Brain Structure and Function*, Springer Science and Business Media Deutschland GmbH, v. 225, n. 8, p. 2553–2562, nov 2020. ISSN 18632661. Disponível em: <https://doi.org/10.1007/s00429-020-02143-1>.   Cited in page 54.

160   PANTONI, L. Cerebral small vessel disease: from pathogenesis and clinical characteristics to therapeutic challenges. *The Lancet Neurology*, Elsevier, v. 9, n. 7, p. 689–701, 2010.   Cited 2 times in pages 55 and 96.

161   WARDLAW, J. M.; SMITH, C.; DICHGANS, M. Small vessel disease: mechanisms and clinical implications. *The Lancet Neurology*, Elsevier, v. 18, n. 7, p. 684–696, 2019.   Cited 2 times in pages 55 and 69.

162   DICHGANS, M.; LEYS, D. Vascular cognitive impairment. *Circulation research*, Am Heart Assoc, v. 120, n. 3, p. 573–591, 2017.   Cited 2 times in pages 55 and 69.

163   WARDLAW, J. M. et al. Neuroimaging standards for research into small vessel disease and its contribution to ageing and neurodegeneration. *The Lancet Neurology*, v. 12, n. 8, p. 822–838, aug 2013. ISSN 14744422.   Cited in page 55.

164   WARDLAW, J. M.; SMITH, C.; DICHGANS, M. Mechanisms of sporadic cerebral small vessel disease: insights from neuroimaging. *The Lancet Neurology*, Elsevier, v. 12, n. 5, p. 483–497, 2013.   Cited 2 times in pages 55 and 56.

165   PASI, M. et al. White matter microstructural damage on diffusion tensor imaging in cerebral small vessel disease: clinical consequences. *Stroke*, Am Heart Assoc, v. 47, n. 6, p. 1679–1684, 2016.   Cited 3 times in pages 55, 56, and 61.

166   Ter Telgte, A. et al. *Cerebral small vessel disease: From a focal to a global perspective*. 2018.   Cited 4 times in pages 55, 69, 96, and 108.

167   SMITH, E. E. et al. Harmonizing brain magnetic resonance imaging methods for vascular contributions to neurodegeneration. *Alzheimer's & Dementia: Diagnosis, Assessment & Disease Monitoring,* Elsevier, v. 11, p. 191–204, 2019.   Cited in page 55.

168   ZOTIN, M. C. Z. et al. Cerebral small vessel disease and vascular cognitive impairment: from diagnosis to management. *Current Opinion in Neurology,* Wolters Kluwer Health, v. 34, n. 2, p. 246, 2021.   Cited in page 55.

169   BLAIR, G. W. et al. Advanced neuroimaging of cerebral small vessel disease. *Current treatment options in cardiovascular medicine,* Springer, v. 19, n. 7, p. 1–17, 2017.   Cited in page 55.

170   GALE, E. M.; CARAVAN, P. *Gadolinium-free contrast agents for magnetic resonance imaging of the central nervous system.* [S.l.]: ACS Publications, 2018. 395–397 p.   Cited in page 55.

171   WONG, W. H. E.; MALLER, J. J. Arterial spin labeling techniques 2009–2014. *Journal of medical imaging and radiation sciences,* Elsevier, v. 47, n. 1, p. 98–107, 2016.   Cited in page 56.

172   PASCHOAL, A. M. et al. Intravoxel incoherent motion mri in neurological and cerebrovascular diseases. *NeuroImage: Clinical,* Elsevier, v. 20, p. 705–714, 2018.   Cited in page 56.

173   LEONI, R. et al. Cerebral blood flow and vasoreactivity in aging: an arterial spin labeling study. *Brazilian Journal of Medical and Biological Research,* SciELO Brasil, v. 50, 2017.   Cited in page 56.

174   SHAMSEER, L. et al. Preferred reporting items for systematic review and meta-analysis protocols (prisma-p) 2015: elaboration and explanation. *Bmj,* British Medical Journal Publishing Group, v. 349, 2015.   Cited in page 56.

175   SALAMI, A. et al. Age-related white matter microstructural differences partly mediate age-related decline in processing speed but not cognition. *Biochimica et Biophysica Acta (BBA)-Molecular Basis of Disease,* Elsevier, v. 1822, n. 3, p. 408–415, 2012.   Cited in page 58.

176   ALEXANDER, A. L. et al. Diffusion Tensor Imaging of the Brain. *Neurotherapeutics,* 2007. ISSN 19337213.   Cited in page 58.

177   PAPMA, J. M. et al. Cerebral small vessel disease affects white matter microstructure in mild cognitive impairment. *Human Brain Mapping,* 2014. ISSN 10970193.   Cited 3 times in pages 12, 58, and 61.

178   D'SOUZA, M. M. et al. Diffusion tensor tractography in cerebral small vessel disease: correlation with cognitive function. *Neuroradiology Journal,* 2018. ISSN 19714009.   Cited in page 58.

179   DUERING, M. et al. Free water determines diffusion alterations and clinical status in cerebral small vessel disease. *Alzheimer's and Dementia,* 2018. ISSN 15525279.   Cited 2 times in pages 58 and 60.

180   NITKUNAN, A. et al. Multimodal MRI in Cerebral Small Vessel Disease. *Stroke,* 2008. ISSN 0039-2499.   Cited 2 times in pages 58 and 69.

181 Van Leijsen, E. M. et al. Progression of white matter hyperintensities preceded by heterogeneous decline of microstructural integrity. *Stroke*, 2018. ISSN 15244628. Cited in page 58.

182 O'SULLIVAN, M. et al. Diffusion tensor MRI correlates with executive dysfunction in patients with ischaemic leukoaraiosis. *Journal of Neurology, Neurosurgery and Psychiatry*, 2004. ISSN 00223050. Cited in page 58.

183 LAWRENCE, A. J. et al. Mechanisms of Cognitive Impairment in Cerebral Small Vessel Disease: Multimodal MRI Results from the St George's Cognition and Neuroimaging in Stroke (SCANS) Study. *PLoS ONE*, 2013. ISSN 19326203. Cited in page 58.

184 DOBRYNINA, L. A. et al. Microstructural Predictors of Cognitive Impairment in Cerebral Small Vessel Disease and the Conditions of Their Formation. *Diagnostics*, 2020. Cited in page 58.

185 De Laat, K. F. et al. Loss of white matter integrity is associated with gait disorders in cerebral small vessel disease. *Brain*, 2011. ISSN 00068950. Cited in page 58.

186 De Laat, K. F. et al. Diffusion tensor imaging and gait in elderly persons with cerebral small vessel disease. *Stroke*, 2011. ISSN 00392499. Cited in page 58.

187 VERGHESE, J. et al. Epidemiology of gait disorders in community-residing older adults. *Journal of the American Geriatrics Society*, 2006. ISSN 00028614. Cited in page 58.

188 CAVALLARI, M. et al. Thalamic fractional anisotropy predicts accrual of cerebral white matter damage in older subjects with small-vessel disease. *Journal of Cerebral Blood Flow and Metabolism*, 2014. ISSN 15597016. Cited in page 58.

189 ZEESTRATEN, E. A. et al. Application of diffusion tensor imaging parameters to detect change in longitudinal studies in cerebral small vessel disease. *PLoS ONE*, 2016. ISSN 19326203. Cited in page 58.

190 ZEESTRATEN, E. A. et al. Change in multimodal MRI markers predicts dementia risk in cerebral small vessel disease. *Neurology*, 2017. ISSN 1526632X. Cited in page 58.

191 Van Der Holst, H. M. et al. Factors associated with 8-year mortality in older patients with cerebral small vessel disease the Radboud University Nijmegen Diffusion Tensor and Magnetic Resonance Cohort (RUN DMC) study. *JAMA Neurology*, 2016. ISSN 21686149. Cited in page 58.

192 LAWRENCE, A. J. et al. A comparison of functional and tractography based networks in cerebral small vessel disease. *NeuroImage: Clinical*, Elsevier, v. 18, p. 425–432, 2018. Cited 3 times in pages 58, 64, and 66.

193 TULADHAR, A. M. et al. Structural network efficiency predicts conversion to dementia. *Neurology*, 2016. ISSN 1526632X. Cited in page 58.

194 TULADHAR, A. M. et al. Structural network changes in cerebral small vessel disease. *Journal of Neurology, Neurosurgery & Psychiatry*, BMJ Publishing Group Ltd, v. 91, n. 2, p. 196–203, 2020. ISSN 0022-3050. Disponível em: <https://jnnp.bmj.com/content/91/2/196>. Cited in page 58.

195   ZHOU, H. et al. Atypical cortical thickness and subcortical volumes in cerebral microbleed patients: A combined freesurfer and diffusion tensor imaging study. *Journal of Medical Imaging and Health Informatics*, 2015. ISSN 21567026.   Cited in page 58.

196   GUNDA, B. et al. ADC histograms from routine DWI for longitudinal studies in cerebral small vessel disease: A field study in CADASIL. *PLoS ONE*, 2014. ISSN 19326203.   Cited in page 58.

197   Van Norden, A. G. et al. Diffusion tensor imaging and cognition in cerebral small vessel disease. The RUN DMC study. *Biochimica et Biophysica Acta - Molecular Basis of Disease*, 2012. ISSN 09254439.   Cited in page 58.

198   Van Norden, A. G. et al. Cognitive function in small vessel disease: The additional value of diffusion tensor imaging to conventional magnetic resonance imaging: The RUN DMC study. *Journal of Alzheimer's Disease*, 2012. ISSN 18758908.   Cited in page 58.

199   BENJAMIN, P. et al. Progression of MRI markers in cerebral small vessel disease: Sample size considerations for clinical trials. *Journal of Cerebral Blood Flow and Metabolism*, 2016. ISSN 15597016.   Cited in page 58.

200   Van Uden, I. W. et al. White matter and hippocampal volume predict the risk of dementia in patients with cerebral small vessel disease: The RUN DMC study. *Journal of Alzheimer's Disease*, 2015. ISSN 18758908.   Cited in page 58.

201   REGINOLD, W. et al. Impact of white matter hyperintensities on surrounding white matter tracts. *Neuroradiology*, 2018. ISSN 14321920.   Cited in page 59.

202   CIULLI, S. et al. Prediction of Impaired Performance in Trail Making Test in MCI Patients with Small Vessel Disease Using DTI Data. *IEEE Journal of Biomedical and Health Informatics*, 2016. ISSN 21682194.   Cited in page 59.

203   LAWRENCE, A. J. et al. Structural network efficiency is associated with cognitive impairment in small-vessel disease. *Neurology*, AAN Enterprises, v. 83, n. 4, p. 304–311, 2014.   Cited 2 times in pages 59 and 93.

204   TULADHAR, A. M. et al. Structural network connectivity and cognition in cerebral small vessel disease. *Human Brain Mapping*, 2016. ISSN 10970193.   Cited in page 59.

205   CHEN, H. F. et al. Microstructural disruption of the right inferior fronto-occipital and inferior longitudinal fasciculus contributes to WMH-related cognitive impairment. *CNS Neuroscience and Therapeutics*, 2020. ISSN 17555949.   Cited in page 59.

206   TULADHAR, A. M. et al. Disruption of rich club organisation in cerebral small vessel disease. *Human Brain Mapping*, 2017. ISSN 10970193.   Cited in page 59.

207   CHEN, X. et al. Disrupted functional and structural connectivity within default mode network contribute to WMH-related cognitive impairment. *NeuroImage: Clinical*, 2019. ISSN 22131582.   Cited in page 59.

208   LEIJSEN, E. M. van et al. Longitudinal changes in rich club organization and cognition in cerebral small vessel disease. *NeuroImage: Clinical*, 2019. ISSN 22131582.   Cited in page 59.

209   DU, J. et al. Structural brain network measures are superior to vascular burden scores in predicting early cognitive impairment in post stroke patients with small vessel disease. *NeuroImage: Clinical*, 2019. ISSN 22131582.   Cited in page 59.

210   LIU, C. et al. Changes of white matter integrity and structural network connectivity in nondemented cerebral small-vessel disease. *Journal of Magnetic Resonance Imaging*, 2020. ISSN 15222586.   Cited in page 59.

211   DU, J. et al. Structural Brain Network Disruption at Preclinical Stage of Cognitive Impairment Due to Cerebral Small Vessel Disease. *Neuroscience*, 2020. ISSN 03064522.   Cited in page 59.

212   BOOT, E. M. et al. Structural network efficiency predicts cognitive decline in cerebral small vessel disease. *NeuroImage: Clinical*, 2020. ISSN 22131582.   Cited in page 59.

213   VERGOOSSEN, L. W. M. et al. Interplay of white matter hyperintensities, cerebral networks, and cognitive function in an adult population: Diffusion-tensor imaging in the maastricht study. *Radiology*, v. 298, n. 2, p. 384–392, 2021. PMID: 33350892. Disponível em: <https://doi.org/10.1148/radiol.2021202634>.   Cited 4 times in pages 59, 67, 69, and 70.

214   BAYKARA, E. et al. A novel imaging marker for small vessel disease based on skeletonization of white matter tracts and diffusion histograms. *Annals of Neurology*, v. 80, n. 4, p. 581–592, 2016. Disponível em: <https://onlinelibrary.wiley.com/doi/abs/10.1002/ana. 24758>.   Cited in page 59.

215   WEI, N. et al. A neuroimaging marker based on diffusion tensor imaging and cognitive impairment due to cerebral white matter lesions. *Frontiers in Neurology*, 2019. ISSN 16642295. Cited in page 59.

216   LOW, A. et al. Peak Width of Skeletonized Mean Diffusivity as a Marker of Diffuse Cerebrovascular Damage. *Frontiers in Neuroscience*, v. 14, 2020. ISSN 1662453X.   Cited in page 60.

217   ALTENDAHL, M. et al. An IL-18-centered inflammatory network as a biomarker for cerebral white matter injury. *PLoS ONE*, 2020. ISSN 19326203.   Cited in page 60.

218   ZHANG, R. et al. Venous disruption affects white matter integrity through increased interstitial fluid in cerebral small vessel disease. *Journal of Cerebral Blood Flow and Metabolism*, 2020. ISSN 15597016.   Cited in page 60.

219   ZHANG, R. et al. Disentangling the pathologies linking white matter hyperintensity and geriatric depressive symptoms in subjects with different degrees of vascular impairment. *Journal of Affective Disorders*, v. 282, 2021. ISSN 15732517.   Cited in page 60.

220   HUANG, P. et al. White Matter Free Water is a Composite Marker of Cerebral Small Vessel Degeneration. *Translational Stroke Research*, 2021. ISSN 1868601X.   Cited in page 60.

221   WILLIAMS, O. A. et al. Diffusion tensor image segmentation of the cerebrum provides a single measure of cerebral small vessel disease severity related to cognitive change. *NeuroImage: Clinical*, 2017. ISSN 22131582.   Cited in page 60.

222   WILLIAMS, O. A. et al. Predicting dementia in cerebral small vessel disease using an automatic diffusion tensor image segmentation technique. *Stroke*, 2019. ISSN 15244628. Cited in page 60.

223 KONIECZNY, M. J. et al. Multi-shell Diffusion MRI Models for White Matter Characterization in Cerebral Small Vessel Disease. *Neurology*, v. 96, n. 5, 2021. ISSN 1526632X. Cited in page 60.

224 TULADHAR, A. M. et al. White matter integrity in small vessel disease is related to cognition. *NeuroImage: Clinical*, 2015. ISSN 22131582. Cited 2 times in pages 60 and 61.

225 HUANG, L. et al. Early Segmental White Matter Fascicle Microstructural Damage Predicts the Corresponding Cognitive Domain Impairment in Cerebral Small Vessel Disease Patients by Automated Fiber Quantification. *Frontiers in Aging Neuroscience*, v. 12, 2021. ISSN 16634365. Cited in page 60.

226 UDEN, I. W. van et al. Baseline white matter microstructural integrity is not related to cognitive decline after 5years: The RUN DMC study. *BBA Clinical*, 2015. ISSN 22146474. Cited in page 60.

227 HOLTMANNSPÖTTER, M. et al. Diffusion magnetic resonance histograms as a surrogate marker and predictor of disease progression in CADASIL a two-year follow-up study. *Stroke*, 2005. ISSN 00392499. Cited in page 60.

228 BAN, S. et al. Diffuse Tract Damage in CADASIL Is Correlated with Global Cognitive Impairment. *European Neurology*, 2019. ISSN 14219913. Cited in page 60.

229 CROALL, I. D. et al. Using DTI to assess white matter microstructure in cerebral small vessel disease (SVD) in multicentre studies. *Clinical Science*, 2017. ISSN 14708736. Cited in page 60.

230 METOKI, A. et al. Mnemonic function in small vessel disease and associations with white matter tract microstructure. *Neuropsychologia*, 2017. ISSN 18733514. Cited 3 times in pages 12, 60, and 61.

231 NORDEN, A. G. van et al. Diffusion tensor imaging of the hippocampus and verbal memory performance: The RUN DMC Study. *Human Brain Mapping*, 2012. ISSN 10659471. Cited in page 61.

232 HOLST, H. M. van der et al. Microstructural integrity of the cingulum is related to verbal memory performance in elderly with cerebral small vessel disease. The RUN DMC study. *NeuroImage*, 2013. ISSN 10538119. Cited in page 61.

233 CAO, W. W. et al. Deep microbleeds and periventricular white matter disintegrity are independent predictors of attention/executive dysfunction in non-dementia patients with small vessel disease. *International Psychogeriatrics*, 2017. ISSN 1741203X. Cited in page 61.

234 LIU, C. et al. Fiber Connectivity Density in Cerebral Small-Vessel Disease Patients With Mild Cognitive Impairment and Cerebral Small-Vessel Disease Patients With Normal Cognition. *Frontiers in Neuroscience*, 2020. ISSN 1662453X. Cited in page 61.

235 LIAO, Z. et al. Microstructural damage of normal-appearing white matter in subcortical ischemic vascular dementia is associated with Montreal Cognitive Assessment scores. *Journal of International Medical Research*, 2019. ISSN 14732300. Cited in page 61.

236 BRANDHOFE, A. et al. T2 relaxation time of the normal-appearing white matter is related to the cognitive status in cerebral small vessel disease. *Journal of Cerebral Blood Flow and Metabolism*, 2020. ISSN 15597016. Cited in page 61.

237 UDEN, I. W. van et al. Diffusion tensor imaging of the hippocampus predicts the risk of dementia; the RUN DMC study. *Human Brain Mapping*, 2016. ISSN 10970193. Cited in page 61.

238 SWARDFAGER, W. et al. Peripheral inflammatory markers indicate microstructural damage within periventricular white matter hyperintensities in Alzheimer's disease: A preliminary report. *Alzheimer's and Dementia: Diagnosis, Assessment and Disease Monitoring*, 2017. ISSN 23528729. Cited in page 61.

239 RAMAN, M. R. et al. Circulating vascular growth factors and magnetic resonance imaging markers of small vessel disease and atrophy in middle-aged adults. *Stroke*, 2018. ISSN 15244628. Cited in page 62.

240 FINSTERWALDER, S. et al. Small vessel disease more than Alzheimer's disease determines diffusion MRI alterations in memory clinic patients. *Alzheimer's and Dementia*, 2020. ISSN 15525279. Cited in page 62.

241 ELDIN, A. E. S. A. M. T. et al. Cognitive and balance impairments in people with incidental white matter hyperintensities. *Egyptian Journal of Neurology, Psychiatry and Neurosurgery*, v. 56, n. 1, 2020. ISSN 16878329. Cited in page 62.

242 ROSARIO, B. L. et al. Cerebral white matter and slow gait: Contribution of hyperintensities and normal-appearing parenchyma. *Journals of Gerontology - Series A Biological Sciences and Medical Sciences*, 2016. ISSN 1758535X. Cited in page 62.

243 HOLST, H. M. van der et al. Baseline Cerebral Small Vessel Disease Is Not Associated with Gait Decline After Five Years. *Movement Disorders Clinical Practice*, 2017. ISSN 23301619. Cited in page 62.

244 HOLST, H. M. van der et al. White matter changes and gait decline in cerebral small vessel disease. *NeuroImage: Clinical*, 2018. ISSN 22131582. Cited in page 62.

245 FINSTERWALDER, S. et al. Minor gait impairment despite white matter damage in pure small vessel disease. *Annals of Clinical and Translational Neurology*, 2019. ISSN 23289503. Cited in page 62.

246 LAAT, K. F. de et al. Diffusion tensor imaging and mild parkinsonian signs in cerebral small vessel disease. *Neurobiology of Aging*, 2012. ISSN 01974580. Cited in page 62.

247 Van Der Holst, H. M. et al. Cerebral small vessel disease and incident parkinsonism. *Neurology*, 2015. ISSN 1526632X. Cited in page 62.

248 CAI, M. et al. Cognition mediates the relation between structural network efficiency and gait in small vessel disease. *NeuroImage: Clinical*, Elsevier Inc., v. 30, jan 2021. ISSN 22131582. Disponível em: <https://pubmed.ncbi.nlm.nih.gov/33887698/>. Cited in page 62.

249 HANNAWI, Y. et al. White Matter Injury Is Associated with Reduced Manual Dexterity and Elevated Serum Ceramides in Subjects with Cerebral Small Vessel Disease. *Cerebrovascular Diseases*, v. 50, n. 1, 2021. ISSN 14219786. Cited in page 62.

250 BROOKES, R. L. et al. Depression in small-vessel disease relates to white matter ultrastructural damage, not disability. *Neurology*, 2014. ISSN 1526632X. Cited in page 62.

251   Van Uden, I. W. et al. White matter integrity and depressive symptoms in cerebral small vessel disease: The RUN DMC study. *American Journal of Geriatric Psychiatry*, 2015. ISSN 15457214.   Cited in page 62.

252   XIE, X.; SHI, Y.; ZHANG, J. Structural network connectivity impairment and depressive symptoms in cerebral small vessel disease. *Journal of Affective Disorders*, 2017. ISSN 15732517. Cited in page 62.

253   PASI, M. et al. White matter microstructural damage and depressive symptoms in patients with mild cognitive impairment and cerebral small vessel disease: The VMCI-Tuscany Study. *International Journal of Geriatric Psychiatry*, 2016. ISSN 10991166.   Cited in page 62.

254   KIM, Y. et al. Vascular Effects on Depressive Symptoms in Cognitive Impairment. *Journal of Alzheimer's disease : JAD*, 2018. ISSN 18758908.   Cited in page 62.

255   HOLLOCKS, M. J. et al. Differential relationships between apathy and depression with white matter microstructural changes and functional outcomes. *Brain*, 2015. ISSN 14602156. Cited in page 62.

256   TAY, J. et al. Apathy is associated with large-scale white matter network disruption in small vessel disease. *Neurology*, 2019. ISSN 1526632X.   Cited in page 62.

257   LISIECKA-FORD., D. M. et al. Involvement of the reward network is associated with apathy in cerebral small vessel disease. *Journal of Affective Disorders*, 2018. ISSN 15732517. Cited in page 62.

258   RAIMONDO, L. et al. Advances in resting state fMRI acquisitions for functional connectomics. *NeuroImage*, Academic Press, v. 243, p. 118503, nov 2021. ISSN 1053-8119. Cited in page 63.

259   LINORTNER, P. et al. White matter hyperintensities alter functional organization of the motor system. *Neurobiology of Aging*, 2012. ISSN 15581497.   Cited 2 times in pages 63 and 66.

260   ZHOU, X. et al. Altered brain function in cerebral small vessel disease patients with gait disorders: a resting-state functional mri study. *Frontiers in Aging Neuroscience*, Frontiers Media SA, v. 12, 2020.   Cited in page 63.

261   PAPMA, J. M. et al. The influence of cerebral small vessel disease on default mode network deactivation in mild cognitive impairment. *NeuroImage: Clinical*, Elsevier, v. 2, p. 33–42, 2013.   Cited 4 times in pages 12, 63, 65, and 66.

262   PANTONI, L. et al. Effect of Attention Training in Mild Cognitive Impairment Patients with Subcortical Vascular Changes: The RehAtt Study. *Journal of Alzheimer's Disease*, 2017. ISSN 18758908.   Cited 2 times in pages 63 and 66.

263   ATWI, S. et al. Attention-related brain activation is altered in older adults with white matter hyperintensities using multi-echo fmri. *Frontiers in Neuroscience*, Frontiers, v. 12, p. 748, 2018.   Cited 2 times in pages 63 and 66.

264   SCHAEFER, A. et al. Early small vessel disease affects frontoparietal and cerebellar hubs in close correlation with clinical symptoms—a resting-state fmri study. *Journal of Cerebral Blood Flow & Metabolism*, v. 34, n. 7, p. 1091–1095, 2014. PMID: 24780899. Disponível em: <https://doi.org/10.1038/jcbfm.2014.70>.   Cited 4 times in pages 63, 66, 69, and 94.

265   CHEN, X. et al. Disrupted functional and structural connectivity within default mode network contribute to wmh-related cognitive impairment. *NeuroImage: Clinical*, Elsevier, v. 24, p. 102088, 2019.   Cited in page 63.

266   DICIOTTI, S. et al. Resting state fmri regional homogeneity correlates with cognition measures in subcortical vascular cognitive impairment. *Journal of the neurological sciences*, Elsevier, v. 373, p. 1–6, 2017.   Cited 3 times in pages 12, 63, and 65.

267   LIU, R. et al. The altered reconfiguration pattern of brain modular architecture regulates cognitive function in cerebral small vessel disease. *Frontiers in Neurology*, 2019. ISSN 16642295.   Cited 2 times in pages 64 and 66.

268   ACHARYA, A. et al. White Matter Hyperintensities Relate to Basal Ganglia Functional Connectivity and Memory Performance in aMCI and SVMCI. *Frontiers in Neuroscience*, 2019. ISSN 1662453X.   Cited 2 times in pages 64 and 66.

269   KARIM, H. T. et al. Resting state connectivity within the basal ganglia and gait speed in older adults with cerebral small vessel disease and locomotor risk factors. *NeuroImage: Clinical*, 2020. ISSN 22131582.   Cited in page 64.

270   GESIERICH, B. et al. Alterations and test–retest reliability of functional connectivity network measures in cerebral small vessel disease. *Human brain mapping*, Wiley Online Library, v. 41, n. 10, p. 2629–2641, 2020.   Cited in page 64.

271   QIN, Y. et al. Functional brain connectome and its relation to mild cognitive impairment in cerebral small vessel disease patients with thalamus lacunes: A cross-sectional study. *Medicine (United States)*, 2019. ISSN 15365964.   Cited 3 times in pages 12, 64, and 65.

272   HWANG, M. et al. Brain Activation and Psychomotor Speed in Middle-Aged Patients with Type 1 Diabetes: Relationships with Hyperglycemia and Brain Small Vessel Disease. *Journal of Diabetes Research*, 2016. ISSN 23146753.   Cited in page 64.

273   GAVAZZI, G. et al. Functional magnetic resonance imaging of inhibitory control reveals decreased blood oxygen level dependent effect in cerebral autosomal dominant arteriopathy with subcortical infarcts and leukoencephalopathy. *Stroke*, 2019. ISSN 15244628.   Cited in page 64.

274   LYU, H. et al. Structural and Functional Disruptions in Subcortical Vascular Mild Cognitive Impairment With and Without Depressive Symptoms. *Frontiers in Aging Neuroscience*, 2019. ISSN 16634365.   Cited 2 times in pages 65 and 66.

275   FRANZMEIER, N. et al. Functional connectivity associated with tau levels in ageing, alzheimer's, and small vessel disease. *Brain*, Oxford University Press, v. 142, n. 4, p. 1093–1107, 2019.   Cited 2 times in pages 65 and 66.

276   MAKEDONOV, I.; BLACK, S. E.; MACINTOSH, B. J. BOLD fMRI in the White Matter as a Marker of Aging and Small Vessel Disease. *PLoS ONE*, 2013. ISSN 19326203.   Cited 2 times in pages 65 and 66.

277   ATWI, S. et al. Cardiac-Related Pulsatility in the Insula Is Directly Associated With Middle Cerebral Artery Pulsatility Index. *Journal of Magnetic Resonance Imaging*, 2019. ISSN 15222586.   Cited 2 times in pages 65 and 66.

278 NYENHUIS, D.; STEBBINS, G. T. Nonconventional MR techniques for imaging cerebral small vessel disease. In: *Cerebral Small Vessel Disease.* [S.l.: s.n.], 2011. ISBN 9781139382694. Cited in page 66.

279 PATEL, B.; MARKUS, H. S. Magnetic resonance imaging in cerebral small vessel disease and its use as a surrogate disease marker. *International Journal of Stroke*, SAGE Publications Sage UK: London, England, v. 6, n. 1, p. 47–59, 2011. Cited in page 66.

280 REIJMER, Y. D. et al. Progression of brain network alterations in cerebral amyloid angiopathy. *Stroke*, Am Heart Assoc, v. 47, n. 10, p. 2470–2475, 2016. Cited in page 66.

281 GOUW, A. A. et al. Heterogeneity of small vessel disease: a systematic review of mri and histopathology correlations. *Journal of Neurology, Neurosurgery & Psychiatry*, BMJ Publishing Group Ltd, v. 82, n. 2, p. 126–135, 2011. Cited in page 66.

282 LEIJSEN, E. M. van et al. Longitudinal changes in rich club organization and cognition in cerebral small vessel disease. *NeuroImage: Clinical*, Elsevier, v. 24, p. 102048, 2019. Cited in page 67.

283 BLAIR, G. W. et al. Intracranial hemodynamic relationships in patients with cerebral small vessel disease. *Neurology*, AAN Enterprises, v. 94, n. 21, p. e2258–e2269, 2020. Cited in page 67.

284 SILVA, P. H. R. da et al. Contrast-agent-free state-of-the-art magnetic resonance imaging on cerebral small vessel disease – part 2: Dti and fmri. *NMR in Biomedicine*, n/a, n. n/a, p. e4743. E4743 NBM-22-0068. Disponível em: <https://analyticalsciencejournals.onlinelibrary.wiley.com/doi/abs/10.1002/nbm.4743>. Cited in page 67.

285 KYNAST, J. et al. White matter hyperintensities associated with small vessel disease impair social cognition beside attention and memory. *Journal of Cerebral Blood Flow & Metabolism*, v. 38, n. 6, p. 996–1009, 2018. PMID: 28685621. Disponível em: <https://doi.org/10.1177/0271678X17719380>. Cited in page 69.

286 LAMBERT, C. et al. Longitudinal patterns of leukoaraiosis and brain atrophy in symptomatic small vessel disease. *Brain*, Oxford University Press, v. 139, n. 4, p. 1136–1151, 2016. Cited 2 times in pages 69 and 93.

287 RIGHART, R. et al. Impact of regional cortical and subcortical changes on processing speed in cerebral small vessel disease. *NeuroImage: Clinical*, Elsevier, v. 2, p. 854–861, 2013. Cited 2 times in pages 69 and 70.

288 JOKINEN, H. et al. Brain atrophy accelerates cognitive decline in cerebral small vessel disease: the ladis study. *Neurology*, AAN Enterprises, v. 78, n. 22, p. 1785–1792, 2012. Cited 2 times in pages 69 and 93.

289 TULADHAR, A. M. et al. Structural network connectivity and cognition in cerebral small vessel disease. *Human brain mapping*, Wiley Online Library, v. 37, n. 1, p. 300–310, 2016. Cited 2 times in pages 69 and 96.

290 VENKATRAMAN, V. K. et al. Executive control function, brain activation and white matter hyperintensities in older adults. *Neuroimage*, Elsevier, v. 49, n. 4, p. 3436–3442, 2010. Cited in page 69.

291 DEY, A. K. et al. Pathoconnectomics of cognitive impairment in small vessel disease: A systematic review. *Alzheimer's & Dementia*, v. 12, n. 7, p. 831–845, 2016. Disponível em: <https://alz-journals.onlinelibrary.wiley.com/doi/abs/10.1016/j.jalz.2016.01.007>. Cited 5 times in pages 69, 70, 94, 95, and 108.

292 CHEN, J. et al. Bilateral distance partition of periventricular and deep white matter hyperintensities: Performance of the method in the aging brain. *Academic Radiology*, v. 28, n. 12, p. 1699–1708, 2021. ISSN 1076-6332. Disponível em: <https://www.sciencedirect.com/science/article/pii/S1076633220304864>. Cited 2 times in pages 69 and 96.

293 MEDRANO-MARTORELL, S. et al. Risk factors analysis according to regional distribution of white matter hyperintensities in a stroke cohort. *European Radiology*, Springer, p. 1–9, 2021. Cited in page 69.

294 ARMSTRONG, N. J. et al. Common Genetic Variation Indicates Separate Causes for Periventricular and Deep White Matter Hyperintensities. *Stroke*, Stroke, v. 51, n. 7, p. 2112–2121, jul 2020. ISSN 1524-4628. Disponível em: <https://pubmed.ncbi.nlm.nih.gov/32517579/>. Cited in page 69.

295 MELAZZINI, L. et al. White matter hyperintensities classified according to intensity and spatial location reveal specific associations with cognitive performance. *NeuroImage: Clinical*, Elsevier, v. 30, p. 102616, 2021. Cited in page 69.

296 HIRAO, K. et al. Association of regional white matter hyperintensity volumes with cognitive dysfunction and vascular risk factors in patients with amnestic mild cognitive impairment. *Geriatrics & Gerontology International*, v. 21, n. 8, p. 644–650, 2021. Disponível em: <https://onlinelibrary.wiley.com/doi/abs/10.1111/ggi.14211>. Cited in page 69.

297 LAMBERT, C. et al. Characterising the grey matter correlates of leukoaraiosis in cerebral small vessel disease. *NeuroImage: Clinical*, Elsevier, v. 9, p. 194–205, 2015. Cited 2 times in pages 69 and 93.

298 HEINEN, R. et al. Small vessel disease lesion type and brain atrophy: The role of co-occurring amyloid. *Alzheimer's & Dementia: Diagnosis, Assessment & Disease Monitoring*, v. 12, n. 1, p. e12060, 2020. Disponível em: <https://alz-journals.onlinelibrary.wiley.com/doi/abs/10.1002/dad2.12060>. Cited 2 times in pages 69 and 93.

299 TANG, J. et al. Coexisting cortical atrophy plays a crucial role in cognitive impairment in moderate to severe cerebral small vessel disease patients. *Discovery medicine*, 2017. ISSN 19447930. Cited 2 times in pages 69 and 93.

300 TULADHAR, A. M. et al. Relationship between white matter hyperintensities, cortical thickness, and cognition. *Stroke*, Am Heart Assoc, v. 46, n. 2, p. 425–432, 2015. Cited 3 times in pages 69, 93, and 109.

301 DUERING, M. et al. Incident subcortical infarcts induce focal thinning in connected cortical regions. *Neurology*, AAN Enterprises, v. 79, n. 20, p. 2025–2028, 2012. Cited 2 times in pages 69 and 94.

302 SEO, S. W. et al. Cortical thinning in vascular mild cognitive impairment and vascular dementia of subcortical type. *Journal of Neuroimaging*, Wiley Online Library, v. 20, n. 1, p. 37–45, 2010. Cited 2 times in pages 69 and 94.

303   KIM, H. J. et al. Clinical effect of white matter network disruption related to amyloid and small vessel disease. *Neurology*, AAN Enterprises, v. 85, n. 1, p. 63–70, 2015. Cited 2 times in pages 69 and 94.

304   DUERING, M. et al. Strategic white matter tracts for processing speed deficits in age-related small vessel disease. *Neurology*, Wolters Kluwer Health, Inc. on behalf of the American Academy of Neurology, v. 82, n. 22, p. 1946–1950, 2014. ISSN 0028-3878. Disponível em: <https://n.neurology.org/content/82/22/1946>. Cited in page 70.

305   NORDEN, A. G. van et al. Causes and consequences of cerebral small vessel disease. The RUN DMC study: A prospective cohort study. Study rationale and protocol. *BMC Neurology*, 2011. ISSN 14712377. Cited 2 times in pages 70 and 97.

306   FOLSTEIN, M. F.; FOLSTEIN, S. E.; MCHUGH, P. R. "Mini-mental state". A practical method for grading the cognitive state of patients for the clinician. *Journal of Psychiatric Research*, 1975. ISSN 00223956. Cited 2 times in pages 71 and 97.

307   WEN, W. et al. White matter hyperintensities in the forties: Their prevalence and topography in an epidemiological sample aged 44-48. *Human Brain Mapping*, v. 30, n. 4, p. 1155–1167, apr 2009. ISSN 10659471. Cited 2 times in pages 71 and 98.

308   HUA, K. et al. Tract probability maps in stereotaxic spaces: analyses of white matter anatomy and tract-specific quantification. *Neuroimage*, Elsevier, v. 39, n. 1, p. 336–347, 2008. Cited in page 71.

309   DESIKAN, R. S. et al. An automated labeling system for subdividing the human cerebral cortex on MRI scans into gyral based regions of interest. *NeuroImage*, Academic Press, v. 31, n. 3, p. 968–980, jul 2006. ISSN 1053-8119. Cited 7 times in pages 71, 72, 79, 84, 99, 100, and 107.

310   BIESBROEK, J. M.; WEAVER, N. A.; BIESSELS, G. J. Lesion location and cognitive impact of cerebral small vessel disease. *Clinical Science*, Portland Press Ltd., v. 131, n. 8, p. 715–728, 2017. Cited 2 times in pages 71 and 97.

311   ASHBURNER, J. A fast diffeomorphic image registration algorithm. *Neuroimage*, Elsevier, v. 38, n. 1, p. 95–113, 2007. Cited in page 71.

312   REESE, T. et al. Reduction of eddy-current-induced distortion in diffusion mri using a twice-refocused spin echo. *Magnetic Resonance in Medicine*, v. 49, n. 1, p. 177–182, 2003. Disponível em: <https://onlinelibrary.wiley.com/doi/abs/10.1002/mrm.10308>. Cited in page 72.

313   YEH, F.-C.; BADRE, D.; VERSTYNEN, T. Connectometry: a statistical approach harnessing the analytical potential of the local connectome. *Neuroimage*, Elsevier, v. 125, p. 162–171, 2016. Cited in page 72.

314   YEH, F.-C. et al. Automatic removal of false connections in diffusion mri tractography using topology-informed pruning (tip). *Neurotherapeutics*, Springer, v. 16, n. 1, p. 52–58, 2019. Cited in page 72.

315   HAYES, A. F. *Introduction to mediation, moderation, and conditional process analysis: A regression-based approach*. [S.l.]: Guilford publications, 2017. Cited in page 74.

316   CRAGGS, L. J. L. et al. White matter pathology and disconnection in the frontal lobe in cerebral autosomal dominant arteriopathy with subcortical infarcts and leukoencephalopathy (cadasil). *Neuropathology and Applied Neurobiology*, v. 40, n. 5, p. 591–602, 2014. Disponível em: <https://onlinelibrary.wiley.com/doi/abs/10.1111/nan.12073>. Cited 2 times in pages 93 and 110.

317   PANTONI, L.; POGGESI, A.; INZITARI, D. The relation between white-matter lesions and cognition. *Current opinion in neurology*, LWW, v. 20, n. 4, p. 390–397, 2007. Cited in page 93.

318   CREMERS, L. G. et al. Altered tract-specific white matter microstructure is related to poorer cognitive performance: The rotterdam study. *Neurobiology of aging*, Elsevier, v. 39, p. 108–117, 2016. Cited 2 times in pages 93 and 108.

319   ARALASMAK, A. et al. Association, commissural, and projection pathways and their functional deficit reported in literature. *Journal of computer assisted tomography*, LWW, v. 30, n. 5, p. 695–715, 2006. Cited in page 94.

320   SPRENG, R. N. et al. Intrinsic architecture underlying the relations among the default, dorsal attention, and frontoparietal control networks of the human brain. *Journal of Cognitive Neuroscience*, v. 25, n. 1, p. 74–86, 2013. ISSN 15308898. Cited 2 times in pages 94 and 96.

321   CHENG, H.-L. et al. Impairments in cognitive function and brain connectivity in severe asymptomatic carotid stenosis. *Stroke*, Am Heart Assoc, v. 43, n. 10, p. 2567–2573, 2012. Cited in page 94.

322   SUN, Y.-w. et al. Abnormal functional connectivity in patients with vascular cognitive impairment, no dementia: a resting-state functional magnetic resonance imaging study. *Behavioural brain research*, Elsevier, v. 223, n. 2, p. 388–394, 2011. Cited in page 94.

323   WU, X. et al. Breakdown of sensorimotor network communication in leukoaraiosis. *Neurodegenerative Diseases*, Karger Publishers, v. 15, n. 6, p. 322–330, 2015. Cited in page 94.

324   MOLLET, G. A. Fundamentals of human neuropsychology. *Journal of Undergraduate Neuroscience Education*, Faculty for Undergraduate Neuroscience, v. 6, n. 2, p. R3, 2008. Cited in page 94.

325   DUM, R. P.; STRICK, P. L. The origin of corticospinal projections from the premotor areas in the frontal lobe. *The Journal of neuroscience : the official journal of the Society for Neuroscience*, J Neurosci, v. 11, n. 3, p. 667–689, 1991. ISSN 0270-6474. Disponível em: <https://pubmed.ncbi.nlm.nih.gov/1705965/>. Cited in page 94.

326   PATEL, M. J. et al. Association of small vessel ischemic white matter changes with bold fmri imaging in the elderly. *Psychiatry Research: Neuroimaging*, v. 204, n. 2, p. 117–122, 2012. ISSN 0925-4927. Disponível em: <https://www.sciencedirect.com/science/article/pii/S0925492712002193>. Cited in page 94.

327   FERREIRA, L. K. et al. Aging effects on whole-brain functional connectivity in adults free of cognitive and psychiatric disorders. *Cerebral cortex*, Oxford University Press, v. 26, n. 9, p. 3851–3865, 2016. Cited in page 94.

328   FERREIRA, L. K.; BUSATTO, G. F. Resting-state functional connectivity in normal brain aging. *Neuroscience & Biobehavioral Reviews*, Elsevier, v. 37, n. 3, p. 384–400, 2013. Cited in page 94.

329   GROOT, J. C. D. et al. Periventricular cerebral white matter lesions predict rate of cognitive decline. *Annals of neurology*, Wiley Online Library, v. 52, n. 3, p. 335–341, 2002. Cited 2 times in pages 95 and 108.

330   LIU, Q. et al. White matter damage in the cholinergic system contributes to cognitive impairment in subcortical vascular cognitive impairment, no dementia. *Frontiers in Aging Neuroscience*, v. 9, p. 47, 2017. ISSN 1663-4365. Disponível em: <https://www.frontiersin.org/article/10.3389/fnagi.2017.00047>. Cited in page 95.

331   CHUDASAMA, Y.; ROBBINS, T. Functions of frontostriatal systems in cognition: comparative neuropsychopharmacological studies in rats, monkeys and humans. *Biological psychology*, Elsevier, v. 73, n. 1, p. 19–38, 2006. Cited in page 95.

332   BUCKNER, R. L. Memory and executive function in aging and ad: multiple factors that cause decline and reserve factors that compensate. *Neuron*, Elsevier, v. 44, n. 1, p. 195–208, 2004. Cited in page 95.

333   NEMY, M. et al. Cholinergic white matter pathways make a stronger contribution to attention and memory in normal aging than cerebrovascular health and nucleus basalis of meynert. *NeuroImage*, v. 211, p. 116607, 2020. ISSN 1053-8119. Disponível em: <https://www.sciencedirect.com/science/article/pii/S105381192030094X>. Cited 2 times in pages 95 and 108.

334   SHI, Y.; WARDLAW, J. M. Update on cerebral small vessel disease: a dynamic whole-brain disease. *Stroke and vascular neurology*, BMJ Specialist Journals, v. 1, n. 3, 2016. Cited in page 96.

335   LAWRENCE, A. J. et al. Pattern and rate of cognitive decline in cerebral small vessel disease: a prospective study. *PloS one*, Public Library of Science San Francisco, CA USA, v. 10, n. 8, p. e0135523, 2015. Cited in page 96.

336   PRINS, N. D. et al. Cerebral small-vessel disease and decline in information processing speed, executive function and memory. *Brain*, Oxford University Press, v. 128, n. 9, p. 2034–2041, 2005. Cited in page 96.

337   KIM, K. W.; MACFALL, J. R.; PAYNE, M. E. Classification of White Matter Lesions on Magnetic Resonance Imaging in Elderly Persons. *Biological Psychiatry*, Elsevier, v. 64, n. 4, p. 273–280, aug 2008. ISSN 0006-3223. Disponível em: <http://www.biologicalpsychiatryjournal.com/article/S0006322308003909/fulltexthttp://www.biologicalpsychiatryjournal.com/article/S0006322308003909/abstracthttps://www.biologicalpsychiatryjournal.com/article/S0006-3223(08)00390-9/abstract>. Cited in page 96.

338   RORDEN, C.; KARNATH, H.-O.; BONILHA, L. Improving lesion-symptom mapping. *Journal of cognitive neuroscience*, MIT Press One Rogers Street, Cambridge, MA 02142-1209, USA journals-info . . . , v. 19, n. 7, p. 1081–1088, 2007. Cited in page 96.

339   MAH, Y.-H. et al. Human brain lesion-deficit inference remapped. *Brain*, Oxford University Press, v. 137, n. 9, p. 2522–2531, 2014. Cited in page 96.

340   GESCHWIND, N. DISCONNEXION SYNDROMES IN ANIMALS AND MAN1. *Brain*, v. 88, n. 2, p. 237–237, 06 1965. ISSN 0006-8950. Disponível em: <https://doi.org/10.1093/brain/88.2.237>. Cited in page 96.

341   GESCHWIND, N. DISCONNEXION SYNDROMES IN ANIMALS AND MAN1. *Brain*, v. 88, n. 3, p. 585–585, 09 1965. ISSN 0006-8950. Disponível em: <https://doi.org/10.1093/brain/88.3.585>. Cited in page 96.

342   CORBETTA, M. et al. Common behavioral clusters and subcortical anatomy in stroke. *Neuron*, Elsevier, v. 85, n. 5, p. 927–941, 2015. Cited in page 96.

343   HERBET, G. et al. Mapping neuroplastic potential in brain-damaged patients. *Brain*, Oxford University Press, v. 139, n. 3, p. 829–844, 2016. Cited in page 96.

344   FOULON, C. et al. Advanced lesion symptom mapping analyses and implementation as BCBtoolkit. *GigaScience*, v. 7, n. 3, 02 2018. ISSN 2047-217X. Giy004. Disponível em: <https://doi.org/10.1093/gigascience/giy004>. Cited 2 times in pages 97 and 98.

345   ALVES, P. N. et al. Unravelling the Neural Basis of Spatial Delusions After Stroke. *Annals of Neurology*, John Wiley & Sons, Ltd, v. 89, n. 6, p. 1181–1194, jun 2021. ISSN 1531-8249. Disponível em: <https://onlinelibrary.wiley.com/doi/full/10.1002/ana.26079https://onlinelibrary.wiley.com/doi/abs/10.1002/ana.26079https://onlinelibrary.wiley.com/doi/10.1002/ana.26079>. Cited in page 97.

346   Thiebaut de Schotten, M.; FOULON, C.; NACHEV, P. Brain disconnections link structural connectivity with function and behaviour. *Nature Communications 2020 11:1*, Nature Publishing Group, v. 11, n. 1, p. 1–8, oct 2020. ISSN 2041-1723. Disponível em: <https://www.nature.com/articles/s41467-020-18920-9>. Cited in page 97.

347   ULRICHSEN, K. M. et al. Structural brain disconnectivity mapping of post-stroke fatigue. *NeuroImage: Clinical*, Elsevier, v. 30, p. 102635, jan 2021. ISSN 2213-1582. Cited in page 97.

348   SALVALAGGIO, A. et al. Post-stroke deficit prediction from lesion and indirect structural and functional disconnection. *Brain : a journal of neurology*, Brain, v. 143, n. 7, p. 2173–2188, jul 2020. ISSN 1460-2156. Disponível em: <https://pubmed.ncbi.nlm.nih.gov/32572442/>. Cited in page 97.

349   AVANTS, B. B. et al. A reproducible evaluation of ANTs similarity metric performance in brain image registration. *NeuroImage*, Neuroimage, v. 54, n. 3, p. 2033–2044, feb 2011. ISSN 1095-9572. Disponível em: <https://pubmed.ncbi.nlm.nih.gov/20851191/>. Cited in page 98.

350   KLEIN, A. et al. Evaluation of 14 nonlinear deformation algorithms applied to human brain MRI registration. *NeuroImage*, Neuroimage, v. 46, n. 3, p. 786–802, jul 2009. ISSN 1095-9572. Disponível em: <https://pubmed.ncbi.nlm.nih.gov/19195496/>. Cited in page 98.

351   ROJKOVA, K. et al. Atlasing the frontal lobe connections and their variability due to age and education: a spherical deconvolution tractography study. *Brain structure & function*, Brain Struct Funct, v. 221, n. 3, p. 1751–1766, apr 2016. ISSN 1863-2661. Disponível em: <https://pubmed.ncbi.nlm.nih.gov/25682261/>. Cited in page 98.

352   Thiebaut De Schotten, M. et al. Damage to white matter pathways in subacute and chronic spatial neglect: a group study and 2 single-case studies with complete virtual "in vivo" tractography dissection. *Cerebral cortex (New York, N.Y. : 1991)*, Cereb Cortex, v. 24, n. 3, p. 691–706, mar 2014. ISSN 1460-2199. Disponível em: <https://pubmed.ncbi.nlm.nih.gov/23162045/>. Cited in page 98.

353 De Schotten, M. T. et al. A lateralized brain network for visuospatial attention. *Nature neuroscience*, Nat Neurosci, v. 14, n. 10, p. 1245–1246, oct 2011. ISSN 1546-1726. Disponível em: <https://pubmed.ncbi.nlm.nih.gov/21926985/>. Cited in page 98.

354 Thiebaut de Schotten, M. et al. Atlasing location, asymmetry and inter-subject variability of white matter tracts in the human brain with MR diffusion tractography. *NeuroImage*, Neuroimage, v. 54, n. 1, p. 49–59, jan 2011. ISSN 1095-9572. Disponível em: <https://pubmed.ncbi.nlm.nih.gov/20682348/>. Cited in page 99.

355 Thiebaut De Schotten, M. et al. From Phineas Gage and Monsieur Leborgne to H.M.: Revisiting Disconnection Syndromes. *Cerebral cortex (New York, N.Y. : 1991)*, Cereb Cortex, v. 25, n. 12, p. 4812–4827, dec 2015. ISSN 1460-2199. Disponível em: <https://pubmed.ncbi.nlm.nih.gov/26271113/>. Cited in page 99.

356 WINKLER, A. M. et al. Permutation inference for the general linear model. *NeuroImage*, Academic Press, v. 92, p. 381–397, may 2014. ISSN 1053-8119. Cited in page 99.

357 MORI, S. S.; CRAIN, B. J. MRI atlas of human white matter. Elsevier, p. 239, 2005. Cited in page 99.

358 GRIFFANTI, L. et al. Classification and characterization of periventricular and deep white matter hyperintensities on mri: a study in older adults. *Neuroimage*, Elsevier, v. 170, p. 174–181, 2018. Cited in page 108.

359 JIANG, C. et al. Ischemic stroke in pontine and corona radiata: Location specific impairment of neural network investigated with resting state fMRI. *Frontiers in Neurology*, Frontiers Media S.A., v. 10, n. MAY, p. 575, 2019. ISSN 16642295. Cited in page 108.

360 QIU, Y. et al. Loss of integrity of corpus callosum white matter hyperintensity penumbra predicts cognitive decline in patients with subcortical vascular mild cognitive impairment. *Frontiers in Aging Neuroscience*, v. 13, p. 43, 2021. ISSN 1663-4365. Disponível em: <https://www.frontiersin.org/article/10.3389/fnagi.2021.605900>. Cited in page 108.

361 PARK, J. et al. Neural Dissociation of Number from Letter Recognition and Its Relationship to Parietal Numerical Processing. *Journal of Cognitive Neuroscience*, NIH Public Access, v. 24, n. 1, p. 39, jan 2012. ISSN 0898929X. Disponível em: </pmc/articles/PMC3357212//pmc/articles/PMC3357212/?report=abstracthttps://www.ncbi.nlm.nih.gov/pmc/articles/PMC3357212/>. Cited in page 109.

362 BOISGUEHENEUC, F. D. et al. Functions of the left superior frontal gyrus in humans: a lesion study. *Brain*, Oxford Academic, v. 129, n. 12, p. 3315–3328, dec 2006. ISSN 0006-8950. Disponível em: <https://academic.oup.com/brain/article/129/12/3315/266905>. Cited in page 109.

363 GOLDMAN-RAKIC, P. S. Circuitry of the frontal association cortex and its relevance to dementia. *Archives of Gerontology and Geriatrics*, Elsevier, v. 6, n. 3, p. 299–309, sep 1987. ISSN 0167-4943. Cited in page 109.

364 DAW, N. D. et al. Cortical substrates for exploratory decisions in humans. *Nature*, Nature Publishing Group, v. 441, n. 7095, p. 876–879, 2006. Cited in page 109.
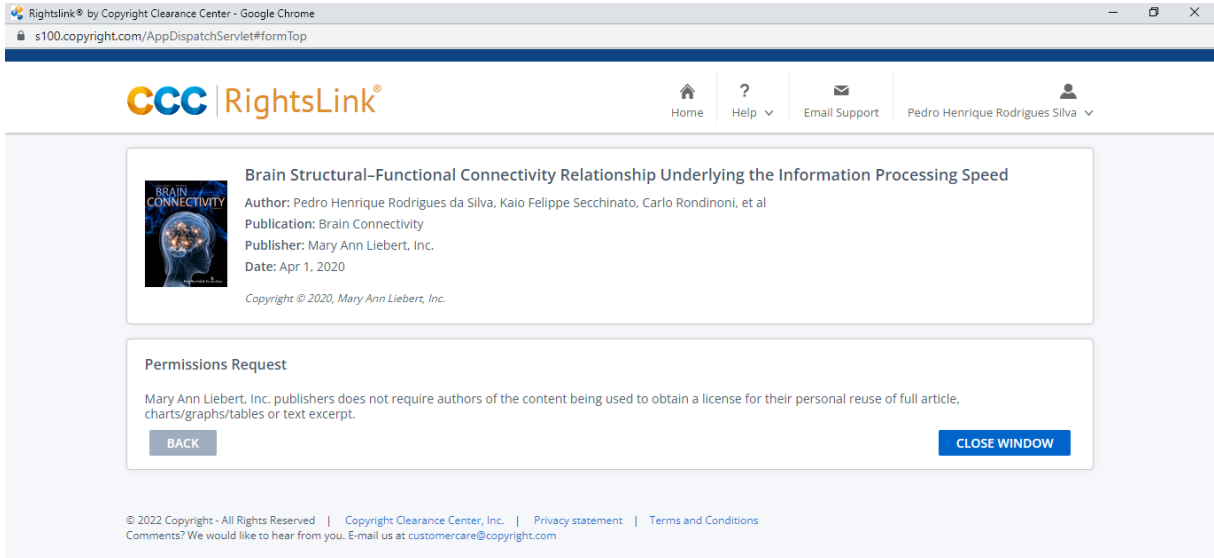
365   BOORMAN, E. D. et al. How Green Is the Grass on the Other Side? Frontopolar Cortex and the Evidence in Favor of Alternative Courses of Action. *Neuron*, Elsevier, v. 62, n. 5, p. 733–743, jun 2009. ISSN 08966273. Disponível em: <http://www.cell.com/article/S0896627309003894/fulltexthttp://www.cell.com/article/S0896627309003894/abstracthttps://www.cell.com/neuron/abstract/S0896-6273(09)00389-4>. Cited in page 109.

366   LATERRA, D. The role of the higher order thalamus during goal-directed behavior and sensory processing. 2019. Disponível em: <http://minerva-access.unimelb.edu.au/handle/11343/238522>. Cited in page 109.

367   BOLANDZADEH, N. et al. The association between cognitive function and white matter lesion location in older adults: a systematic review. *BMC neurology*, BioMed Central, v. 12, n. 1, p. 1–10, 2012. Cited in page 110.

368   WEN, W. et al. Gray matter reduction is correlated with white matter hyperintensity volume: A voxel-based morphometric study in a large epidemiological sample. *NeuroImage*, Academic Press, v. 29, n. 4, p. 1031–1039, feb 2006. ISSN 1053-8119. Cited in page 110.

369   BRUGULAT-SERRAT, A. et al. White matter hyperintensities mediate gray matter volume and processing speed relationship in cognitively unimpaired participants. *Human Brain Mapping*, John Wiley & Sons, Ltd, v. 41, n. 5, p. 1309–1322, apr 2020. ISSN 1097-0193. Disponível em: <https://onlinelibrary.wiley.com/doi/full/10.1002/hbm.24877https://onlinelibrary.wiley.com/doi/abs/10.1002/hbm.24877https://onlinelibrary.wiley.com/doi/10.1002/hbm.24877>. Cited in page 110.

370   HOTZ, I. et al. Associations of subclinical cerebral small vessel disease and processing speed in non-demented subjects: A 7-year study. *NeuroImage: Clinical*, Elsevier, v. 32, p. 102884, jan 2021. ISSN 2213-1582. Cited in page 110.

A

Table 18 – Tracts from a preliminary study using the HCP1021 tractography atlas (included in the DSI Studio package).

Cortical Regions Pair	Tracts
right Cuneus (BA 17) – left Lingual Gyrus (BA 17)	Corpus callosum, left cerebellum, left inferior longitudinal fasciculus
right Cuneus (BA 17) -left Declive	Corpus callosum, left cerebellum, middle cerebellar peduncle
right Cuneus (BA 17) - left Precuneus (BA 7)	left cingulum, right cingulum, right u fiber, corpus callosum, right cerebellum
right Cuneus (BA 17) - left Superior Parietal Lobule (BA 7)	Corpus callosum
right Cuneus (BA 17) - right Middle Frontal Gyrus (BA 6)	right corticothalamic pathway, corpus callosum
left Lingual Gyrus (BA 17) - left Declive	left inferior fronto-occipital fasciculus, left inferior longitudinal fasciculus, corpus callosum, left cerebellum, r cerebellum, middle cerebellar peduncle, vermis
left Lingual Gyrus (BA 17) - left Superior Parietal Lobule (BA 7)	left corticothalamic pathway, corpus callosum
left Lingual Gyrus (BA 17) - left Precuneus (BA 7)	left corticothalamic pathway, corpus callosum
left Declive - left Superior Parietal Lobule (BA 7)	left parieto pontine tract, corpus callosum, left cerebellum, middle cerebellar peduncle
left Declive - left Precuneus (BA 7)	corpus callosum, left cerebellum
left Declive - left Inferior Frontal Gyrus (BA 9)	No tract was observed
left Declive - left Middle Frontal Gyrus (BA 6)	left parieto pontine tract, corpus callosum, left cerebellum, middle cerebellar peduncle
left Declive - right Middle Frontal Gyrus (BA 6)	right parieto pontine tract, right fronto pontine tract, corpus callosum
left Superior Parietal Lobule (BA 7) - left Precuneus (BA 7)	left corticostriatal pathway, left corticothalamic pathway, left cingulum, left inferior longitudinal fasciculus, left u fiber, corpus callosum
left Superior Parietal Lobule (BA 7) - left Inferior Frontal Gyrus (BA 9)	left superior longitudinal fasciculus, left u fiber
left Superior Parietal Lobule (BA 7) - left Middle Frontal Gyrus (BA 6)	left corticothalamic pathway, left superior longitudinal fasciculus, left u fiber, corpus callosum
left Superior Parietal Lobule (BA 7) - r Middle Frontal Gyrus (BA 6)	Corpus callosum
left Precuneus (BA 7) - left Inferior Frontal Gyrus (BA 9)	left superior longitudinal left fasciculus, left u fiber
left Precuneus (BA 7) - left Middle Frontal Gyrus (BA 6)	left corticothalamic pathway, corpus callosum
left Precuneus (BA 7) - right Middle Frontal Gyrus (BA 6)	Corpus callosum
left Inferior Frontal Gyrus (BA 9) - left Middle Frontal Gyrus (BA 6)	left corticostriatal pathway, left arcuate fasciculus, left frontal aslant tract, left superior longitudinal fasciculus, left u fiber, corpus callosum
left Inferior Frontal Gyrus (BA 9) - right Middle Frontal Gyrus (BA 6)	Corpus callosum
left Middle Frontal Gyrus (BA 6) - right Middle Frontal Gyrus (BA 6)	Corpus callosum

B Article Reuse License

Figure 25 – "Brain structural-functional connectivity relationship underlying the information processing speed" article reuse license

C Article Reuse License

SPRINGER NATURE LICENSE
TERMS AND CONDITIONS

Jan 17, 2022

This Agreement between Universidade de São Paulo -- Pedro Henrique Rodrigues Silva
("You") and Springer Nature ("Springer Nature") consists of your license details and the
terms and conditions provided by Springer Nature and Copyright Clearance Center.

License Number	5231430389961
License date	Jan 17, 2022
Licensed Content Publisher	Springer Nature
Licensed Content Publication	Brain Structure and Function
Licensed Content Title	Non-classical behavior of the default mode network regions during an information processing task
Licensed Content Author	Pedro Henrique Rodrigues da Silva et al
Licensed Content Date	Sep 16, 2020
Type of Use	Thesis/Dissertation
Requestor type	academic/university or research institute
Format	print and electronic
Portion	full article/chapter
Will you be translating?	no
Circulation/distribution	50000 or greater
Author of this Springer Nature content	yes

Title	Brain structural and functional Networks: from connections to cognition. A study applied to Cerebral Small Vessel Disease
Institution name	Universidade de São Paulo
Expected presentation date	Mar 2022
Requestor Location	Universidade de São Paulo Rua Prudente de Moraes, 315 São João da Boa Vista, Outra 13870-050 Brazil Attn: Universidade de São Paulo
Total	0.00 USD

Terms and Conditions

Springer Nature Customer Service Centre GmbH
Terms and Conditions

This agreement sets out the terms and conditions of the licence (the **Licence**) between you and **Springer Nature Customer Service Centre GmbH** (the **Licensor**). By clicking 'accept' and completing the transaction for the material (**Licensed Material**), you also confirm your acceptance of these terms and conditions.

1. Grant of License

1. 1. The Licensor grants you a personal, non-exclusive, non-transferable, world-wide licence to reproduce the Licensed Material for the purpose specified in your order only. Licences are granted for the specific use requested in the order and for no other use, subject to the conditions below.

1. 2. The Licensor warrants that it has, to the best of its knowledge, the rights to license reuse of the Licensed Material. However, you should ensure that the material you are requesting is original to the Licensor and does not carry the copyright of another entity (as credited in the published version).

1. 3. If the credit line on any part of the material you have requested indicates that it was reprinted or adapted with permission from another source, then you should also seek permission from that source to reuse the material.

2. Scope of Licence

2. 1. You may only use the Licensed Content in the manner and to the extent permitted by these Ts&Cs and any applicable laws.

2. 2. A separate licence may be required for any additional use of the Licensed Material, e.g. where a licence has been purchased for print only use, separate permission must be obtained for electronic re-use. Similarly, a licence is only valid in the language selected and does not apply for editions in other languages unless additional translation rights have been granted separately in the licence. Any content

owned by third parties are expressly excluded from the licence.

2. 3. Similarly, rights for additional components such as custom editions and derivatives require additional permission and may be subject to an additional fee. Please apply to Journalpermissions@springernature.com/bookpermissions@springernature.com for these rights.

2. 4. Where permission has been granted **free of charge** for material in print, permission may also be granted for any electronic version of that work, provided that the material is incidental to your work as a whole and that the electronic version is essentially equivalent to, or substitutes for, the print version.

2. 5. An alternative scope of licence may apply to signatories of the STM Permissions Guidelines, as amended from time to time.

3. Duration of Licence

3. 1. A licence for is valid from the date of purchase ('Licence Date') at the end of the relevant period in the below table:

Scope of Licence	Duration of Licence
Post on a website	12 months
Presentations	12 months
Books and journals	Lifetime of the edition in the language purchased

4. Acknowledgement

4. 1. The Licensor's permission must be acknowledged next to the Licenced Material in print. In electronic form, this acknowledgement must be visible at the same time as the figures/tables/illustrations or abstract, and must be hyperlinked to the journal/book's homepage. Our required acknowledgement format is in the Appendix below.

5. Restrictions on use

5. 1. Use of the Licensed Material may be permitted for incidental promotional use and minor editing privileges e.g. minor adaptations of single figures, changes of format, colour and/or style where the adaptation is credited as set out in Appendix 1 below. Any other changes including but not limited to, cropping, adapting, omitting material that affect the meaning, intention or moral rights of the author are strictly prohibited.

5. 2. You must not use any Licensed Material as part of any design or trademark.

5. 3. Licensed Material may be used in Open Access Publications (OAP) before publication by Springer Nature, but any Licensed Material must be removed from OAP sites prior to final publication.

6. Ownership of Rights

6. 1. Licensed Material remains the property of either Licensor or the relevant third party and any rights not explicitly granted herein are expressly reserved.

7. Warranty

IN NO EVENT SHALL LICENSOR BE LIABLE TO YOU OR ANY OTHER PARTY OR ANY OTHER PERSON OR FOR ANY SPECIAL, CONSEQUENTIAL, INCIDENTAL OR INDIRECT DAMAGES, HOWEVER CAUSED, ARISING OUT OF OR IN CONNECTION WITH THE DOWNLOADING, VIEWING OR USE OF THE MATERIALS REGARDLESS OF THE FORM OF ACTION, WHETHER FOR BREACH OF CONTRACT, BREACH OF WARRANTY, TORT, NEGLIGENCE, INFRINGEMENT OR OTHERWISE (INCLUDING, WITHOUT LIMITATION, DAMAGES BASED ON LOSS OF PROFITS, DATA, FILES, USE, BUSINESS OPPORTUNITY OR CLAIMS OF THIRD PARTIES), AND
WHETHER OR NOT THE PARTY HAS BEEN ADVISED OF THE POSSIBILITY OF SUCH DAMAGES. THIS LIMITATION SHALL APPLY NOTWITHSTANDING ANY FAILURE OF ESSENTIAL PURPOSE OF ANY LIMITED REMEDY PROVIDED HEREIN.

8. Limitations

8. 1. _BOOKS ONLY:_ Where **'reuse in a dissertation/thesis'** has been selected the following terms apply: Print rights of the final author's accepted manuscript (for clarity, NOT the published version) for up to 100 copies, electronic rights for use only on a personal website or institutional repository as defined by the Sherpa guideline (www.sherpa.ac.uk/romeo/).

8. 2. For content reuse requests that qualify for permission under the STM Permissions Guidelines, which may be updated from time to time, the STM Permissions Guidelines supersede the terms and conditions contained in this licence.

9. Termination and Cancellation

9. 1. Licences will expire after the period shown in Clause 3 (above).

9. 2. Licensee reserves the right to terminate the Licence in the event that payment is not received in full or if there has been a breach of this agreement by you.

Appendix 1 — Acknowledgements:

For Journal Content:
Reprinted by permission from [**the Licensor**]: [**Journal Publisher** (e.g. Nature/Springer/Palgrave)] [**JOURNAL NAME**] [**REFERENCE CITATION** (Article name, Author(s) Name), [**COPYRIGHT**] (year of publication)

For **Advance Online Publication papers:**
Reprinted by permission from [**the Licensor**]: [**Journal Publisher** (e.g. Nature/Springer/Palgrave)] [**JOURNAL NAME**] [**REFERENCE CITATION** (Article name, Author(s) Name), [**COPYRIGHT**] (year of publication), advance online publication, day month year (doi: 10.1038/sj.[JOURNAL ACRONYM].)

For Adaptations/Translations:
Adapted/Translated by permission from [**the Licensor**]: [**Journal Publisher** (e.g. Nature/Springer/Palgrave)] [**JOURNAL NAME**] [**REFERENCE CITATION** (Article name, Author(s) Name), [**COPYRIGHT**] (year of publication)

Note: For any republication from the British Journal of Cancer, the following credit line style applies:

Reprinted/adapted/translated by permission from [**the Licensor**]: on behalf of Cancer Research UK: : [**Journal Publisher** (e.g. Nature/Springer/Palgrave)] [**JOURNAL NAME**] [**REFERENCE CITATION** (Article name, Author(s) Name), [**COPYRIGHT**] (year of publication)

For **Advance Online Publication** papers:
Reprinted by permission from The [**the Licensor**]: on behalf of Cancer Research UK: [**Journal Publisher** (e.g. Nature/Springer/Palgrave)] [**JOURNAL NAME**] [**REFERENCE CITATION** (Article name, Author(s) Name), [**COPYRIGHT**] (year of publication), advance online publication, day month year (doi: 10.1038/sj.[JOURNAL ACRONYM])

For Book content:
Reprinted/adapted by permission from [**the Licensor**]: [**Book Publisher** (e.g. Palgrave Macmillan, Springer etc) [**Book Title**] by [**Book author**(s)] [**COPYRIGHT**] (year of publication)

Other Conditions:

Version 1.3